PROJECT ADVISORY COMMITTEE

Subcommittee on

Engineering

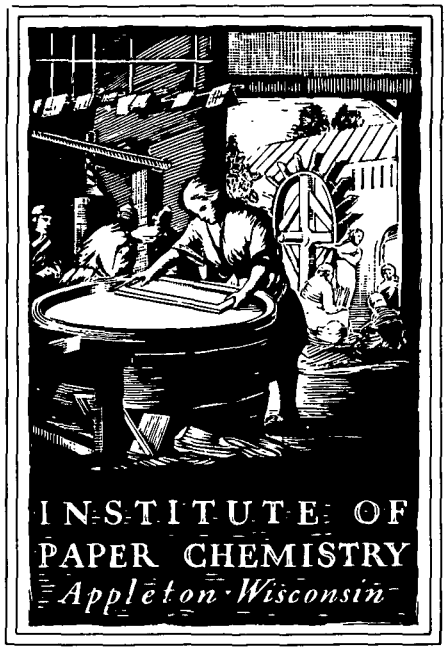

IPC STAFF STATUS REPORTS

This information represents a review of on-going research for use by the Project Advisory Subcommittees. The information is not intended to be a definitive progress report on any of the projects and should not be cited or referenced in any paper or correspondence external to your company.

Your advice and suggestions on any of the projects will be most welcome.

FOR MEMBER COMPANIES ONLY

NOTICE & DISCLAIMER

The Institute of Paper Chemistry (IPC) has provided a high standard of professional service and has exerted its best efforts within the time and funds available for this project. The information and conclusions are advisory and are intended only for the internal use by any company who may receive this report. Each company must decide for itself the best approach to solving any problems it may have and how, or whether, this reported information should be considered in its approach.

IPC does not recommend particular products, procedures, materials, or services. These are included only in the interest of completeness within a laboratory context and budgetary constraint. Actual products, procedures, materials, and services used may differ and are peculiar to the operations of each company.

In no event shall IPC or its employees and agents have any obligation or liability for damages, including, but not limited to, consequential damages, arising out of or in connection with any company's use of, or inability to use, the reported information. IPC provides no warranty or guaranty of results.

This information represents a review of on-going research for use by the Project Advisory Committees. The information is not intended to be a definitive progress report on any of the projects and should not be cited or referenced in any paper or correspondence external to your company.

Your advice and suggestions on any of the projects will be most welcome.

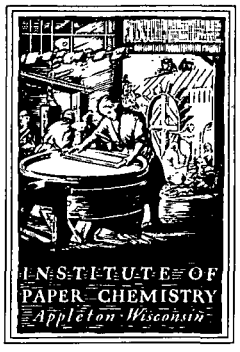

THE INSTITUTE OF PAPER CHEMISTRY
Post Office Box 1039
Appleton, Wisconsin 54912
Phone: 414/734-9251
Telex: 469289

March 4, 1988

TO: Members of the Engineering Project Advisory Committee

Enclosed is advance reading material for the March 29-30 meeting of the Engineering Project Advisory Committee. Included are status reports for active projects, an agenda, and a current committee membership list.

Rooms have been reserved in the Continuing Education Center, and meals will be provided as stated on the agenda. If you haven't already indicated your attendance, please do so at your earliest convenience by returning your registration form or calling Jennifer Schuh at 414/738-3320. Also enclosed is the Security Card with the number to gain entrance into the Continuing Education Center.

For all Project Advisory Committee meetings, the Institute invites its member companies to send one or more representatives to attend the review sessions (first day) of any or all of the meetings. These invitations were mailed in February. PAC members from member companies are also welcome to attend the other meetings, and may stay in the CEC and attend meetings and meals of their choice, at no cost. If you wish to attend any of the other meetings, but haven't registered, please call Jennifer Schuh to do so. A meeting schedule is enclosed for your information.

We look forward to meeting with you on March 29-30.

Sincerely,

Clyde

Clyde H. Sprague, Director
Engineering Division

CHS/lms
Enclosures

THE INSTITUTE OF PAPER CHEMISTRY

Project Advisory Committee Spring Meetings
Member Dues - Funded Research Reviews

March 22, 23, 24, 29, and 30

1988

Continuing Education Center
Appleton, Wisconsin
(414) 734-9251

Committee	Review Schedule	Research Area*
Pulping Processes	Tuesday, March 22 8:30 AM - 5:30 PM Dinner at 6:00 PM	Chemical Recovery: Recovery Furnace Processes Bleached Chemical Pulp: Pulping Oxygen Bleaching High Lignin Pulps: Strength Development Microstructure of Wood Fibers Analytical Techniques
Paper Properties	Wednesday, March 23 8:30 AM - 5:30 PM Dinner at 6:00 PM	Board Properties and Performance Process, Properties, Product Relationships Internal Strength Enhancement Strength Improvement and Failure Mechanisms On-line Measurement of Paper Mechanical Properties
Systems Analysis	Thursday, March 24 1:00 PM - 5:30 PM Dinner at 6:00 PM	MAPPS Simulator Development Continuing Module Development Performance Attribute Modeling Optimization with MAPPS MAPPS Applications and Field Experience

*NOT IN ORDER OF AGENDA

Committee	Review Schedule	Research Area*
Engineering	Tuesday, March 29 10:00 AM - 5:30 PM Dinner at 6:00 PM	Corrosion: Kraft Liquor Corrosivity Corrosion Control in Paper Mills Corrosion-Resistant Coatings Papermaking: Higher Consistency Processing Wet Pressing Impulse Drying
Forest Genetics	Wednesday, March 30 1:00 PM - 5:00 PM Dinner at 6:00 PM	Somatic Embryogenesis Initiation of Embryogenic Callus Tissue Culture Biochemistry Somatic Embryo Development Tissue Culture Biochemistry

TABLE OF CONTENTS

PRELIMINARY AGENDA

ENGINEERING
PROJECT ADVISORY COMMITTEE

March 29-30, 1988

Continuing Education Center (CEC)
The Institute of Paper Chemistry
Appleton, Wisconsin

Tuesday, March 29, 1988

11:00am	-- INTRODUCTION	Sprague/Chairman
11:15	-- CORROSION AND MATERIALS ENGINEERING GROUP	
	- Recovery Boiler Corrosion	Crowe
12:00	LUNCH	
1:00pm	- Fundamentals of Corrosion Control in Paper Mills	Staff
	- Fundamentals of Kraft Liquor Corrosivity	Crowe
2:00	-- PAPERMAKING PROCESSES GROUP	
	- Impulse Drying	Sprague
2:45	-- BREAK	
3:00	- Fundamentals of Wet Pressing	Lindsay
3:45	- Medium Consistency Processing	Staff
4:00	- Fiber and Paper Performance Attributes in Process Simulation (MAPPS)	Jones
5:30	-- COCKTAILS	
6:00	-- DINNER - CEC DINING ROOM	

Wednesday, March 30, 1988

7:15am -- BREAKFAST - CEC DINING ROOM

COMMITTEE ACTIVITIES

8:00am	-- Project Reviews	Committee and Staff
9:30	BREAK	
9:45	-- Continued Discussion	
10:30	-- Report Preparation	Committee
11:00	-- Adjourn	
	-- LUNCH - CEC DINING ROOM	

NOTE: The fall Engineering PAC meeting is scheduled for October 20-21, 1988.

ENGINEERING

Project Advisory Committee

Dr. Robert Rounsley (Chairman) - 6/89*
Research Fellow
Mead Corporation
8th & Hickory Street
Chillicothe, OH 45601
(614) 772-3581

Mr. Sven S. Arenander - 6/90
Group Leader
Union Camp Corporation
P.O. Box 3301
Princeton, NJ 08543-3301
(609) 896-1200

Dr. William C. Bliesner - 6/90
Technical Director
Thilmany Pulp & Paper Company
P.O. Box 600
Kaukauna, WI 54130
(414) 766-4611

Mr. Percy E. Brooks - 6/90
Manager, Pulp & Paper Engineering
Georgia-Pacific Corporation
133 Peachtree Street, N.E.
P.O. Box 105605
Atlanta, GA 30348-5605
(404) 521-4618

Mr. LeRoy H. Busker - 6/88
Director, Research & Planning
Beloit Corporation
Rockton R & D Center
1165 Prairie Hill Road
Rockton, IL 61072
(608) 364-7961

Mr. Max D. Moskal - 6/88
Project Manager
Stone Container Corporation
616 Executive Drive
Willowbrook, IL 60521
(312) 655-6949

Mr. M. Thomas Neill - 6/88
Vice President R&D
Abitibi-Price Inc.
Research Centre
Sheridan Park
Mississauga, Ontario L5K 1A9
CANADA
(416) 822-4770

Dr. W.B.A. Sharp - 6/90
Group Leader
Westvaco Corporation
Laurel Research Center
11101 Johns Hopkins Road
Laurel, MD 20707
(301) 792-9100

Dr. John Smuk - 6/89
Manager of Process Engineering
Research and Development Center
Potlatch Corporation
P.O. Box 510
Cloquet, MN 55720
(218) 879-2393

Mr. Benjamin Thorp - 6/89
Senior Vice President
Research and Engineering
James River Corporation
P.O. Box 2218
Richmond, VA 23217
(804) 644-5411

Dr. Jerry Wallace - 6/89
Mill Manager
Appleton Papers Inc.
East Main Street
Roaring Spring, PA 16673-1480
(814) 224-2131

Dr. Yung Duk Woo - 6/89
Senior Engineer
Papermaking R&D Department
Weyerhaeuser Paper Company
Tacoma, WA 98477
(206) 924-6428

*date of retirement
2/18/88

S T A T U S R E P O R T S

To The

Engineering Project Advisory Committee

March 29-30, 1988
The Institute of Paper Chemistry
Continuing Education Center
Appleton, Wisconsin

THE INSTITUTE OF PAPER CHEMISTRY

Appleton, Wisconsin

Status Report

to the

ENGINEERING PROJECT ADVISORY COMMITTEE

Project 3628

RECOVERY BOILER FIRESIDE CORROSION

March 29, 1988

PROJECT SUMMARY FORM

DATE: March 29, 1988

PROJECT NO.: 3628 - Recovery Boiler Fireside Corrosion

PROJECT LEADER: D.C. Crowe

IPC GOAL:

Improve safety and increase the operating life of equipment by proper selection of materials of construction and by identifying suitable process conditions.

OBJECTIVE:

To understand the causes of corrosion in the kraft recovery boiler, as a basis for devising methods of reducing corrosion damage.

CURRENT FISCAL BUDGET: $ 75,000.

SUMMARY OF RESULTS SINCE LAST REPORT: (September 1987 - March 1988)

Experimental equipment consisting of two tube furnaces has been started up. Preliminary runs have been completed and described. A new mechanism for air port corrosion has been proposed and an experimental plan for its investigation and comparison with other theories is presented for review. Study of probe designs has been initiated for in-situ air port corrosion studies, and some of this work is described.

INTRODUCTION

Fireside corrosion of recovery boiler components in the lower furnace is a chronic and costly problem. The major concern is the possibility of a smelt explosion if the water should leak from the tubes or smelt spouts, with the possibility of injury to personnel and loss of production. Operating costs include periodic inspection and repairs, plus downtime. Recently, the cost of insurance has increased due to the large number of recovery boiler accidents.

Corrosion of recovery boilers is a many-faceted problem. Some of the history of studies of lower furnace problems was summarized in the last PAC report. Corrosion of the lower furnace has been of special concern. Current repair or protection schemes such as thermal spray coatings, composite tubing, and pin studding are costly and sometimes not entirely successful. Relationships between corrosion of boiler tubes, furnace conditions, and operating practices are unknown. The mechanisms of corrosion are not well understood, in large part because the environments in problem areas are poorly characterized.

Corrosion can be severe around air ports, smelt spouts and at the liquid level line of the molten smelt. This research program will focus on problem areas in the boiler. One of these problems, addressed in this report, is air port corrosion. Wastage of stainless steel from composite air ports exposes the underlying carbon steel, leaving it unprotected. This is a serious concern to the industry. The corrosion has been attributed to NaOH condensation, but NaOH is unstable in the boiler and often has not been detected in corrosion deposits. Doubts about this theory remain in the minds of many corrosion engineers. An alternative mechanism for this corrosion is proposed and a test program to investigate it is outlined for review. By obtaining a better understanding of the corrosion mechanism, remedial measures may be devised, and conditions which stimulate corrosion may be avoided. The proposed mechanism should be considered to be speculative until experimental evidence in support of it can be obtained.

AN ALTERNATIVE MECHANISM OF RECOVERY BOILER AIR PORT CORROSION

by David C. Crowe and John H. Cameron

Abstract

Localized corrosion at recovery boiler air ports has been attributed to condensed sodium hydroxide but the role of NaOH has not been proved. An alternative mechanism, described here, involves corrosion by chloride and pyrosulfate.

Introduction

Corrosion of air ports has been an enduring problem of recovery boilers. In the 1960s, Plumley, Lewis and Tallent[1] concluded after field and lab studies, that wastage of carbon steel observed near air ports might be due to a gas-solid reaction, perhaps involving the localized concentration of oxygen, carbon dioxide and sulfur-containing gases. They thought metal wastage around air ports was not due to excessive metal temperatures resulting from high heat transfer rates.

Some localized corrosion in recovery boilers has been attributed to condensation of sodium hydroxide at lower temperatures. Clement,[2] investigating corrosion on the windbox side of flat stud boilers, argued that corrosion was due to reaction of iron, condensed NaOH and O_2 to form Fe_2O_3 and then non-protective $NaFeO_2$. Hydroxide condensation was further implicated by Bruno[3].

Moberg[4] summarized gas phase research carried out in Scandinavia to look at various steels over a range of temperatures and gas composition. They concluded that chromium steels possessed superior resistance to corrosion. In fact, stainless steels used for composite tubes have successfully reduced general corrosion rates in kraft recovery boilers.

More recently, localized wastage of stainless steel from composite tubes primarily near air ports of high pressure boilers was reported at a meeting of the National Association of Corrosion Engineers[5]. This has become a great concern to the industry. Corrosion and cracking was described further by Wensley[6] and was attributed to the condensation of hydroxide.

Barna and Rogan[7] have reported on the appearance and occurrence of corrosion of composite tubes at port openings. They considered that the corrosion process depends on formation of crevices that have the capability of accumulating deposits and that form a non gas-tight seal between the furnace and casing side of the tubing. They suggested that hydroxide vapors condense at deposits and form a molten phase at the deposit/substrate interface.

Wensley[8] reported that tube cladding wastage and the preferential corrosion of the stainless cladding from flat studs often occurred together. He also noted that those openings which evidently experienced higher temperature conditions

in service, resulting in both flat stud burn-back and flat stud notch cracking, were less likely to exhibit pronounced stainless cladding wastage. Conversely, areas of cladding wastage experienced less flat stud burn-back and notch cracking. This suggests that stainless steel removal is a low temperature phenomenon. Wensley also reported measurements of the waterwall tube temperatures between the primary and secondary air ports which were between 300 and 350 C, as measured by chordal thermocouples, confirming that the temperatures of the tubes are fairly low.

In contrast, in a failure analysis of a cracked composite recovery boiler tube, Odelstam[9] determined that the tube had reached temperatures as high as 500-550 C. Perhaps these temperatures should be considered to be the top of the operating range for tube temperatures. In explaining the preferential corrosion of stainless steel, he referenced work by Rahmel which indicated that carbon steel is more resistant to molten hydroxide than are Cr and CrNi steels. The corrosion rate depends on the Na_2O_2 content in the pure NaOH melt which in turn depends on oxygen and steam partial pressure in the gas above the melt. The chromium is especially reactive to form chromate (Na_2CrO_4) via:

$$4\ NaOH + Cr_2O_3 + 3/2\ O_2 \rightarrow 2\ Na_2CrO_4 + 2\ H_2O \qquad (1)$$

This reaction would remove the protective chromium oxide passive layer from the stainless steel, causing rapid corrosion.

The NaOH condensation mechanism has been recently summarized by Odelstam et al.[10] According to that theory, the NaOH may condense if the hot furnace gas is cooled rapidly and then placed in contact with low (<1ppm) CO_2 air. Laboratory results were described in which severe corrosion of 304L SS occurred at the interface between molten NaOH/Na_2CO_3 and air. Compared to the 304 SS, type 310 stainless steel corroded less and carbon steel less than either stainless steel. In areas in contact with the furnace gas with high CO_2 concentration, the NaOH would react to form harmless carbonates and sulfates. They also reported tests confirming that NaOH and Cr_2O_3 react to form Na_2CrO_4, and presented analysis of corrosion deposits containing high NaOH concentrations.

There is some uncertainty about the extent to which carbon steel is attacked but it is generally considered to be attacked more slowly than stainless steel. This observation, based on damage of composite tubes, would be consistent with corrosion caused by NaOH, in which stainless steel may be corroded more quickly than carbon steel.

The conditions under deposits where the corrosion occurs are poorly understood. Bruno[3] had perhaps the most to report regarding deposits (formed on carbon steel in lower pressure boilers). Sulfur content of these deposits was very low. He reported that deposits from the Iggesund recovery boiler began to melt at 250 C. Deposits containing 12% NaOH were encountered in a boiler (280 C, 64 bar) near the primary and secondary air ports. Sodium sulfide (2.1%) and sodium sulfate (2.8%) were very low, although other analyses of deposits from around air ports showed higher sulfate concentrations. Clement[2] described chemical accumulations at air ports, with a black and red deposit ($NaFeO_2$) next to the tube, yellow and green layers outside that, and extending into a gray layer of unreacted "Hydrochrome" refractory material. The pH was about 12 and sulfur (as SO_3) was less than 2%. The temperature in the area was about 315 C (600 F).

Odelstam et al.[10] have provided analyses of deposits showing high NaOH composition. No analysis for NaCl or $Na_2S_2O_3$ was reported and the method of analysis for NaOH was not described. The high NaOH levels may form by the reverse of reaction (1) during an analytical titration procedure. Other analyses of corrosion deposits from air ports have not provided evidence of NaOH condensation. Retrieval of representative corrosion deposits is very difficult, especially because corrosion is localized and unpredictable.

Reservations regarding the condensation of NaOH remain based on the difficulty of producing NaOH fume in the recovery boiler, as described by Cameron[11]. Pejryd and Hupa[12] have made equilibrium calculations for the gas composition in the kraft furnace. These calculations show that NaOH vapor is a stable species only at temperatures above 800 C. In the temperature range from 800 to 1300 C, the equilibrium CO_2 concentration is several orders of magnitude greater than the equilibrium NaOH concentration. It is unlikely that NaOH could condense in such an atmosphere without reacting with the CO_2 to form Na_2CO_3.

Alternative Mechanism

Recent research by Cameron[11] indicates that KCl and NaCl are major volatile species from melts similar to those found within the recovery furnace and that very little NaOH vapor is produced. Liden and Pejryd [13] have noted that KCl (g) and NaCl (g) may be emitted in about equal amounts, even though potassium is a minor constituent of the liquor. These salts may deposit on cooler surfaces within the furnace. On exposure to SO_3 or SO_2, they would be expected to form pyrosulfates $Na_2S_2O_7$ and $K_2S_2O_7$ via the equations:

$$2\,NaCl\,(s) + 2\,SO_3\,(g) + 1/2\,O_2 \text{---> } Na_2S_2O_7\,(l) + Cl_2\,(g) \qquad (2)$$

$$2\,NaCl\,(s) + 2\,SO_2\,(g) + 3/2\,O_2 \text{ ---> } Na_2S_2O_7\,(l) + Cl_2\,(g) \qquad (3)$$

Therefore, pyrosulfate should be considered as a possible corrosive agent within the recovery boiler.

Although pyrosulfate is known to be a corrosive agent [14, 15, 16], it has not been considered as a potential agent for the corrosion observed with composite tubes. This appears to be a result of equilibrium studies by Backman and Hupa[17] which show that $Na_2S_2O_7$ is unstable at the SO_2 levels and temperatures found within a recovery boiler. Backman and Hupa concluded that $Na_2S_2O_7$ could only occur if the SO_x concentration exceeds 5000 ppm. Since the SO_2 concentration in kraft furnaces is in the range of 50 to 500 ppm, $Na_2S_2O_7$ would be expected to be unstable and therefore, was eliminated from consideration as a corrosive agent. These conclusions differ from the findings of Coats, Dear and Penfold.[18] They have measured the relation between the partial pressure of SO_3 and melting point temperatures of alkali pyrosulfates. For example, at 425 C (800 F) about 3000 ppm of SO_3 is necessary to form $Na_2S_2O_7$ or about 200 ppm SO_3 to form $K_2S_2O_7$.

While $Na_2S_2O_7$ may be unstable at the SO_x levels in the recovery furnace, there are conditions under which it will occur. Fielder et al.[19] and Anderson and Hung[20] have shown that NaCl will react rapidly with SO_2 or SO_3 at 400 C and SO_x level less than 1000 ppm to form $Na_2S_2O_7$ via equation 2. Fielder et al.[19] found that on exposure to SO_2-SO_3-O_2, a NaCl sample was essentially molten $Na_2S_2O_7$ after 10 min. at 401 C. By raising the temperature to 500 C in a stream of O_2, the $Na_2S_2O_7$ slowly converted to a non-adhering film of Na_2SO_4. They proposed that for the temperature range 401 to 450 C (750 to 840 F), molten $Na_2S_2O_7$ is the

principal film product that is formed when NaCl is exposed to the oxides of sulfur. Reid has noted that, below 482 C (900 F) equilibrium favors SO_3 over SO_2. Thus as furnace gas cools, SO_3 may be more stable and it may react via equation 2.

The corrosion in the area of the air ports in the recovery boiler may result from pyrosulfate. Based on the work of Fielder et al.[13], and the conclusions of Cameron [11] that NaCl and KCl are the major volatile species in the recovery boiler, production of pyrosulfate appears to be possible. This would occur in areas where the temperature is in the range 400 to 450 C (750 to 840 F) and chloride, SO_3 and O_2 are present. On the cold side of the waterwall, and in areas in contact with air these conditions may be present. The molten nature of the pyrosulfate would account for the appearance of the tube wastage where it is suggestive of erosion by a liquid phase. Backman, Hupa, and Hyoty[17] have noted that $Na_2S_2O_7$ - $K_2S_2O_7$ mixtures might have a low eutectic temperature (down to 280 C). This is within the region of temperatures anticipated on recovery boiler waterwall tubes.

The role of pyrosulfates in corrosion has been reviewed by Reid [14]. Work by Corey, Cross and Reid [15] has indicated that at tube-metal temperatures of 425 C (800 F), pyrosulfates probably contribute to metal loss.

$$3\,Na_2S_2O_7 + Fe_2O_3 \rightarrow 3\,Na_2SO_4 + Fe_2(SO_4)_3 \qquad (4)$$

$$4\,Na_2S_2O_7 + Fe_3O_4 \rightarrow 4\,Na_2SO_4 + FeSO_4 + Fe_2(SO_4)_3 \qquad (5)$$

$$3\,Na_2S_2O_7 + Fe_2O_3 \rightarrow 2\,Na_3Fe(SO_4)_3 \rightarrow 3\,Na_2SO_4 + Fe_2O_3 + 3\,SO_3 \qquad (6)$$

Removal of the oxide layers would expose the underlying steel to rapid oxidation and sulfidation. Nevertheless, pyrosulfates have not been found in corrosion products of recovery boiler in concentrations high enough to be identified by X-ray diffraction. However, they may decompose prior to analysis. Corrosion by pyrosulfates would be restricted to a range from 750-900 F (400- 480 C). This range agrees closely with the results of Fielder et al.[19] for pyrosulfate formation and may occur on recovery boiler waterwall tubes.

Besides forming pyrosulfate, chlorides may increase the oxidation appreciably above 400 C (750 F) by destroying the protective spinel layer on

austenitic stainless steels. When alkalies are also present, chromium is lost from the surface as volatile chromic chloride, increasing the oxidation rate to replace the normal chromium oxide film [14]. This may account for the severe attack of stainless steel alloys. Reaction of chloride and chromium oxide spinel may generate hydroxide. A possible reaction, involving oxidation and formation of high pH is:

$$4\,KCl + Cr_2O_3 + H_2O + 2\,e^- \rightarrow 2\,CrCl_2 + 2\,K_2O + 2\,OH^- \qquad (7)$$

The hydroxide may then react via equation (1) to produce chromate and the $CrCl_2$ may react elsewhere in the deposit where P_{O_2} is higher, forming chromate or Cr_2O_3. Chiang et al.[21] have suggested a similar process involving $Cr_2(SO_3)_3$ in Ni - Cr alloys instead of $CrCl_2$. In that process, Cr_2O_3 reacts to form $Cr_2(SO_3)_3$ which migrates outward and reprecipitates where P_{O_2} is higher. Chloride concentrations in the corrosion deposit were low according to Bruno [3]. This would be consistent with volatilization to Cl_2 via equation 2. Further detailed analysis of deposits would be useful to determine the presence and distribution of chloride.

Alexander[22] found that the effect of increasing chloride concentration in mixtures of sulfates and chlorides was more marked with austenitic than with ferritic steels at temperatures of 400 - 700 C (750 to 1290 F). Apparently, the chloride destroyed the normally protective spinel oxide layer. They observed that when chromium-containing steels were heated with coatings rich in chloride, a green deposit, strongly resembling chromic oxide, Cr_2O_3, was formed. This deposit could have been formed only by the volatilization of chromium. They thought that the volatile chromium compound was CrO_2Cl_2, $CrCl_3$ or CrO_3. Work by Pickering, Beck and Fontana was quoted in which results were attributed to corrosion via:

$$24\,KCl + 10\,Cr_2O_3 + 9\,O_2 \rightarrow 12\,K_2CrO_4 + 8\,CrCl_3 \qquad (8)$$

This reaction commenced at about 400 C (750 F). This reaction might account for the observation of chromate in smelt deposits and the greenish yellow color observed in deposits from corroded areas of boilers.

Shinata et al. [23] have studied NaCl induced hot corrosion of stainless steels, and concluded that, in the range 650-900 C (1200-1650 F), chromium is oxidized selectively, leaving a non-protective Cr_2O_3 scale. Corrosion losses increased with increasing chromium content. This raises the question whether a similar process takes place in the recovery boiler at lower temperatures, to preferentially attack chromium alloys. If this is the case, then the accelerated wastage of stainless steel from composite tubes may be rationalized in terms of a mechanism involving chloride. Vaughan et al.[16] determined that chloride produced during refuse firing is responsible for serious corrosion. They noted that low temperature corrosion could be attributed to chlorine formed by oxidation of HCl or by conversion of alkali chlorides to sulfates and pyrosulfate. Resistance to chloride may be very important in preventing recovery boiler corrosion. This question needs to be resolved, and may provide the key to improved performance of air ports.

Chromates may arise for many reasons, not necessarily due to reaction of chromium with hydroxides. At higher temperature (975 C), Fryburg et al.[24,25] have indicated that chromium oxide may react to form chromate via:

$$Cr_2O_3 + 2\,Na_2SO_4\,(l) + 3/2\,O_2 \rightarrow 2\,Na_2CrO_4\,(l) + 2\,SO_3\,(g) \qquad (9)$$

Although temperatures are too low on the tube surface, the reaction may occur in the deposit. This could account for the presence of chromate in the corrosion deposit.

A mechanism of lower temperature corrosion relevant to the recovery boiler may share some features with a mechanism described by Luthra and Shores[26] for corrosion at 600-900 C (1110-1650 F). It involves formation of a liquid sulfate phase and sulfidation of the surface, thereby retarding formation of a protective Cr_2O_3 scale. In a study of corrosion of cobalt alloys, Luthra [27] has suggested that the major oxidant is SO_3. It diffuses in via counter transport of $S_2O_7^{2-}$ and SO_4^{2-}. Oxygen (from SO_3) is consumed at the scale surface to form SO_2. The SO_2 (or SO_3^{2-}) will diffuse away from the surface. Low P_{O_2} at the metal surface will ensure that the Cr_2O_3 film is non-protective

Conclusions

Results described in the literature to date do not provide unequivocal evidence of NaOH condensation and may be based on false premises regarding the presence of NaOH in recovery boilers. The published information on corrosion of air ports is consistent with an alternative corrosion process involving chloride and pyrosulfate. Work is underway at the Institute of Paper Chemistry to examine ways in which chloride and pyrosulfate might accelerate corrosion of stainless steel near recovery boiler air ports.

References

1. A.L.Plumley, E.C.Lewis and R.G.Tallent, TAPPI 49(1):72A- 81A (1966).
2. J.L.Clement, TAPPI 53(2): 269 (1970).
3. F.Bruno, PulpPap.Ind.Corr.Prob. 4: 68 (1983), Swedish Corrosion Institute, Stockholm (1983).
4. O.Moberg, PulpPap.Ind.Corr.Prob. 1: 125-136 (1974).
5. NACE T-5H-1 Task Group on Recovery Boiler Fireside Corrosion, Minutes of Meeting, Atlanta, Sept 19, 1985.
6. D.A.Wensley, Corrosion and Cracking of Composite Boiler Tubes, p.231-245 in 1986 Kraft Recovery Operations Seminar, TAPPI, Atlanta (1986).
7. J.L.Barna and J.B.Rogan, Proc.TAPPI 1986 Engineering Conf. pp.377-385 (1986).
8. D.A.Wensley, Matl. Perf. 26(11): 53-55 (1987).
9. T.Odelstam, pp.277-288 in Proc. 1987 Kraft Recovery Operations (Orlando) TAPPI Press, Atlanta (1987).
10. T. Odelstam, H.N.Tran, D.Barham, D.W.Reeve, M.Hupa and R.Backman, pp.585-590 in TAPPI 1987 Engineering Conference Proceedings, TAPPI, Atlanta (1987).
11. J.H.Cameron, "Vaporization from Alkali Carbonate Melts", Institute of Paper Chemistry Technical Paper Series No. 237 (April 1987) accepted by Pulp and Paper Science.
12. L.Pejryd and M.Hupa, TAPPI 1984 Pulping Conf., San Francisco, TAPPI, Atlanta (1984).
13. J.Liden and L.Pejryd, Nord.PulpPap.Res.J. 1(1): 22 -25 (1986).
14. W.T.Reid, External Corrosion and Deposits, American Elsevier, New York (1971).

15. R.C.Corey, B.J.Cross and W.T.Reid, Trans ASME 67: 289 - 302 (1945).
16. D.A.Vaughan, H.H.Krause and W.K.Boyd, pp.473-493 in Ash Deposits and Corrosion Due to Impurities in Combustion Gases, ed. R.W.Bryers, Hemisphere Pub.Co./ McGraw Hill, New York, 1978.
17. R.Backman, M.Hupa and P.Hyoty, PulpPap.Ind.Corr.Prob. 4: 76-81 (1983).
18. A.W.Coats, D.J.A.Dear and D.Penfold, J.Inst.Fuel, 41:129 (1968).
19. W.L Fielder, C.A.Stearns and F.J.Kohl, Proc.Electrochem.Soc. 83: 251-265 (1983) and J.Electrochem.Soc. 131: 2414-2417 (1984).
20. A.B.Anderson and S.C.Hung, J.Am.Chem.Soc. 105: 7541 (1983).
21. K.Y.Chiang, F.S.Pettit and G.H.Meier, pp. 519 - 530 in High Temperature Corrosion, ed. R.A.Rapp, NACE, Houston (1983).
22. P.A.Alexander, pp.571 - 582 in The Mechanism of Corrosion by Fuel Impurities, Proc. Int'l Conf. Marchwood Eng. Labs, Butterworths, London, 1963.
23. Y. Shinata, F.Takahashi and K.Hashiura, Mat.Sci.Eng. 87: 399 - 405 (1987).
24. G.C.Fryburg, F.J.Kohl and C.A.Stearns, J.Electrochem.Soc. 131: 2985-2987 (1984).
25. G.C.Fryburg, F.J.Kohl, C.A.Stearns and W.L.Fielder, J.Electrochem.Soc. 129: 571-585 (1982).
26. K.L.Luthra and D.A.Shores, J.Electrochem.Soc. 127(10): 2202-2210 (1980).
27. K.L.Luthra, pp. 507 - 512 in High Temperature Corrosion ed. R.A.Rapp, NACE, Houston (1983).

PROGRESS:

1. Some preliminary corrosion tests have been completed. The primary objective of these tests has been to commission laboratory equipment which can be used for studies of recovery boiler corrosion, and to gain experience in conducting these experiments. The results should provide some baseline data for subsequent testing of steels in powdered smelt using tube furnaces. One furnace is an electrical tube furnace (110 V, 5A) with temperature controller, chromel alumel thermocouple and variable transformer as the main pieces of equipment. The second furnace (220 V) has a temperature controller, thermocouples and over-temperature shut-off. The furnace tubes are alumina, fitted with universal seals. Metal samples are contained in smelt-filled alumina combustion boats.

Results of corrosion measurements for 1018 carbon steel and 304 stainless steel showed similar corrosion rates for both materials of about 0.2 mpy after 2

week exposure at 300 C. The smelt composition was 80 % Na_2CO_3, 12 % Na_2SO_4 and 8 % Na_2S, and an oxygen free nitrogen atmosphere was used. At 300 C, the carbon steel coupons and one of the stainless steel coupons were covered with a black film. One of the stainless steel samples had a green colored film on its surface. At higher temperature, the green deposit was observed on all coupons. The weight loss results are listed in Table 1.

Table 1

Corrosion rates of 1018 and 304 steels.

Temperature	1018 Carbon Steel	304 Stainless
300	0.19, 0.21 mpy	0.27, 0.23
500	0.57, 3.92	0.62, 1.72
400	0.42, 0.42	0.40, 0.27
600	0.84, 1.88	11.73, 1.35

2. The gas metering systems have been designed and partly constructed. A system for adding H_2O to the flue gas has been designed. A nitrogen/CO_2/O_2 gas stream will be saturated with H_2O at a controlled temperature to obtain the desired final H_2O content.

3. Conceptual design is complete for a corrosion probe for use in the recovery boiler air port. It will be inserted through the primary windbox of a boiler so that the tip of the probe is located at the upper crotch of an air port, where corrosion has been observed. The probe will be oriented at approximately a 45 degree angle pointing downward. The probe will be comprised of a stainless steel outer tube enclosing an aluminum or kanthal inner tube. The inner tube will contain molten sulfur (mp 113 C, bp 445 C). The use of sulfur is based on a suggestion by W. T. Reid in "External Corrosion and Deposits", American Elsevier, NY (1971). The sulfur pool will be heated by a cartridge heater immersed in it. Cooling will be provided by a cooling coil located outside the windbox. The cartridge heater will be controlled by a temperature controller using a thermocouple located between the aluminum internal tube and the external stainless steel tube. At the tip of the probe will be a small cup which will fill with smelt or be filled prior to the test. This cup will also serve as the corrosion coupon. This design will help to maintain the corrosion deposit on the corroded surface after withdrawal from the furnace. Molten sulfur will be used to maintain the temperature of the probe because it will not pose an explosion hazard if it leaks into the boiler, and it is

molten throughout the range of temperatures of interest. Uniform temperature inside the probe should be attained by thermal convection of the sulfur.

PLANS FOR NEXT PERIOD:

Experimental Plan for Laboratory Study

This study will focus on obtaining information on the effects of potentially corrosive species in simulated kraft smelts to aid in identifying the relevant mechanisms of corrosion under smelt deposits.

Simulated smelts

1. 80 % Na_2CO_3, 12 % Na_2SO_4, 8 % Na_2S.
2. Smelt 1 with 10 % NaOH addition.
3. Smelt 1 with 5 % NaCl addition.
4. Smelt 1 with 5 % $Na_2S_2O_7$ addition.
5. Smelt 1 with 5 % KCl addition.
6. Smelt 1 with 5 % $Na_2S_2O_3$ addition.
7. Smelt 1 with 5 % S addition.
8. Smelt 1 with 5 % Na_2SO_3 addition.

The Na_2S used in the smelt is formed from $Na_2S \cdot 9H_2O$ in a vacuum furnace under nitrogen atmosphere at approximately 190 C. The temperature is brought up slowly to prevent flashing. After cooling, the smelt is then ground to a fine powder within a nitrogen filled glove bag, placed in a jar and sealed. Mixing with Na_2CO_3 and Na_2SO_4 is also done under a nitrogen atmosphere, and again is ground to a fine powder. Care is taken to exclude air from the smelt until placed in the furnace. Smelt analysis will be performed on smelts used in initial tests to determine smelt stability at these temperatures.

Materials

1. 1018 Carbon Steel.
2. A210 Carbon Steel.
2. 304 Stainless Steel.

Gas Atmosphere

1. 1.0 % H_2S, 1.0 % O_2, 2 % H_2O, 10 % CO_2, balance N_2.
2. Additions of 0.1 % SO_2 and SO_3 to Gas 1.

The gas will be metered into the furnace and after exiting the furnace will be passed through an NaOH solution to remove the H_2S before venting into the fume hood. Gas analysis will be performed to determine gas stability at the test temperatures. A system to produce and introduce the SO_2/SO_3 mixture needs to be devised.

Temperatures

1. 300 C
2. 400 C
3. 500 C

Air Port Corrosion Probe

Detailed design of the corrosion probe will be done. Construction and bench testing will then commence.

Other Plans

1. Document corrosion problems in smelt spouts and relevant corrosion mechanisms as a first step in designing a research program to study smelt spout corrosion problems.

2. Obtain samples of smelt and flue gases withdrawn from the vicinity of air ports and smelt spouts of operating boilers and perform chemical analyses to obtain a better knowledge of local conditions in the boiler.

3. Establish the range of gas environment conditions for use in gas phase oxidation/sulfidation tests.

Related Experimental Plans of John Cameron, Chemical Recovery Group

Experiments are proposed in the Chemical Recovery Group to support the concept that $Na_2S_2O_7$ is an active agent for composite tube corrosion near air ports. Earlier experiments have shown that NaCl is more volatile than NaOH from Na_2CO_3 - Na_2S melts. The present experiments will determine the deposit composition on a cooled probe above a Na_2CO_3 - Na_2S melt and any change in composition through reaction with furnace gases (specifically SO_2). The experiments will be conducted in a reactor system using a probe at 300 to 500 C (the temperature range for air port corrosion). The deposit could be exposed to SO_2

or could be formed in an SO_2 environment. If the initial deposit is mainly NaCl, SO_2 may convert this deposit to $Na_2S_2O_7$. Pyrosulfate is known to be a highly corrosive agent and if it can be shown that the deposit contains $Na_2S_2O_7$, then this must be considered to be an active agent in composite tube corrosion.

POTENTIAL FUTURE ACTIVITIES

1. Devise an apparatus for investigation of lower furnace corrosion. The apparatus should continuously replenish molten smelt at the corroding steel surface, with the steel cooled to form a layer of frozen smelt.

2. Develop and validate real-time corrosion testing methods for use in operating boilers.

SIGNIFICANCE TO THE INDUSTRY:

An improved knowledge of corrosion mechanisms in recovery boilers will aid in the design of remedial measures which will extend the operating life and improve safety.

THE INSTITUTE OF PAPER CHEMISTRY

Appleton, Wisconsin

Status Report

to the

ENGINEERING PROJECT ADVISORY COMMITTEE

Project 3309

FUNDAMENTALS OF CORROSION CONTROL IN PAPER MILLS

March 29, 1988

PROJECT SUMMARY FORM

DATE: March 29, 1988

PROJECT NO.: 3309 - Fundamentals of Corrosion Control in Paper Mills

PROJECT LEADER: Staff

IPC GOAL:

Increase the useful life of equipment by proper selection of construction materials and by identifying suitable process conditions.

OBJECTIVE:

To improve the life of paper machine suction rolls through corrosion and corrosion fatigue studies to establish mechanisms that limit lifetime and to identify failure preventive measures.

CURRENT FISCAL BUDGET: $150,000

SUMMARY OF RESULTS SINCE LAST REPORT: (October 1987 - February 1988)

Near threshold fatigue crack growth testing in aggressive environments has been conducted on 1N Bronze suction roll material using compact tension specimens. The test environment contained 3000 ppm Cl^- with pH 1. The test was conducted to compare the resistance of this alloy to that of the cast CA15 and duplex stainless steel materials. The crack growth rate of the 1N Bronze was significantly increased in this environment, relative to a less harsh environment, as were the crack growth rates of the duplex stainless steels. The threshold stress intensity for 1N bronze is approximately 1.5 ksi-$\sqrt{in.}$ The duplex stainless steels have threshold stress intensities of about 4 ksi-$\sqrt{in.}$ with the exception of the wrought 3RE60 material which has a threshold stress

intensity of about 1.7 ksi-$\sqrt{in.}$ Thus, the performance of the 1N bronze material is inferior to the cast duplex stainless steels in all environments tested.

Crack initiation studies via rotating bar bending tests in several different environments with pH levels above 3 have not differentiated between alloys 63 and 75, in contrast to their difference in service performance. Testing has been continued in order to determine if changes in the test environment can produce differences in the performance of these two alloys. Results of recent tests completed in Environment I (10,000 ppm Cl^-, pH 1) and Environment J (10,000 ppm Cl^-, 50 ppm S_2O_3, pH 1) again indicate a slight reduction in the 10^8 cycle fatigue strength for both alloys, but no difference between the fatigue resistance of the two alloys is evident. Although additional S-N tests remain to be done, it is clear that increasingly severe environments will have a deleterious effect on the fatigue strength, but the increased severity of the environment still fails to discriminate between alloys with vastly different service performance. None of the environments tested so far would have predicted the different service performance of these two suction roll alloys.

Exposures of ring weld coupons with high residual stresses have been made in a 10,000 ppm Cl^-, pH 3 environment to observe if stress corrosion cracking would occur. Ring weld coupons were processed in three different ways: 1) no ring weld condition, 2) ring weld applied and, 3) ring welded and stress relieved. The stress relief heat treatment was as follows; two hours at 550°C, followed by a slow cool to 425°C, followed by air cooling to room temperature. Accelerated corrosion and SCC of the weld area was observed on all welded non-stress-relieved coupons (case 2), with the exception of Alloy 63. Coupons in the as-received and ring weld stress relieved condition exhibited no accelerated or abnormal corrosion characteristics.

Metallographic studies (fractographic, microstructural, compositional) have been initiated to determine the influence of microstructure on crack propagation. Differences have been observed in the metallography of the suction roll alloys which may cause differences in service performance.

PLANS FOR NEXT PERIOD:

1. Extend near-threshold fatigue crack growth testing to include a newly developed roll material, Alloy 86. Continue near threshold fatigue testing of all current test materials using an environment which simulates the composition of the electrolyte in a pit or crevice.

2. Investigate the effect of superimposed mean stresses on the long-lifetime crack initiation resistance of suction roll alloys in simulated white waters, to simulate residual stress effects. Because of the cost of equipment for conducting these tests, they will be initiated under contract in an outside laboratory.

3. Continue the rotating bending fatigue testing and alternating testing of Alloys 63 and 75 in a simulated pit environment containing saturated amounts of ferric chloride and chromic chlorides with the pH adjusted to 1 with HCl.

4. Solicit vendor cooperation to investigate the magnitude of residual stresses present in partially machined suction rolls or rolls that have had cosmetic welding done on them.

5. Extend the investigation of crack path through the suction roll microstructures in an effort to identify those metallurgical phases which are responsible for rapid cracking and those which may be responsible for crack retardation in the materials tested in near threshold fatigue studies.

6. Investigate corrosion current transients of suction roll materials with different simulated white waters utilizing tests that permit a quantitative evaluation of the dissolution rates occurring at the crack tip.

7. Investigate the effects of notches and surface roughness on fatigue crack growth initiation behavior in suction roll alloys exposed to simulated white water environments.

SIGNIFICANCE TO THE INDUSTRY:

The near-threshold crack growth behavior of two additional classes of suction roll alloys (CA15, 1N Bronze) is consistent with their service performance records, lending additional credence to this test method as a predictor of service performance of suction rolls.

The crack initiation behavior of suction rolls, as determined by fully reversed loading S-N tests, continues to be of little value in differentiating between suction roll alloys.

Observation of SCC, which occurred in most of the alloys which had autogenous cosmetic ring weld applied and no subsequent heat treatment annealling, indicates the need for proper annealing of rolls with cosmetic welds.

THE INSTITUTE OF PAPER CHEMISTRY

Appleton, Wisconsin

Status Report

to the

ENGINEERING PROJECT ADVISORY COMMITTEE

Project 3556

FUNDAMENTALS OF KRAFT LIQUOR CORROSIVITY

March 29, 1988

PROJECT SUMMARY

DATE: March 29, 1988

PROJECT NO.: 3556 - Fundamentals of Kraft Liquor Corrosivity

PROJECT LEADER: D.C. Crowe

IPC GOAL:

Increase the useful life of equipment by proper selection of materials of construction and by identifying suitable process conditions.

OBJECTIVE:

To understand the causes of corrosion and corrosion-assisted cracking of carbon steels exposed to kraft liquor as a basis for developing methods for reducing corrosion damage in kraft process streams.

CURRENT FISCAL BUDGET: $ 75,000

SUMMARY OF RESULTS SINCE LAST REPORT: (September 1987 - March 1988)

Bench testing of modifications to the microprocessor-based corrosion monitoring system is almost complete and field testing will commence in the next period. Investigation of the effects of velocity on corrosion of carbon steel in kraft white liquor is in progress; initial results have shown dramatic increases in corrosion rate due to flow. Tests to determine stress corrosion cracking susceptibility of carbon steel in actual mill digester liquors have been completed.

INTRODUCTION

This project has comprised an extensive study of corrosion and stress corrosion cracking in kraft liquor. The effects of liquor composition have been investigated, reference electrodes have been demonstrated and corrosion rate

measurement techniques have been applied in mill studies. Current activities include development of a corrosion monitoring system, study of velocity effects, and investigation of stress corrosion cracking of carbon steel in kraft digester liquor.

CORROSION MONITORING SYSTEM

Introduction

The objective of the development of this system is to provide a reliable tool for on-line monitoring in kraft white liquor, and to demonstrate and promote its application. The microprocessor-based corrosion monitoring system has been built to measure corrosion rates via the linear polarization resistance technique, and to collect and store the data. The instrument and stored data may be monitored remotely by telephone when installed at the mill.

Progress

Some improvements and minor corrections to the software have been made during the last period. Laboratory testing has been performed to assure the reliable and accurate operation of the entire system.

Plans for Next Period

The monitoring system will be field tested for approximately a month. A report describing the system will be prepared.

VELOCITY EFFECTS

Introduction

Corrosion rates in kraft white liquor increase dramatically as the velocity of the liquor is increased. This effect is especially pronounced in piping. An improved understanding of the relationship between the corrosion rate and the velocity will assist equipment designers in sizing equipment or choosing materials to minimize

the costs of corrosion. The objective of this work is to provide data to pipe designers which relates corrosion rate to flow parameters such as velocity in pipes.

Testing of the effects of velocity conducted using pipe loops is cumbersome and slow. The rotating cylinder electrode (RCE) is an alternative which will allow systematic and relatively rapid investigation of the effects of velocity. Smaller quantities of liquor may be used compared to flow loops, providing better control of liquor conditions. Work is in progress to confirm that the RCE may be used successfully to model the flow in pipes or other geometries in kraft white liquor. Corrosion rates in a pipe loop will be compared with rates measured using a rotating cylinder electrode.

Rotating Cylinder Electrode

Introduction

The rotating cylinder electrode (RCE) permits the application of methods of hydrodynamics and mass transfer in analogy to service conditions in different geometries. The electrode geometry is useful for simulating turbulent conditions. The rotating cylinder also has the advantages of uniform current density and uniform diffusion layer thickness. The fluid mechanics of the rotating cylinder are described in the Appendix to this report. Correlation of corrosion with other geometries is also described.

Experimental Approach

1) Kinematic viscosity of simulated white liquor will be measured so that Reynolds numbers (Re) can be calculated for various rotational rates of the RCE. [Complete] These values of kinematic viscosity will be used also in the pipe loop study.

2) Corrosion rate will be determined at various potentials via weight loss tests. This will illustrate how the potential influences the corrosion rate in flowing liquor and will determine the potential at which to conduct tests. If potential is

uncontrolled, its changes will confound observed variation in corrosion rate due to velocity changes. Polarization curves at a range of rotation rates will be obtained as part of this task, to assist in selecting test potentials. [Complete]

3) Data relating corrosion rate to velocity will be collected. The corrosion rate will be related to shear stress, Re and mass transfer coefficient for the RCE and compared with relations between corrosion rate, Re, shear and mass transfer in the flow loop to determine if they are similar. If they are, the RCE may be used to study velocity effects.

4) Convert RCE corrosion rate data to pipe corrosion rate data to produce information needed by pipe designers. A variety of liquor compositions and materials would be tested.

5) Verify the validity of the polarization resistance technique in the flow situation so that it may be used for corrosion rate measurement or for on-line monitoring.

Progress

The rotating cylinder electrode apparatus is illustrated schematically in Fig.1. The working electrode is composed of a stainless steel shaft surrounded by a tightly fitting Teflon sleeve in the portion exposed to liquor. This shaft fits directly into the motor-generator to minimize vibration. The test electrode is cylindrical and is drilled and tapped on both ends. One end fits onto the bottom of the shaft, the other end has a Teflon and Delrin cap to maintain uniform flow below the working electrode. The rotation speed is controlled using a Servodyne controller. The speed was checked with a tachometer. An automatic temperature controller maintains the temperature within 2 C. A Princeton Applied Research Model 350 corrosion system was used to perform the polarization studies.

Preliminary weight loss tests were performed in 100 g/L NaOH + 30 g/L Na_2S at 1000 rpm over a range of exposure time and temperature. The results are summarized in Table 1. The corrosion potential was measured periodically during the test. It varied during the test, so that electrodes passivated at different times.

Because of these differences in the potential, the measured corrosion rates varied from test to test, confounding any effect of velocity on corrosion rate.

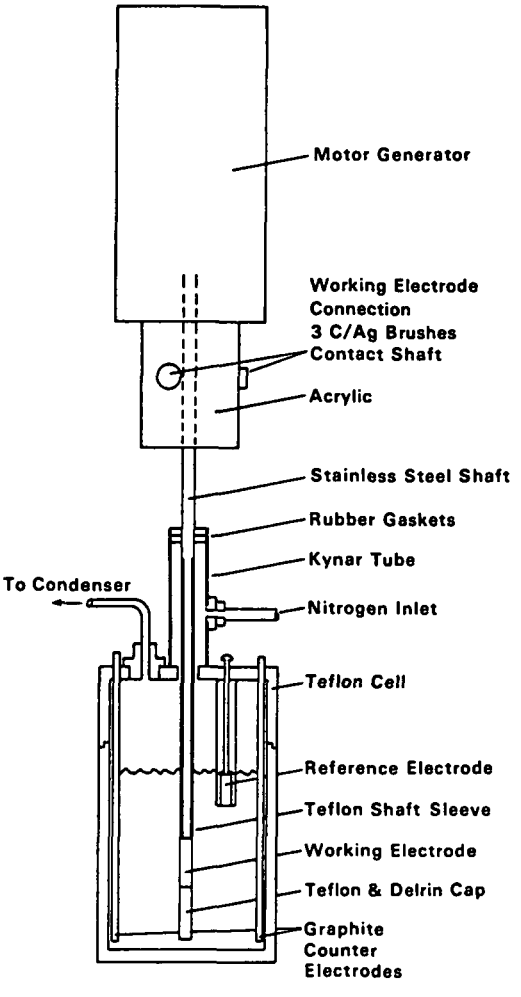

Figure 1. Schematic drawing of the rotating cylinder electrode apparatus.

The kinematic viscosity of simulated liquor at 90 C was measured for use in calculating Reynolds number, friction factor and shear stress on the rotating electrodes. The viscosity was measured using a Cannon-Fenske Routine Viscometer tube calibrated at 90 C using distilled water. The kinematic viscosity (dynamic viscosity divided by the density) was measured as 0.5256 cSt +/-1.2%. The liquor velocity at 1000 rpm is ($\omega d/2$) = 0.478 m/s so that the Reynolds number at 1000 rpm is approximately 8350 for the electrodes used in this study. The Schmidt

number, γ/D, was estimated to be 5256, assuming a diffusion constant of 10^{-6} cm^2/s. The friction factor calculated from equation 6 (in the Appendix) was 0.0105. A shear stress of approximately 1.35 N/m^2 was calculated using equation 13 (in the Appendix). These conditions will be duplicated as closely as possible in the flow loop for comparison.

Table 1

Results of Preliminary Tests

Exposure time, h	Temperature, C	Weight loss, mpy
24	60	47.8
	70	14.0
	80	44.7
	90	119.1
48	60	45.6
	70	31.9
	80	77.4
	90	65.9
72	60	94.4
	70	53.8
	80	33.5
	90	284.7

A second series of weight loss tests was conducted at 90 C and 1000 rpm with controlled potentials, and the results are shown in Table 2. These results illustrate the strong effect of potential on corrosion rates. The corrosion rate of 1786 mpy is the highest ever measured in this laboratory in white liquor.

Table 2

Corrosion Rate vs. Potential

Corrosion Potential	Corrosion rate
100 mV(SSSE)	7.8 mpy
50	30.5
0	118.0
- 50	1786.1
-100	1761.8
-150	196.4
-200	57.5
-250	23.2

The polarization behavior at a range of rotational speeds is shown in Fig. 2. The active/passive peak increased in size with rotation rate and was shifted to higher potential. Work is in progress to measure corrosion rate as a function of rotation rate at the potential where corrosion rates are highest.

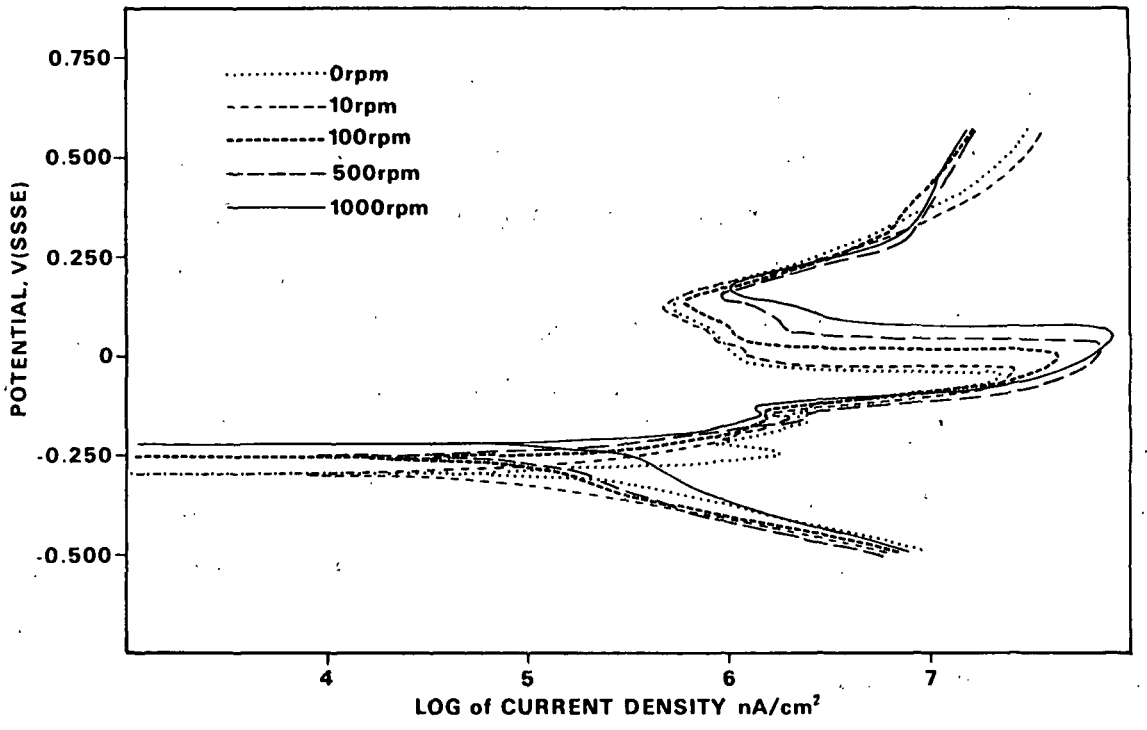

Figure 2. Polarization curves obtained for carbon steel at a range of rotational rates, 90 C, 1 mV/s scan rate.

Plans for Next Period

1) Continue with the experimental plan described above to compare the corrosion rates measured in the RCE and pipe loops. Collect corrosion rate data for various rotation rates (velocities) and liquor compositions using the RCE.

2) Perform preliminary tests with stainless steels used in white liquor pipe systems.

Flow Loop

Introduction

The flow loop will be used to reproduce flow conditions encountered in pipes in mills. It will be used in comparisons of the corrosion rate for similar hydrodynamic conditions in pipes and for the RCE.

Progress

Construction of the flow loop has been completed. It has a heated liquor storage tank, a pump, flow detector, piping and probes. The finished set up is illustrated in Fig. 3. Figure 4 shows a close up view of the test section with four steel pipe sections separated from each other, and from the inlet and outlet sections by Teflon spacers. These are shown disassembled in Fig. 5. The central teflon spacer has a silver reference electrode inserted into it for making measurements of the corrosion potential. The inlet and outlet sections of the pipe may be used as the counter electrodes. This assembly is tightened together using the threaded tie rods. The inside of the pipe sections are machined to match the Teflon spacers and so maintain undisturbed flow past the test sections.

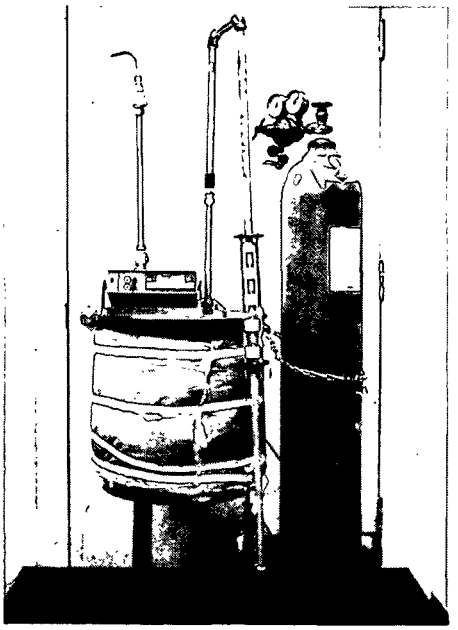

Figure 3. Construction of the flow loop has been completed.

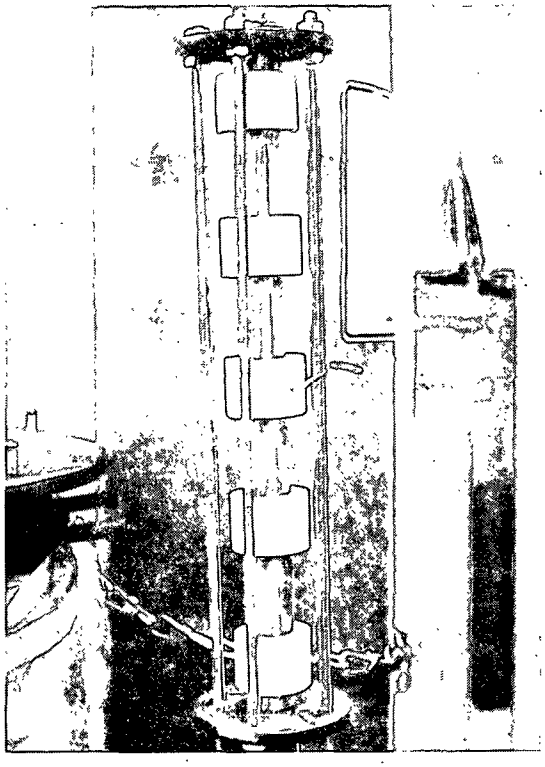

Figure 4. The test section showing the test pieces and the Teflon spacers.

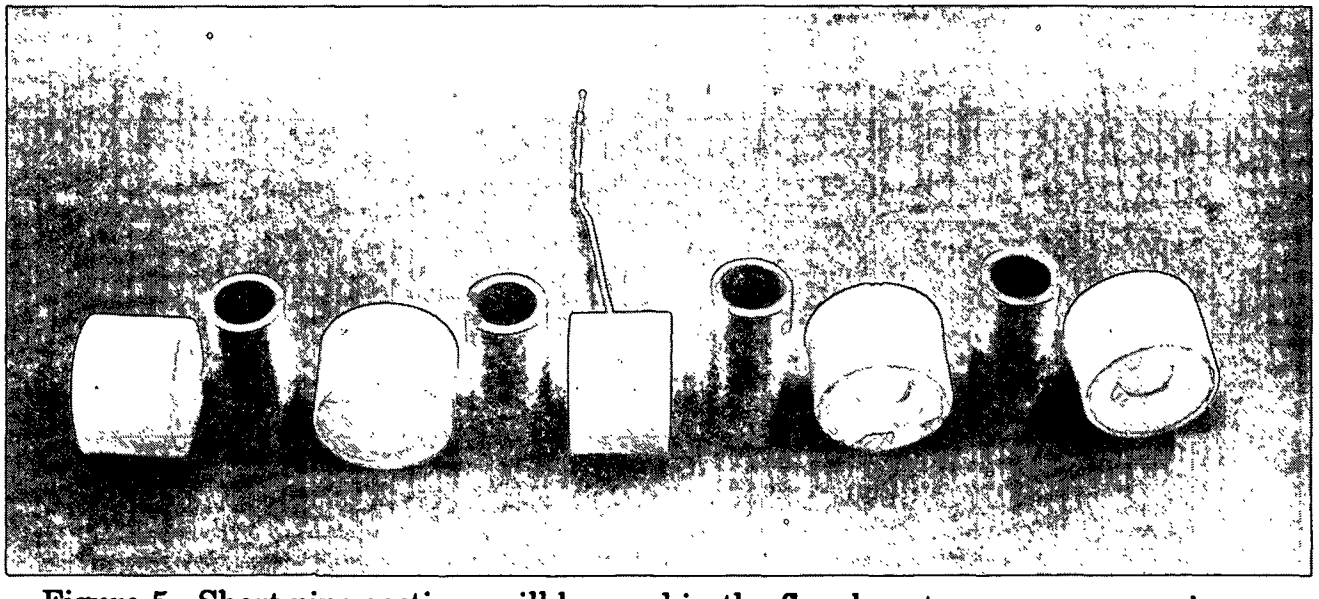

Figure 5. Short pipe sections will be used in the flow loop to measure corrosion rates by weight loss.

Plans for Next Period

1. Weight loss tests will be performed in the flow loop at a range of flow rates and correlated with Re, shear and mass transfer for comparison with the RCE.

2. Polarization curves obtained in the flow loop at a range of flow rates will be compared with curves obtained on the rotating cylinder electrode.

STRESS CORROSION CRACKING OF CARBON STEEL IN ACTUAL DIGESTER LIQUORS

Introduction

The extent of stress corrosion cracking in kraft continuous digesters is observed to vary from vessel to vessel, but the reasons for this variation are unknown. Slow strain rate tests of A516 Gr. 70 digester steel have been performed in real mill liquors to determine susceptibility to stress corrosion cracking for comparison purposes. Additional tests were performed in simulated liquors with the same major inorganic species as in the mill liquors to determine whether the behavior could be attributed to these species alone.

Progress

Previous reports have outlined progress on investigation of stress corrosion susceptibility in mill liquors. Liquor samples were obtained from top separator/ top circulation lines of four Kamyr continuous digesters. Slow strain rate tests have been completed in the liquor from these mills plus simulated liquors with the same concentrations of inorganic constituents as the mill E9 and mill P6 liquors. The objective of testing with this simulated liquor was to determine whether the major inorganic species control stress corrosion susceptibility, or whether organic species and trace inorganics have a significant effect. Liquor analyses are summarized in Table 3.

Table 3

DIGESTER LIQUOR COMPOSITION

	Mill M5	Mill P6	Mill E9	Mill H10
NaOH, g/L	14.1	39.5	50.7	25.4
Na_2S, g/L	11.1	18.9	21.6	14.5
Na_2CO_3, g/L	30.7	16.6	26.6	17.3
$Na_2S_2O_3$, g/L	2.5	2.5	6.8	2.8
Na_2SO_3, g/L	1.3	2.6	4.8	1.5
Na_2SO_4, g/L	3.4	2.2	7.7	3.3
NaCl, g/L	1.2	1.5	0.5	0.4
Na_2S_x, g/L	0.7	0.2	-	0.6

Data from slow strain rate tests in mill liquors and the simulated liquors are plotted in Fig. 6 - 11. Cracking susceptibility is measured by the percent reduction in diameter of the test specimen. If a specimen does not experience stress corrosion cracking (SCC), it will elongate, neck and finally fail in a ductile mode. The % reduction in its diameter will be large. On the other hand, if cracking occurs during the test, the specimen will fail early in the test at a primary crack in its surface. The fracture surface will be brittle and many secondary cracks will be present. The specimen will not have necked down, so its diameter will be closer to the original, that is the % reduction in diameter will be a low value. Thus the percent reduction in diameter will provide a measure of susceptibility to SCC. The number of cracks in the failed specimens will also provide a measure of SCC susceptibility.

The polarization curves differed in shape in the various mill liquors. In mill M5 and H10 liquors low current peaks were observed, as would be expected for relatively weak liquors. Curves for steel in liquor from mills P6 and E9 had large active/passive peaks typically found in stronger liquors. The peak was smaller in the simulated E9 liquor, indicating some difference between the real and simulated liquors. The polarization curve in the simulated P6 liquor was similar in shape and size to the real liquor.

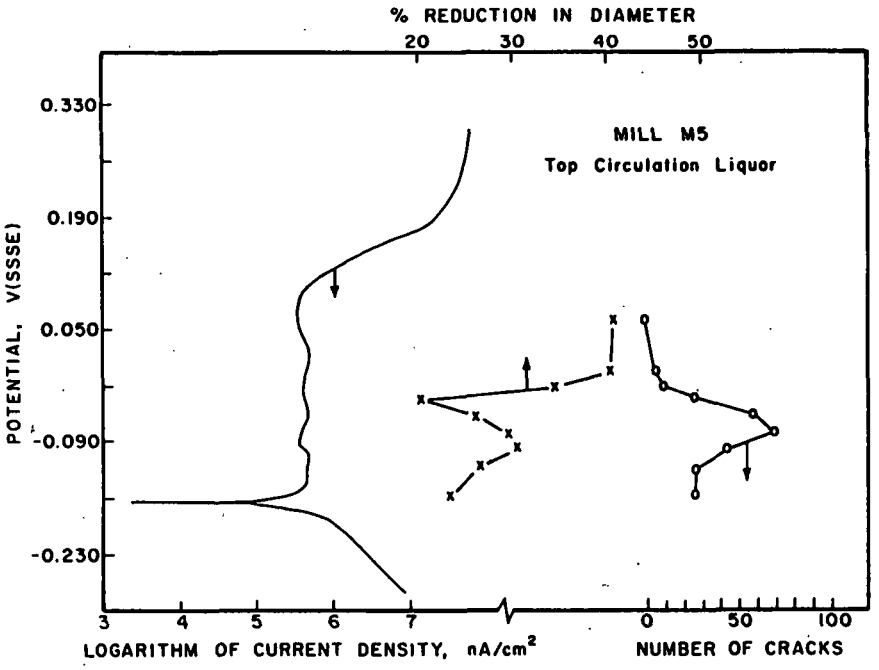

Figure 6. Polarization curve and percent reduction in diameter of stress cracks in test samples as a function of potential for mild steel in mill M5 liquor, illustrating the susceptibility to stress corrosion in the active/ passive range.

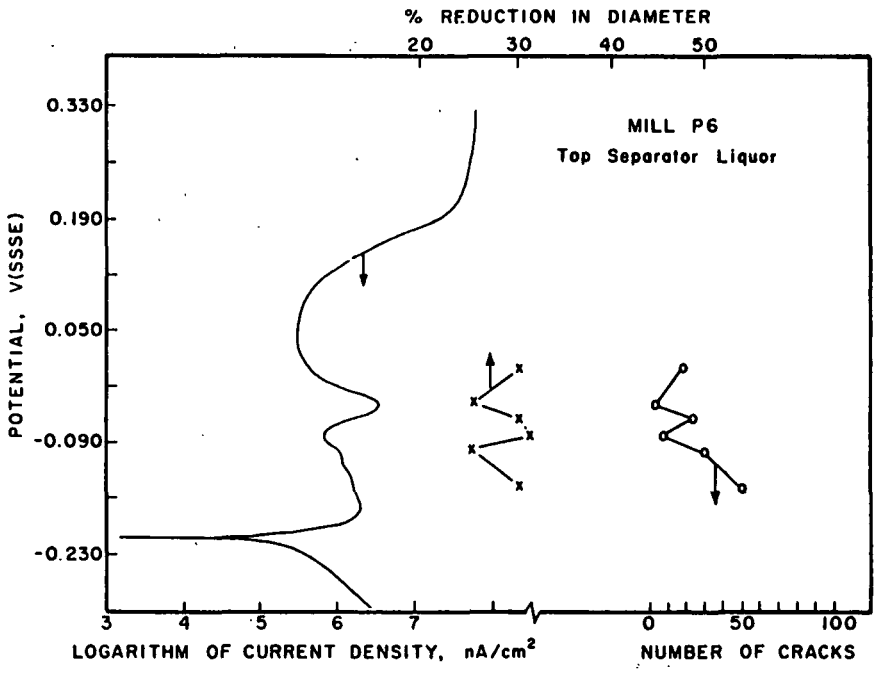

Figure 7. Polarization curve, percent reduction in diameter and number of cracks in test samples as a function of potential for mild steel in mill P6 liquor.

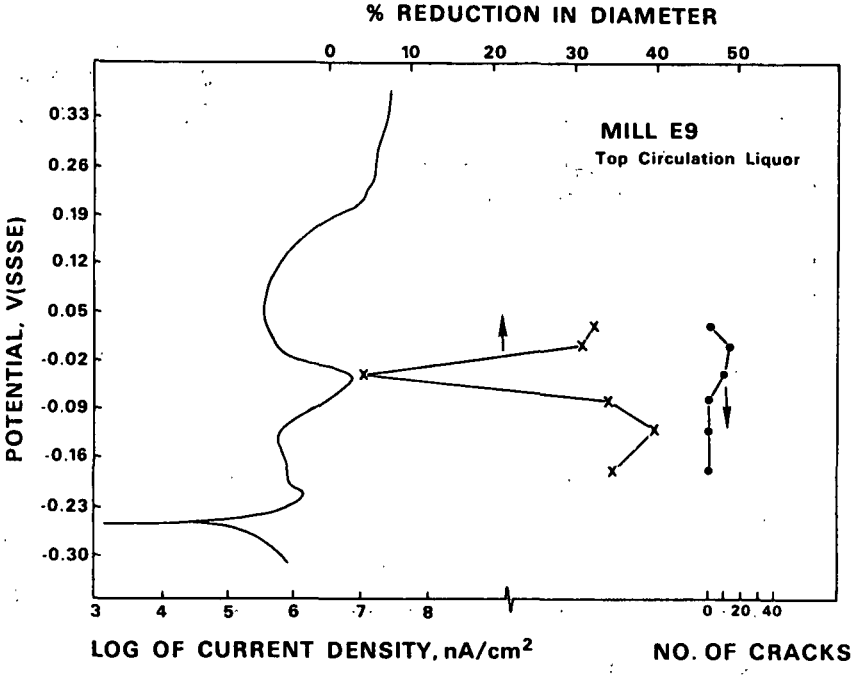

Figure 8. Polarization curve, percent reduction in diameter and number of cracks in test samples as a function of potential for mild steel in mill E9 liquor.

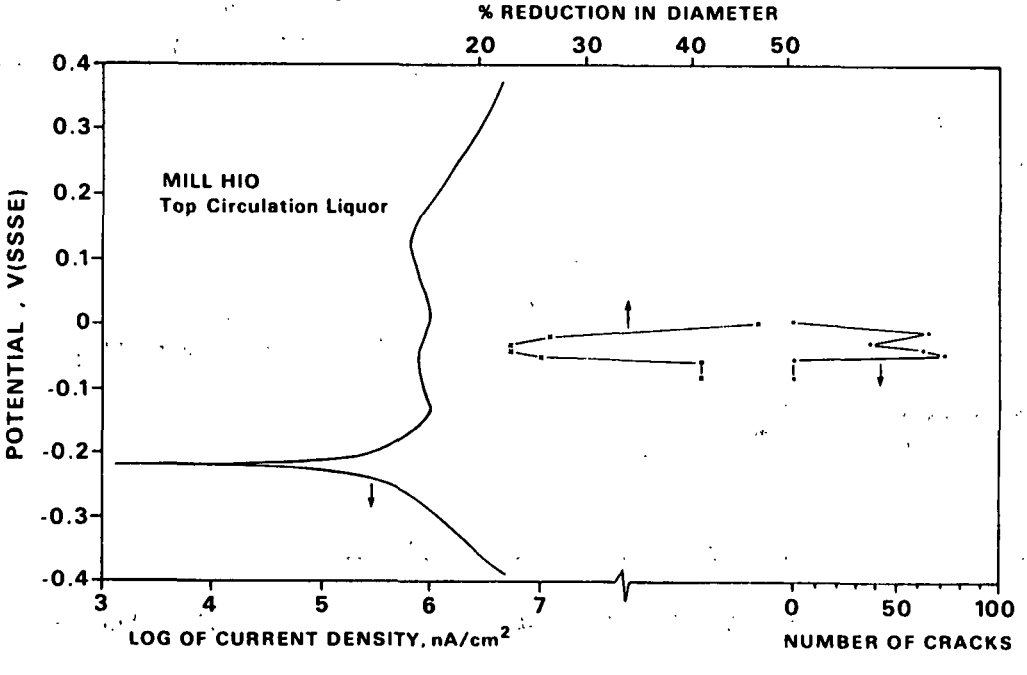

Figure 9. Polarization curve, percent reduction in diameter and number of cracks in test samples as a function of potential for mild steel in mill H10 liquor.

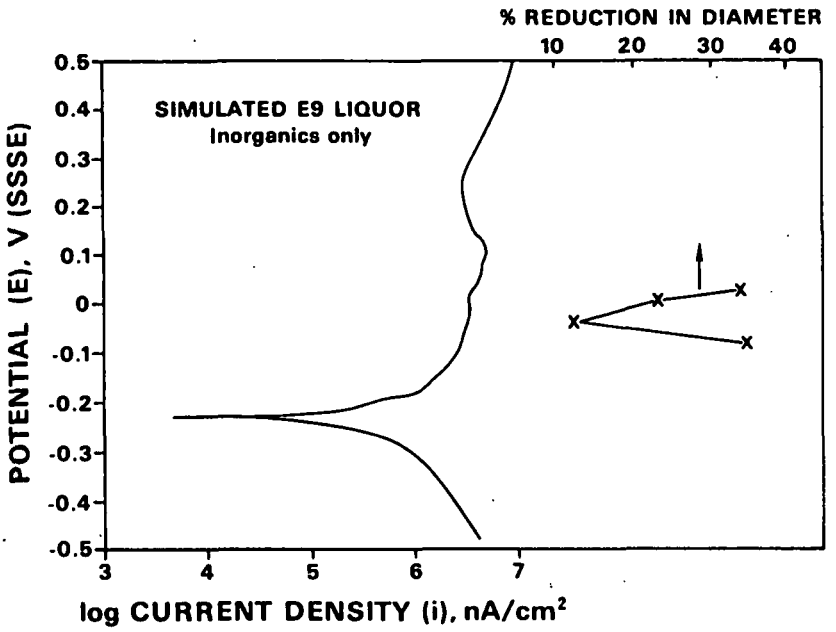

Figure 10. Polarization curve, percent reduction in diameter in test samples in simulated E9 liquor containing the major inorganic species of the E9 liquor.

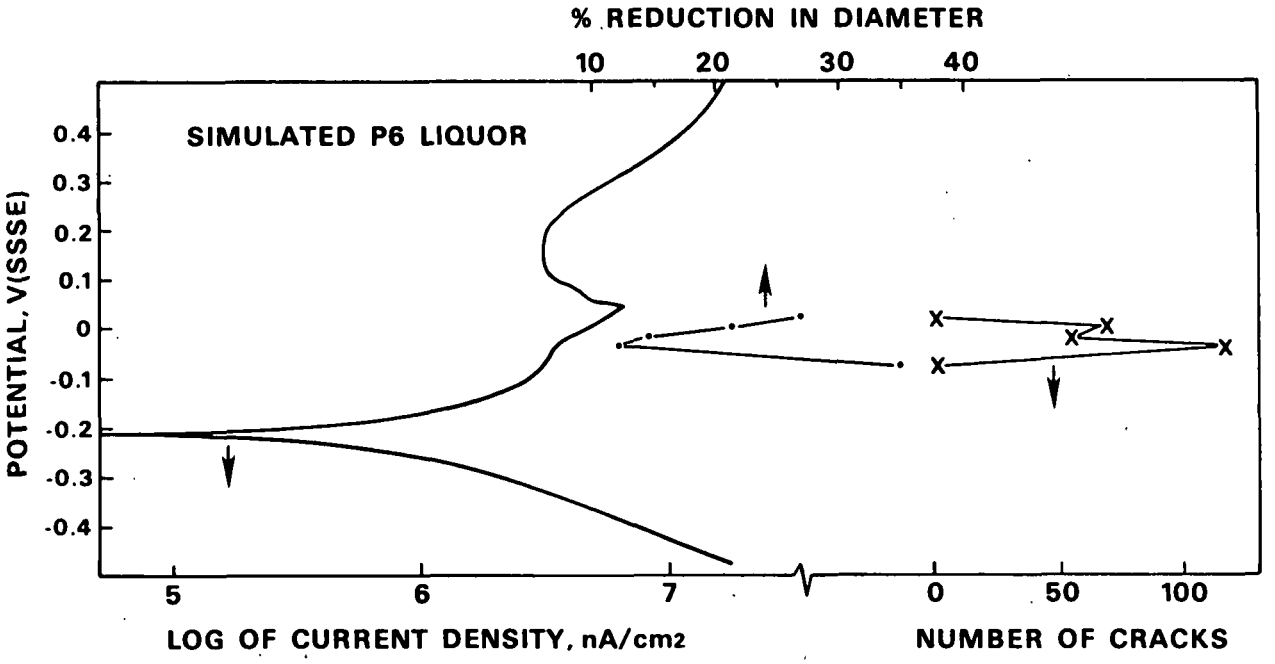

Figure 11. Polarization curve, percent reduction in diameter and number of cracks in test samples in simulated P6 liquor containing the major inorganic species of the P6 liquor.

The number of cracks in failed specimens, and the % reduction in diameter were used to indicate the zone of SCC. In mill M5 liquor, a large numbers of cracks in the specimens were associated with the SCC range, as measured by % reduction in diameter, Fig. 6. In mill P6 liquor, fewer cracks were observed at potentials where the % reduction in diameter indicated SCC susceptibility. The cracking zone measured at mill H10 was very disctinct, spanning -20 to -55 mV, with the % reduction in diameter and number of cracks in good agreement. The range and severity of cracking were similar at mill M5 which had relatively similar liquor composition. Simulated P6 liquor caused more severe cracking than the real mill liquor. The number of cracks was low in real mill E9 liquor, Fig. 8. However, innumerable cracks were observed on the samples in the simulated E9 liquor, suggesting that organics in the real liquor may have inhibited crack initiation. The other simulated liquor, P6, caused fewer cracks than simulated E9 liquor. That liquor had less thiosulfate, carbonate and hydroxide.

The range for cracking varied from mill to mill. For mill M5 liquor, cracking occurred in the range from +10 to -100 mV(SSSE). For mill P6 liquor, cracking was not severe, as judged by relatively high % reduction in diameter measurements but the range was wide; cracking was most severe at -40 mV(SSSE) with cracking at potentials below 20 mV(SSSE). In mill E9 liquor, the cracking range spanned +20 to -40 mV(SSSE) and was severe as measured by % reduction in diameter. A similar range was observed with the simulated E9 liquor. The lack of organics in the simulated E9 liquor did not appear to have a strong influence on the range for stress corrosion. This suggests that the major inorganic species determine the range for cracking, but not necessarily the severity. The differences between mills may be related to different concentrations of inorganic species mainly NaOH and Na_2S. The Na_2S concentration was high at mill P6, but the NaOH and $Na_2S_2O_3$ were lower, which may have reduced SCC. At mill H10, the cracking zone was from +20 to -80 mV, very similar to mill M5. In these weaker liquors at mills M5 and H10, the cracking zone was wider. The E9 liquor had a high thiosulfate concentration which may have caused severe SCC. The cracking zone correlates

with the active/passive peak of the polarization curve. This peak was in the region of 0 mV(SSSE). The variation in cracking zone appears to be related to the liquor composition through its effect on the polarization curve.

Conclusion

This concludes work investigating stress corrosion cracking of kraft liquor. Differences in kraft liquor compositions in real mill liquors have been shown to affect the susceptibility to SCC considerably. It appears that the organics or trace inorganics in real liquor are beneficial; they reduce the severity of SCC. Liquors with higher NaOH, Na_2S and $Na_2S_2O_3$ concentration increase SCC susceptibility and narrow the cracking range.

SIGNIFICANCE TO THE INDUSTRY

Modern corrosion measurement techniques and equipment have been developed and demonstrated for use in kraft liquor systems. Some operating parameters which increase corrosion rates have been identified. The effects of major liquor constituents on corrosivity of white liquors have been determined.

APPENDIX - Fluid Mechanics of the Rotating Cylinder Electrode

There are three regimes of flow on the rotating electrode: laminar, vortex, and turbulent. The hydrodynamics in each regime is described below. Correlations with other geometries, and application to corrosion studies are described also.

Laminar Regime

For the rotating cylinder, the critical Reynolds number, Re_{crit}, is about 200, that is, below the critical Reynolds number, the flow is laminar. In the laminar region there is very little mass transfer. Flow within storage tanks or clarifiers would be laminar. For the rotating electrode, the flow is laminar at < ~10 rpm. According to Gabe (4), Cornet and Kappesser found that in the range $5 < Re < 200$, for a Schmidt number equal to 460, the Sherwood number was 37. This suggested that the fluid was rotating with the inner cylinder and not contributing to mass transfer, thus resulting in a constant Sherwood number. Gabe (4) documented other mass transport equations for the laminar region.

[Note. The Reynolds number, $Re = Vd/\gamma$ where V is the peripheral velocity (m/s), d is the specific diameter (m), and γ is the kinematic viscosity (m^2/s). Re is essentially the ratio of velocity and viscous forces. The Schmidt number, $Sc = \gamma/D$ where D is the diffusivity (cm^2/s). The higher the Schmidt number, the thinner the diffusion layer. The Sherwood number, $Sh = kd/D$ where k is the mass transfer coefficient. The Sherwood number is a dimensionless mass transfer coefficient.]

Vortex Regime

Taylor vortices develop above a critical Taylor number, Ta. The flow is laminar but the vortices give superimposed radial and axial motion. Gabe (4) noted that others had found that instability occurs when:

$$Ta = 29.3, \text{ where } Ta = Re\,((R_2 - d)/(R_2 + d))^{0.5} \quad (1)$$

and where R_2 is the cell diameter and d is the rotating cylinder diameter. For Ta > 400, true turbulent flow develops.

Turbulent Regime

The Reynolds, Schmidt and Sherwood numbers can be related in the turbulent regime.

For a smooth cylinder:

According to Eisenberg, Tobias and Wilke (3),

$$Sh = 0.079\,Re^{0.7}\,Sc^{0.356} \qquad (2)$$

This means that the mass transfer coefficient, k, may be related to the velocity and the rates of diffusion of corrosion reaction products and reactants. The mass transfer coefficient is related to the limiting current density via:

$$i_L = knFC \qquad (3)$$

where i_L is the limiting corrosion current, n is the number of electrons, F is Faraday's number and C is the bulk concentration. Combining equations 2 and 3 and rearranging:

$$i_L = 0.0791\,zFCV^{0.7}(d/\gamma)^{-0.3}(\gamma/D)^{-0.644} \qquad (4)$$

This can also be expressed as:

$$(k_L/V)\,Sc^{0.644} = 0.0791\,Re^{-0.3} \qquad (5)$$

where k_L is the mass transfer coefficient at the limiting current density, that is, the reaction is diffusion controlled. This relation was confirmed by plotting the logarithm of both sides, at limiting current for a known reaction on a rotating electrode (3). Thus mass transfer rates may be predicted based on the velocity and other physical properties.

Friction factor on the rotating electrode may also be predicted using the Reynolds number (3). In the turbulent regime, $10^3 < Re < 10^5$,

$$f/2 \sim 0.079\,Re^{-0.3} \qquad (6)$$

For a rough cylinder, the relationship between the non-dimensional constants is different:

On rough cylinders, the friction factor will be slightly different, as affected by the surface. Kappesser et al. (2) quoted work by Makrides and Hackerman estimating that above Re_{crit}, where the friction factor, f, is independent of angular velocity.

$$f/2 = (1.25 + 5.76 \log d/\varepsilon)^{-2} \quad (7)$$

where ε is the characteristic roughness dimension and d is the cylinder diameter. Thus a roughness factor is incorporated into the friction factor. For a smooth rotating cylinder and $600 < Re < 250{,}000$ they found that for both rough and smooth cylinders:

$$Sh = (f/2)\, Re\, Sc^{0.356} \quad (8)$$

which may be obtained from equations 2 and 5.

The shear stress is given by:

$$\tau = \eta\, (dV/dy) \quad (9)$$

where y is the distance from the surface and η is the viscosity. According to Silverman (10), the shear stress in the fluid at the surface of the RCE is given by:

$$\tau = (f/2)\, \rho\, \omega^2\, r^2 \quad (10)$$

where r is the RCE radius.

Correlations with Other Geometries

Historically, investigators have related corrosion in two geometries (e.g. pipe and cylinder) by equating the mass transfer rates. The pipe velocity is then expressed in terms of the corresponding rotation rate of the rotating electrode. This assumes there is a direct quantitative relationship between the mass transfer rates and the corresponding product of Re and Sc.

Wranglen et al. (5) equated equation 4 with a similar expression for tubes to get, for turbulent conditions:

$$\log Re_{tube} = 0.67 + 0.833 \log Re_{cyl} \quad (11)$$

They claimed that, using this, experimental results for the rotating electrode could be recalculated to apply to tube flow.

Equation 2 was used by Ellison and Schmeal (9) for carbon steel corrosion of rotating cylinders in H_2SO_4. They used the Harriot-Hamilton equation:

$$Sh = 0.0096\, Re^{0.913}\, Sc^{0.346} \qquad (12)$$

for pipes, for a range of mass transfer coefficients used for the rotating electrode. Their model of the corrosion reaction assumed mass transfer to be controlling, and their results supported that assumption for both rotating electrode and pipes, so that they thought the corrosion rates measured in one geometry could be applied in other geometries with the same mass transfer coefficient.

Silverman (10) has criticized this approach of directly equating the mass transfer relations in two geometries because velocity profiles and the friction factor dependencies on Re are different in the two geometries. Furthermore, equating mass transfer is invalid if the fluid velocity effect is caused by erosion rather than convective mass transfer. Instead, he suggests that the shear forces must be equivalent in the two geometries to predict behavior. For the rotating cylinder:

$$\tau_{cyl} = (f/2)\, \rho\, \omega^2\, r^2 = 0.079\, Re^{-0.3}\, \rho\, \omega^2\, r^2 \qquad (13)$$

where ω is the rotation rate and ρ is the density. A similar expression is available for pipes.

$$\tau = (0.079/2)\, Re^{-0.25}\, r\, V^2 \qquad (14)$$

Using the Harriot-Hamilton relation, equation 12, to estimate mass transfer and

$$C.R. = Sh\, (C_w - C_b)\, (D/d) \qquad (15)$$

where C.R. is the corrosion rate, he predicted corrosion rates in pipe at a given shear stress. A similar approach is proposed for our study in white liquor.

Application to Corrosion Studies

Corrosion processes are not always diffusion controlled. Furthermore, anodic and cathodic reactions may occur, often on separate areas. Thus, corrosion rate is not proportional to mass transfer or other hydrodynamic parameter. The situation must be appraised for each system being studied. Erosion of the surface film may be another problem.

Ellison and Wen (1) noted that mass transfer corrosion may be distinguished from corrosion erosion. With direct erosion, metal loss rate varies as velocity to the 2nd to 6th power. With convective mass transfer, the corrosion rate varies as velocity to the nth power where n is always less than 1.5. Furthermore for erosion corrosion, an induction period exists. An investigation of similar relationships may determine the importance of spalling to corrosion in white liquor.

Efird (7) plotted τ vs. velocity. Then he determined critical velocity for breakaway corrosion on Cu/Ni alloys in seawater and from the plots he obtained a critical shear stress (N/m^2). [Determination of a critical shear stress for spalling in white liquor should be of value to equipment engineers.]

Mahato et al. (8) were concerned that buildup of corrosion products would significantly affect mass transfer in steel pipe. In their work, the mass transfer coefficient in the turbulence layer controlled the overall mass transfer process. Overall, mass transfer was almost independent of Re for long exposures.

Silverman chose a rotation rate to obtain the τ anticipated in a pipe. Using equation 2 for the RCE, and comparing with a time averaged Sherwood number calculated from weight loss data:

$$Sh = (\Delta w / M\ t)\ (1/A)\ (1/(C_{wall}-C_{bulk})\ (d/D) \qquad (16)$$

where Δw is weight loss, M is molecular weight, t is time, A is area, C is the concentration of diffusing species, d is the diameter of the cylinder and D is the diffusivity. From equations 2 and 16, he obtained two similar values for mass transfer coefficient, k. Kinematic viscosity was obtained from tables, D was assumed. He then used his calculated k values to predict corrosion rates in pipes, which unfortunately he did not confirm.

Cameron and Chiu (11) have used the RCE to study inhibitors for use in pipelines; they equated shear stresses in the two geometries.

Silverman and Zerr (12) used a RCE to investigate use of Alloy 26-1 in concentrated H_2SO_4. They concluded that practical and rapid velocity testing is possible using the polarization scans generated with the rotating cylinder electrode.

The use of the RCE and comparison with pipe flow and annular pipe flow has been studied by Chen et al. (15) The polarization resistance technique was also evaluated for use with the RCE, and was found to be accurate and reliable.

Guanti and Hack (13) used the RCE to model in the laboratory the flow conditions in service on a cathodically polarized surface or on anodically polarized zinc, relevant to flow on the hull of a ship.

Kalishek (14) determined that mass transfer to the rotating cylinder electrode surface was rate controlling in kraft white liquor.

Conclusion

The rotating cylinder electrode testing technique is based on well established hydrodynamic theory and has been demonstrated to be useful for study of flow effects on corrosion. Its relevance in kraft white liquor should be confirmed by performing parallel tests with a flow loop at similar conditions. Then the method may be used with confidence to systematically investigate velocity effects.

References

1. B.T.Ellison and C.J.Wen, Lectures in Electrochemical Eng, AIChE Symposium Series, 77(204) 161-169.
2. R.Kappesser, I.Cornet, R.Greif, J.Electrochem.Soc. 118: 1957-1959 (1971).
3. M.Eisenberg, C.W.Tobias and C.R.Wilke, J.Electrochem.Soc. 101: 306-319 (1954).
4. D.R.Gabe, J.Appl.Electrochem. 4: 91-108 (1974).

5. G.Wranglen, J.Berendson and G.Karlberg, p.461-473 in Physiochemical Hydrodynamics, ed. B.Spalding, Advance Publishers, London (1977).

7. K.D.Efird, Corrosion 33: 3-8 (1977).

8. B.K.Mahato, C.Y.Cha and L.W.Shemilt, Cor.Sci. 20: 421-441 (1980).

9. B.T.Ellison and W.R.Schmeal, J.Electrochem.Soc. 125(4): 524-531 (1978).

10. D.C.Silverman, Corrosion 40 (5): 220-226 (1984).

11. G.R.Cameron and A.S.Chiu, Paper 86, Corrosion 85, NACE, Houston (1985).

12. D.C.Silverman and M.E.Zerr, Corrosion 42(11): 633-640 (1986).

13. R.J.Guanti and H.P.Hack, Paper 267, Corrosion 87, NACE, Houston (1987).

14. R.Kalishek, M.Sc. A190 Report, Institute of Paper Chemistry, Appleton, 1987.

15. T.-Y. Chen, A.Moccari and D.D.Macdonald, MTI Publication No. 23, Project 15, RF Project No. 712720, Materials Technology Institute, Columbus, Ohio, May 15, 1986.

THE INSTITUTE OF PAPER CHEMISTRY

Appleton, Wisconsin

Status Report

to the

ENGINEERING PROJECT ADVISORY COMMITTEE

Project 3470

FUNDAMENTALS OF DRYING

March 29, 1988

PROJECT SUMMARY FORM

DATE: February 10, 1988

PROJECT NO.: 3470 - Fundamentals of Drying

PROJECT LEADER: Clyde Sprague

IPC GOAL:

Reduction of the "necessary minimum" complexity in number and/or sophistication of process steps.

OBJECTIVE:

To develop an understanding and a database sufficient for the commercialization of advanced water removal systems, based on high-intensity drying principles. This new technology will reduce capital costs, increase machine productivity, reduce the amount of energy used, and improve paper properties.

CURRENT FISCAL BUDGET:

$150,000 from Institute funds, plus $350,000 through a Department of Energy grant (as Project 3595). This grant is for a total amount of $1.5 million over four years; 1988 is the third grant year for the project.

The Fourdrinier Kraft Board Group has funded part of the work on linerboard and medium issues in impulse drying with grants for $30,000 in 1987 and $100,000 in 1988.

SUMMARY OF RESULTS SINCE LAST REPORT: (October '87 - February '88)

Project 3470 has continued to emphasize research on impulse drying, with the objective of gathering data to support development of the process to the point of commercialization. Impulse drying may be defined as drying a wet sheet under short time, high pressure and high temperature conditions.

Previous work on the project has demonstrated that impulse drying produces very high drying rates at low drying energy requirements, offering the potential for smaller dryer sections and improved energy use. Furthermore, impulse drying en-

hances a wide variety of paper properties, with the potential for improved products, better property control, and the substitution of lower cost furnishes at equal product strength.

An Annual Report for the project, covering the period between September, 1986 and November, 1987 has been completed and should be available by the end of March, 1988. This report contains a summary of previous work on property development, plus recent work on the mechanisms of impulse drying and early results from the pilot roll impulse dryer.

The major project activity over the past six months has been the design and equipment procurement for a second nip for the pilot roll impulse dryer. The second nip will be very similar to the first, but in a reversed position to treat the opposite side of the sheet. The second nip will allow the Institute to evaluate the effects of impulse drying alternate sides of the sheet on two-sidedness of newsprint and fine papers webs. The general arrangement of the second nip is illustrated in Figure 1.

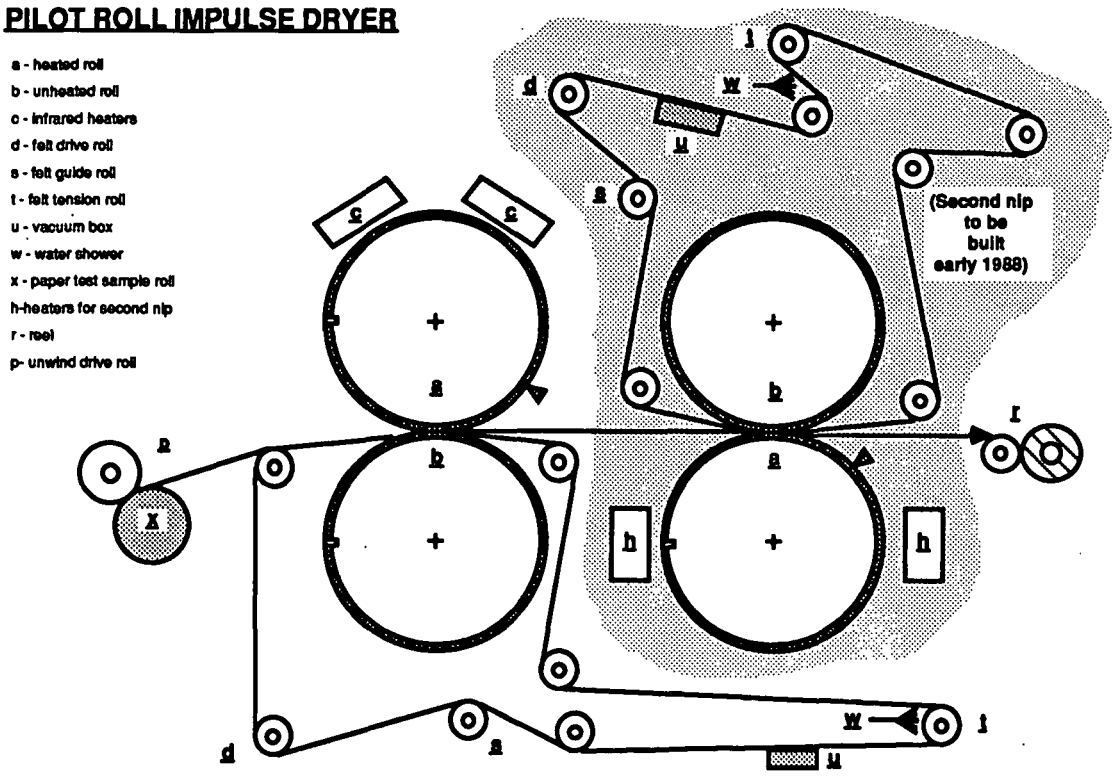

Figure 1. Final design of the pilot roll impulse dryer, showing the configuration of the second nip which will be built during 1988.

Most design details of the second nip are similar to those of the first nip, which were discussed with the PAC in previous meetings. However, the second nip will be heated using an electrical induction heating system manufactured by Inductoheat and provided to the Institute as a partial donation. This system will allow the heat supply to the hot roll to be controlled in much narrower bands than is possible with the infrared heaters used on the first nip. We will be able to selectively heat portions of the roll surface as narrow as three inches wide. These fine adjustments will allow us to investigate the potential of impulse drying to remove wet streaks from wet paper webs.

The design and construction of the second nip are proceeding on schedule, with startup anticipated in time for the Executives' Conference meeting in May, 1988.

Most of the experimental time on the project recently has been consumed by contract research, particularly by activities on the major Fourdrinier Kraft Board Group study of the effects of impulse drying on the convertability of linerboard and medium. The detailed results of this program cannot be reported here. However, the effects of impulse drying were found to be generally positive on the conversion process to combined board.

The limited project-funded experimentation recently has been concerned withdeveloping a better understanding of delamination phenomena, which may represent the principal obstacle to the commercial development of impulse drying. The phenomenon of delamination during intense impulse drying of moderate to heavy basis weight sheets was reported in earlier work at the Institute of Paper Chemistry. Burton (1) observed delamination in an unbleached softwood kraft pulp beaten to 550 ml CSF at basis weights of 100 grams per square meter and heavier. Lower basis weight sheets (40 to 50 grams per square meter) of this furnish did not exhibit blistering or delamination. These observations are consistent with the probable mechanisms of impulse drying. Very thick or highly refined sheets will exhibit greater resistance to the flow of vapor and liquid than thin or coarse webs. If the flow resistance of the web becomes so large that the high pressure steam produced during impulse drying cannot dissipate before the mechanical restraint on the sheet is relieved, the sheet may not be strong enough to sustain the pressurized vapor. Blistering or delamination may then result.

More recent project work (2) indicated that several commercially important grades, including southern pine linerboard, lightweight coating rawstock, writing papers and newsprint showed excellent resistance to delamination. None of these materials delaminated at commercially useful temperatures (below 700°F), although delamination could be produced in all of these furnishes if severe enough conditions were applied. The sheets used for this study were all produced from realistic furnish samples obtained from commercial mills, and so should reasonably predict performance of these materials in practice. It is probable, however, that commercially important furnishes exist which are more susceptible to delamination than those previously studied. At present, there is no way to predict the delamination potential of a furnish without impulse drying actual samples of the material.

An improved understanding of delamination will be essential so that the impulse drying process can accommodate as many furnish types and as wide a range of impulse drying conditions as possible. Work on the mechanisms of delamination is currently underway in three Master's research problems at the Institute, supported by increased emphasis on delamination in the funded research work.

The work on delamination to date involved a limited study to determine whether increasing the flow resistance of southern pine kraft linerboard by refining would produce delamination and, if so, how much refining would be required to induce the problem. A secondary objective of the study was to determine which laboratory test would best detect the onset of delamination, as visual examination is not always reliable as small blisters can heal during subsequent drying. Some preliminary results were presented at the October 1987 PAC meeting; the completed results will be reviewed below.

For this experiment, a sample of the southern pine unbleached kraft pulp used in earlier work on this project was refined in a Valley beater. Samples were extracted over time to achieve a series of samples separated by 50 ml intervals in Canadian Standard Freeness. The pulp samples were then made up at 200 grams per square meter basis weight, pre-pressed to 35% solids, and impulse dried without preheating at 700°F and 400 psi peak pressure for 30 milliseconds. Delamination was noted visually below 600 ml CSF, and later confirmed by z-direction tensile strength tests.

The increasing flow resistance of the web with refining is suggested by Figure 2. Previous work was done at a refining level of 650 ml CSF, at which impulse drying under these conditions would produce a final sheet solids of about 41% solids. Reducing refining towards 750 ml CSF improves the final solids level by about three percentage points; increasing refining towards 350 ml CSF produces only a minor reduction in water removal. Sheets of this furnish produced from 650 ml CSF pulp do not delaminate, but a 50 ml decrease in freeness will produce delamination. The change in final solids level between these refining levels is minimal. The problem is therefore probably not produced by flow resistance alone, but may also involve changes in the amount of heat released to the sheet. Changing the sheet pore structure and pore size distributions by refining might influence both the boiling and water resupply mechanisms of impulse drying, resulting in increased steam production. This question requires further study in the coming year.

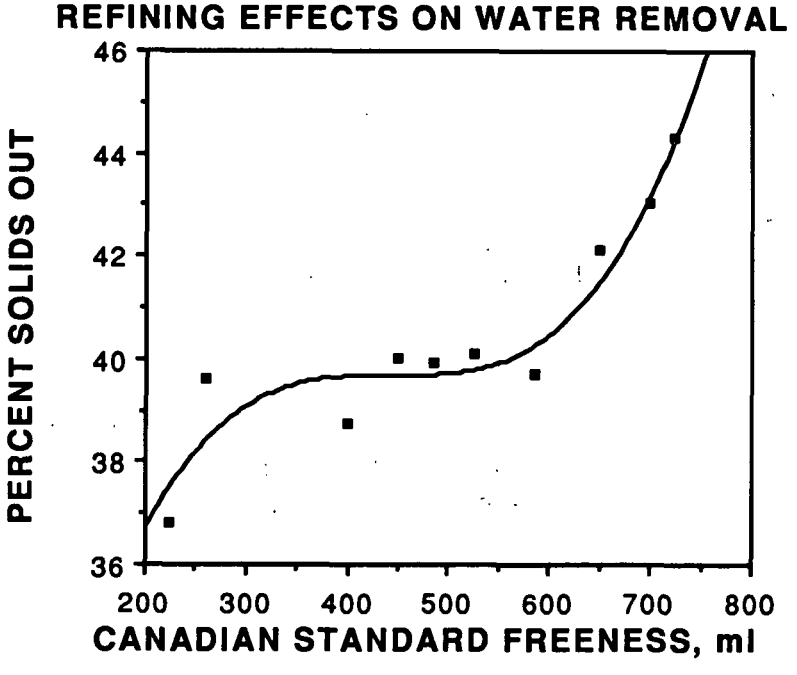

Figure 2. Water removal observed during a web delamination study on 200 gram per square meter linerboard initially at 35% solids. All impulse drying was done at 700°F, 400 psi peak pressure and 30 milliseconds. Delamination was observed for all samples refined below 600 ml CSF.

The effects of delamination on internal bond strength or z-direction tensile strength is shown in Figure 3. Internal bonding improves with refining down to 600 ml CSF, after which delamination begins to reduce bonding. Impulse drying increases internal bonding by almost 20 percent when compared with a pressed and conventionally dried sample at 650 ml CSF, which suggests that no "incipient" delamination was underway at that condition.

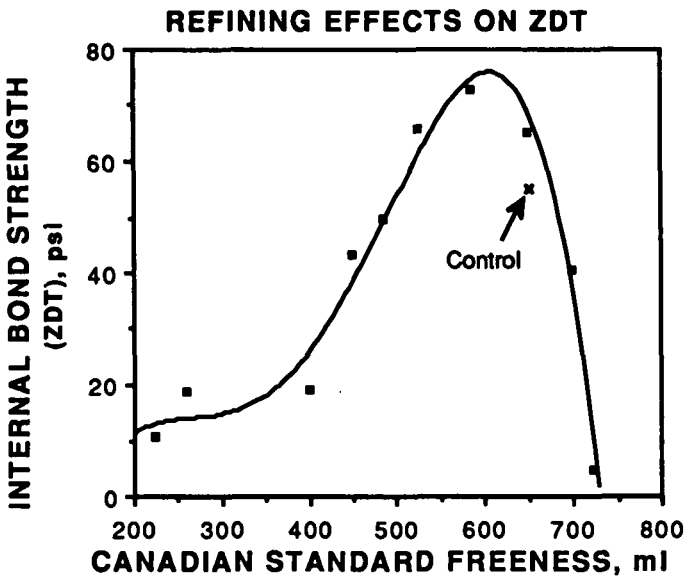

Figure 3. Internal bond strength measurements indicating web delamination in 200 gram per square meter linerboard initially at 35% solids. All impulse drying was done at 700°F, 400 psi peak pressure and 30 milliseconds. Delamination was observed for all samples refined below 600 ml CSF.

Apparent density (Figure 4) followed similar trends, but does not give as clear a picture of the onset of delamination as the internal bond strength test. The density data would suggest that no loss in average density occurred down to 550 ml CSF, well below the actual delamination limit. Density changes are thus not an adequate diagnostic for delamination.

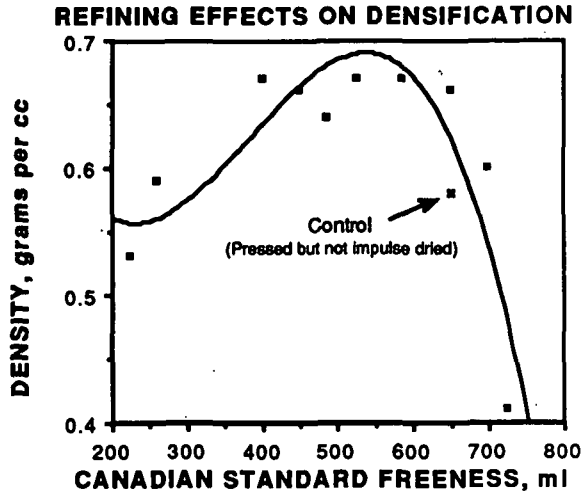

Figure 4. Changes in apparent IPC soft platen density indicating web delamination in 200 gram per square meter linerboard initially at 35% solids. All impulse drying was done at 700°F, 400 psi peak pressure and 30 milliseconds. Delamination was observed for all samples refined below 600 ml CSF.

However, STFI (Figure 5) is sensitive to loss of sheet internal bonding, and can give a clear indication of the start of delamination. As STFI is considerably faster and easier to run than the ZDT internal bonding test, it appears to be a very good means to detect delamination.

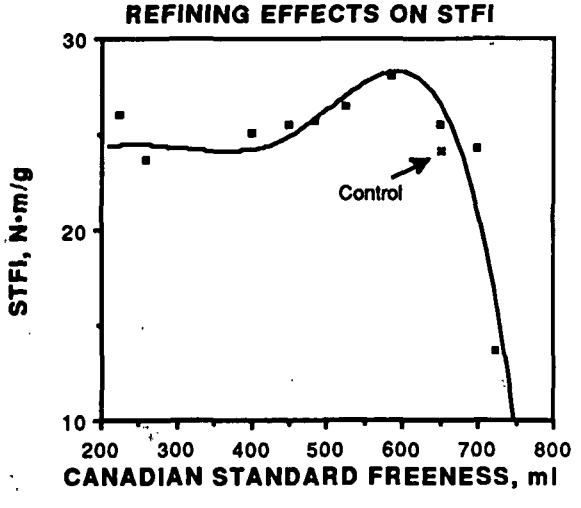

Figure 5. STFI compressive test results for 200 gram per square meter linerboard initially at 35% solids refined to induce delamination. All impulse drying was done at 700°F, 400 psi peak pressure and 30 milliseconds. Delamination was observed for all samples refined below 600 ml CSF.

This preliminary study has thus demonstrated that delamination can be induced by refining. Further work is necessary to understand the heat release, flow resistance, and wet web strength phenomena which appear to govern delamination.

Several student research projects are now underway which are related to Project 3470. W. Bartz' MS project on modelling the whole-mill energy effects of impulse drying will be completed by mid-March, 1988 and should provide the groundwork for more detailed future studies of the economic consequences of impulse drying. D. Arnold's Masters work on developing density gradient measurement techniques will also be complete by mid-March. Newly initiated Masters projects include J. Burkhead's work on bulk development in impulse drying, R. Santkuyl's project on delamination mechanisms, and a program by J. Zavaglia to apply flash x-ray visualization to detecting the development of vapor layers in wet paper webs during impulse drying. Gary Rudemiller is continuing to make good progress in a PhD program to define the heat transfer phenomena which drive impulse drying.

PLANS FOR NEXT PERIOD:

Construction of the second nip of the roll impulse dryer will be expedited to meet an early May, 1988 startup date. Once the construction is complete, a series of experiments will be run to identify combinations of impulse drying conditions which minimize two-sidedness in typical newsprint, light-weight coating rawstock and writing paper furnishes. Once good sheets can be produced, the conversion performance of these grades will be tested. Printing quality in particular will be evaluated using accepted methods suitable to each grade. These experiments will answer the principal questions about the suitability of impulse dried sheets for use in the production of a wide range of important grades.

Further mechanistic work on delamination phenomena will be performed in the funded research project to supplement student work which is already underway. The heat flux and sheet internal deformation and temperature measurement techniques developed in earlier work on impulse drying will be applied to over-refined southern kraft linerboard to understand what changes in heat and water transport accompany the onset of delamination. Once the mechanistic changes which accompany the visible

effects of delamination are identified, work will continue to learn how to modify the impulse drying process to eliminate delamination in sensitive grades.

A timeline for these activities is presented in Figure 7.

SIGNIFICANCE TO THE INDUSTRY

Impulse drying is a new technology which offers the potential for reduced capital costs, increased machine productivity, reduced energy use, and improved paper properties. Commercialization of impulse drying could produce fundamental changes in the pulp and papermaking process as a whole, as equivalent products can be made from less costly furnishes with lower capital and energy costs.

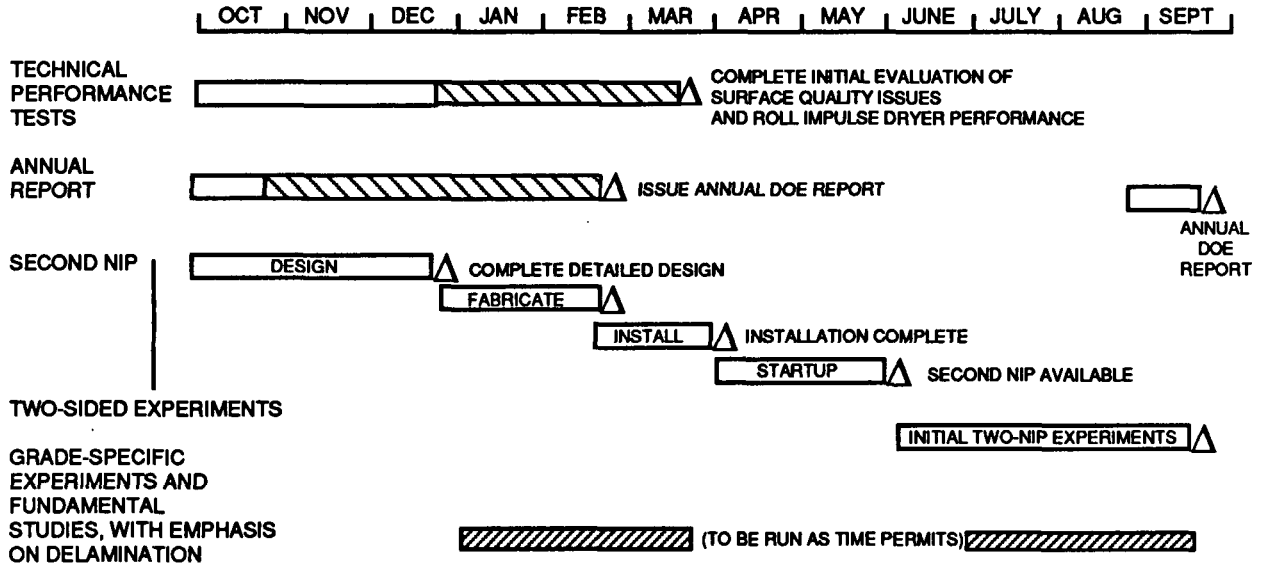

Figure 6. Timeline for project activities during 1988.

REFERENCES

1. Burton, S.W., A Dynamic simulation of impulse drying, Master's Problem, The Institute of Paper Chemistry, May, 1983

2. Lavery, H.P., High-Intensity Drying Processes-Impulse Drying, Report 2 for Department of Energy Contract FG02-85CE40738, DOE/CE/40738-T2, February 1987

THE INSTITUTE OF PAPER CHEMISTRY

Appleton, Wisconsin

Status Report

to the

ENGINEERING PROJECT ADVISORY COMMITTEE

Project 3480

DISPLACEMENT DEWATERING

March 29, 1988

PROJECT SUMMARY FORM

DATE: Feb. 15, 1988

PROJECT NO.: 3480 – DISPLACEMENT DEWATERING

PROJECT LEADER: Jeff Lindsay

IPC GOAL:

Develop novel processes for efficient water removal with enhanced control over paper properties.

CURRENT FISCAL BUDGET: $150,000

OBJECTIVE:

Develop a pilot-scale displacement device which demonstrates that high water removal rates can be achieved while maintaining control over paper properties such as bulk.

SUMMARY OF RECENT PROGRESS:

Experimental equipment for investigating displacement processes has been designed and constructed, as shown in Figure 1. Using the existing MTS hydraulic press, the equipment allows mechanical pressure and gas pressure to be simultaneously applied to a paper sheet in a specified, transient manner. A pressure chamber has been designed to allow superheated steam as well as heated air to be applied to the sheet.

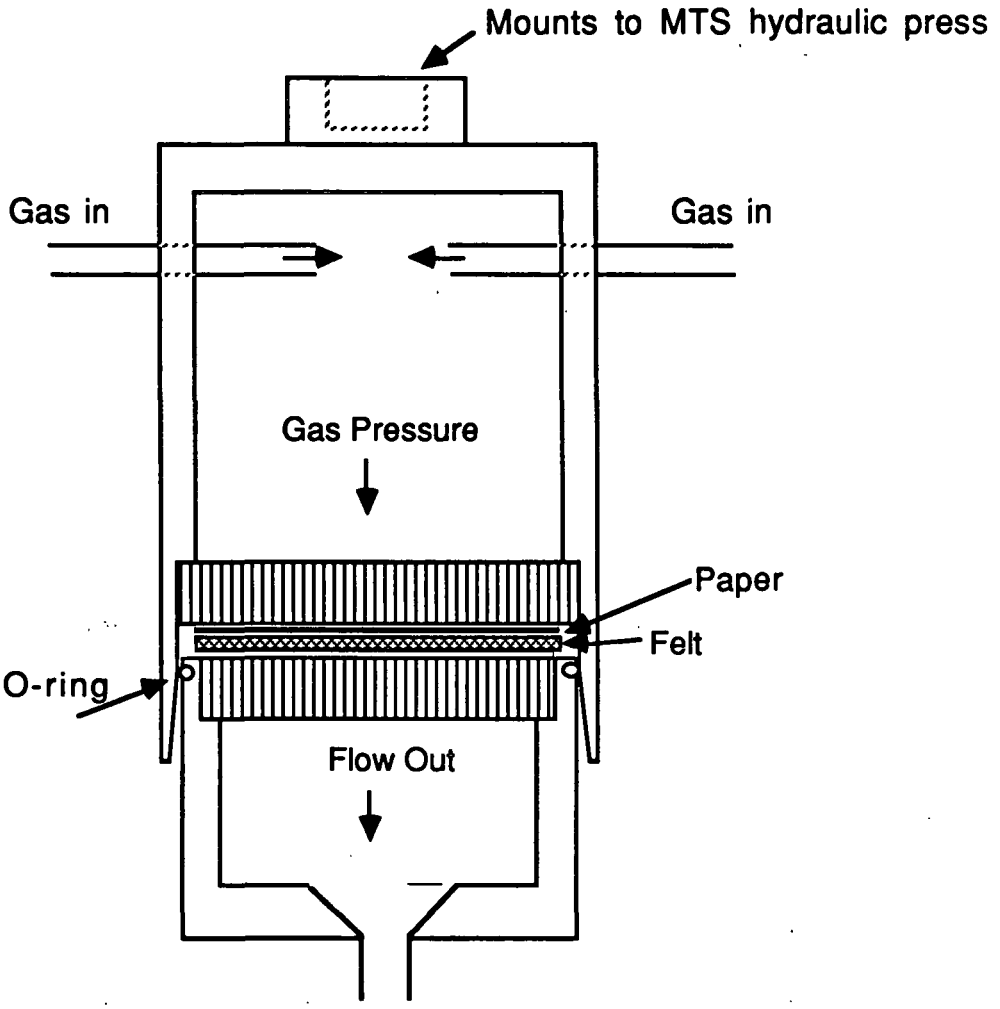

Figure 1. Displacement dewatering equipment (gas supply valves and pressure chamber not shown).

Testing has been delayed because of extreme demands on the MTS hydraulic press for impulse drying research, but some preliminary tests have been made and time has been scheduled for extensive testing beginning in March. Early work will aim at finding operating conditions (nip residence time, mechanical loading, gas pressure, gas temperature) which allow efficient gas-phase displacement of water in several types of paper.

A numerical model, for displacement processes, MIPPS (Moving Interface Problems in Porous Systems), has been developed and is undergoing further refinement. Predictions of vapor pressure development during impulse drying events have been made in order to understand possible delamination mechanisms as well as heat transfer processes. MIPPS is now being modified to deal with direct displacement dewatering in which the gas is applied rather than generated by phase change.

The issue of anisotropic permeability is of interest in displacement dewatering and wet pressing. Simple measurements of the lateral and transverse permeabilities in linerboard were reported in the last PAC report. The previous method permitted measurements only at low compression. The new displacement apparatus provides additional means to measure lateral and transverse permeabilities under various compressive loads. The key to lateral measurements is using a solid plate in place of the lower drilled plate in Figure 1, and replacing the upper plate with a plate having a single small hole in the center. The upper chamber of Figure 1 will then be filled with colored water that will be maintained at a known, constant pressure using compressed gas above the liquid. The colored water will be forced to move in the plane of the initially saturated sheet (the O-ring seals must be removed to permit flow out the sides of the sheet). The theory has recently been developed to determine the permeabilities in the x and y directions as a function of the size and shape of the resulting colored zone in the paper after a specified time. Measurements of the normal permeability can also be made with the apparatus using the original drilled plates, again with pressurized fluid being forced through the sheet. Knowledge of the x, y, and z direction permeabilities as a function of mechanical

compression will be valuable for future pressing and displacement work. Surprisingly, there appear to be no previous measurements of lateral permeability in paper.

PLANS FOR NEXT PERIOD:

1. Begin experimental displacement work with the new apparatus.
2. Continue refinement of MIPPS. Apply it to displacement dewatering using applied steam and air.
3. Measure lateral permeability (x and y directions) and normal permeability in a variety of papers under compressive stress.

SIGNIFICANCE TO THE INDUSTRY:

Displacement dewatering offers the potential of efficient water removal as well as enhanced control over physical properties such as bulk. Developments in the science of displacement phenomena may also lead to improvements in the proven technology of impulse drying.

THE INSTITUTE OF PAPER CHEMISTRY

Appleton, Wisconsin

Status Report

to the

ENGINEERING PROJECT ADVISORY COMMITTEE

Project 3479

MEDIUM CONSISTENCY PROCESSING

March 29, 1988

PROJECT SUMMARY FORM

DATE: February 17, 1988

PROJECT NO.: 3479 - Medium Consistency Processing

PROJECT LEADER: Staff

IPC GOAL: Reduction in complexity of forming systems

OBJECTIVE:

To develop experimental and computational techniques necessary to better understand the behavior of fiber suspensions over a range of consistencies encompassing both current and potential future operations.

To apply a better knowledge of fiber suspension microrheology to increase paper machine wet-end consistencies from current levels of 0.1-1.5% to 2.0-10.0%, depending on grade without loss of machine speed or paper physical properties.

Ultimately, to apply any new knowledge or techniques developed in this area to other high speed multiphase flow problems of interest to the industry.

CURRENT FISCAL BUDGET: $150,000

SUMMARY OF RESULTS SINCE LAST REPORT: (October, 1987 - February, 1988)

Background

Medium consistency forming has the potential of reducing both capital and energy costs, and improving formation and physical properties control. Previous attempts have produced paper which appeared felted, with inferior in-plane properties. This can be traced to lack of control of out-of-plane fiber orientation in the sheet. Without the ability to measure fiber orientation at

actual process conditions, process development must proceed by trial and error. The initial objective of this project has been to develop some means for measuring the fiber orientation distribution in concentrated fiber suspensions during high speed flows.

Flash x-ray radiography (FXR) will be used to study fiber orientation distribution in both idealized and practical flow situations. The objective of any idealized flow experiments will be to assess to what extent fiber orientation distribution can be controlled under the best of conditions. If significant results cannot be realized here, it would be unlikely that any improvement can be made in practical flows.

To evaluate the idealized flow, a four element test was designed, see Table 1, using convergent flow test sections. Initial testing was done with the H-P 300 KV FXR system. To properly image the tracer, Kodak AA film with an X-omatic fine screen was used. However, after evaluating the H-P 150 KV at a thinner test section cross-section, it was determined that this unit performed better. Silver wire of 35 micron diameter coated with nylon was selected for the tracer fiber. The tracers will be disbursed throughout a slurry of 50 micron nylon fibers that constitute a model flow system.

Table 1. Experimental plan.

Quadrant #	Consistency, %	Velocity	Imaging
1	High	High	FXR
2	Low	High	Optical
3	Low	Low	Optical
4	High	Low	FXR

Computational studies are important in modeling different configurations in fluid flow studies. Initial work in this area was done with an early version of the code FLUENT, through an agreement with Lawrence University on their VAX computer.

Progress

A key element for the evaluation of the data generated is the acquisition of an image analyzer. With the recent awarding of a DOE proposal to IPC, we will now have this capability. The image analysis system includes a MicroVAX computer, which can also be used for computational work. We now have the source code of FLUENT, which will allow expansion of the total number of nodes beyond 10,000 - a requirement for simulating three-dimensional flows. In addition, a revised version of FLUENT will be soon available which has the capability of body-fitted coordinates in models of fluid flows.

The necessary equipment to cut the tracer fibers to the proper lengths needed for the tests is in operation. Although somewhat slow, it allows us to do this in-house.

Current Activities

The high concentration-high speed element of the test design has been run with the 1 mm and 2 mm fibers. The 1 mm fibers were run at a volumetric consistency of 9.8% and 6.5%, while the 2 mm fibers were run at volumetric consistencies of 2.5% and 3.7%. Exit velocities for both lengths were 7.5 m/s and 15 m/s. Because we varied the conditions of the experiment within the test quadrant, we can look at the data from these conditions to see if any pattern is developing in flow orientation.

To maximize the performance of the image analysis equipment, we decided to reverse the radiographs to positive prints. This process will allow us to increase the contrast of the tracer fibers and allow easier identification. At this point we are optimizing this process.

Images for the test element that has been completed have been digitized and data files have been written. These data are being evaluated to see if there is any fiber orientation occurring, under the different conditions, as the flow converges in a planer converging duct.

PLANS FOR THE NEXT PERIOD

1. To complete the other elements of the test design with 1 and 2 mm fibers.
2. Repeat the tests with a circular convergent duct.
3. Investigate longer model fibers, 3-3.5 mm.
4. To form a sheet using a high consistency headbox.

SIGNIFICANCE TO THE INDUSTRY

Higher consistency forming has the potential to reduce both capital and energy costs. Perhaps more important is the potential to obtain novel three dimensional sheet properties.

Flash x-ray radiography has demonstrated the ability to provide unique information regarding several multiphase flow problems of interest to the industry. Current applications include black liquor sprays, coating flows, and impulse drying.

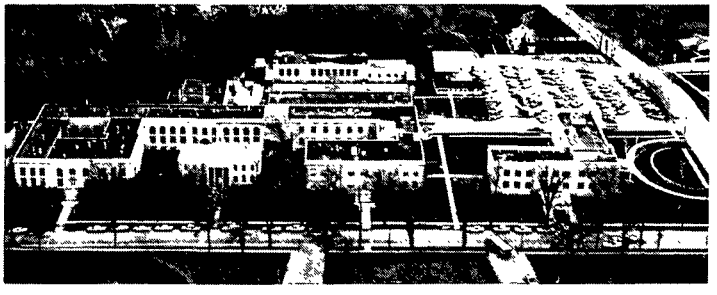

THE INSTITUTE OF PAPER CHEMISTRY, APPLETON, WISCONSIN

S L I D E M A T E R I A L

To The

Engineering Project Advisory Committee

March 29-30, 1988
The Institute of Paper Chemistry
Continuing Education Center
Appleton, Wisconsin

NOTICE & DISCLAIMER

The Institute of Paper Chemistry (IPC) has provided a high standard of professional service and has exerted its best efforts within the time and funds available for this project. The information and conclusions are advisory and are intended only for the internal use by any company who may receive this report. Each company must decide for itself the best approach to solving any problems it may have and how, or whether, this reported information should be considered in its approach.

IPC does not recommend particular products, procedures, materials, or services. These are included only in the interest of completeness within a laboratory context and budgetary constraint. Actual products, procedures, materials, and services used may differ and are peculiar to the operations of each company.

In no event shall IPC or its employees and agents have any obligation or liability for damages, including, but not limited to, consequential damages, arising out of or in connection with any company's use of, or inability to use, the reported information. IPC provides no warranty or guaranty of results.

This information represents a review of on-going research for use by the Project Advisory Committees. The information is not intended to be a definitive progress report on any of the projects and should not be cited or referenced in any paper or correspondence external to your company.

Your advice and suggestions on any of the projects will be most welcome.

TABLE OF CONTENTS

Project 3628

RECOVERY BOILER CORROSION

David Crowe

March 29, 1988

PROJECT 3628

RECOVERY BOILER CORROSION

David C. Crowe

OBJECTIVE

Understand the mechanism of high temperature corrosion in the recovery boiler so that corrosion control options may be identified.

Costs of Recovery Boiler Corrosion:

- Possible Explosion: Injuries, *Fatalities*, Loss of Production.
- Inspection, Repairs and Downtime.
- Increasing Insurance Premiums.

Results Since Last Report:

1. Start-up of two tube furnaces and completion of preliminary runs.
2. Experimental plan for air port corrosion study.
3. Conceptual design of an air port corrosion probe.

Lower Furnace Corrosion Problems

1. Composite Tube at Air Ports
2. Smelt Spouts, Liquid Level
3. Oxidation/Sulfidation of Waterwall.

Sodium Hydroxide Attack

$4\ Fe + 3\ O_2 + 4\ NaOH \rightarrow 4\ NaFeO_2 + 2\ H_2O$

$2\ Fe + 2\ H_2O + 2\ NaOH \rightarrow 2\ NaFeO_2 + 3\ H_2$

$2\ NaOH + Fe_2O_3 \rightarrow 2\ NaFeO_2 + H_2O$

$4\ NaOH + Cr_2O_3 + 3/2\ O_2 \rightarrow 2\ Na_2CrO_4 + 2\ H_2O$

$NaFeO_2$ and high pH may be due to:

$Na_2CO_3 + Fe_2O_3 \rightarrow 2\ NaFeO_2 + CO_2$ (>820 C)

$2\ NaFeO_2 + H_2O \rightarrow 2\ NaOH + Fe_2O_3$

Alternative Theories

$2\ NaCl + 2\ SO_3 + 1/2\ O_2 \rightarrow Na_2S_2O_7$ (l) $+ Cl_2$

$3\ Na_2S_2O_7 + Fe_2O_3 \rightarrow 3\ Na_2SO_4 + Fe_2(SO_4)_3$

$Na_2S_2O_7 + Fe_2O_3 \rightarrow 2\ NaFeO_2 + 2\ SO_3$ (?)

$24\ KCl + 10\ Cr_2O_3 + 9\ O_2 \rightarrow 12\ K_2CrO_4 + 8\ CrCl_3$

PROGRESS:

1. Commissioning of the tube furnace.
2. Preliminary tests of 1018 & 304 steels.
3. Design and construction of gas metering system.
4. Conceptual design of a corrosion probe for use in the air port.
   - heated with molten sulfur.

Experimental Plan

Simulated Smelt

80 % Na_2CO_3, 12 % Na_2SO_4, 8 % Na_2S
with NaOH, NaCl, $Na_2S_2O_7$, KCl,
$K_2S_2O_7$, $Na_2S_2O_3$, S, Na_2SO_3.

Gas

1 % H_2S, 1 % O_2, 2 % H_2O, 10 % CO_2, N_2
with SO_2 & SO_3
300, 400, 500 C

Materials

1018, A210, 304 steel

Related Plans of John Cameron

- Determine the deposit composition on a cooled probe above a Na_2CO_3 - Na_2S melt. NaCl may be more volatile than NaOH.

- What happens to this deposit when exposed to SO_2 ?

Future Activities:

1. Sample smelt and flue gas near air ports and smelt spouts.

2. Document smelt spout problems and relevant corrosion mechanisms.

3. Develop an experimental plan for gas phase oxidation/ sulfidation tests.

Other Potential Activities:

1. Devise a test apparatus which will continuously replenish molten smelt at the corroding steel surface.

2. Develop methods for in-situ corrosion testing.

SIGNIFICANCE TO THE INDUSTRY:

An improved knowledge of corrosion mechanisms in recovery boilers will aid in the design of remedial measures which will extend the operating life and improve safety.

Table 1
Corrosion rates of 1018 and 304 steels.

Temp., C	1018 Carbon Steel	304 Stainless
300	0.19, 0.21 mpy	0.27, 0.23
500	0.57, 3.92	0.62, 1.72
400	0.42, 0.42	0.40, 0.27
600	0.84, 1.88	11.73, 1.35

MOLTEN SMELT CORROSION

Greg Kulas

March 29, 1988

AN INVESTIGATION OF THE FIRESIDE SULPHIDATION OF KRAFT RECOVERY BOILER WATERWALL TUBES

Gregory S. Kulas

THESIS OBJECTIVES

1) **Construct an apparatus for investigating the corrosion of a metal sample covered with a frozen smelt layer and exposed to a molten smelt**

2) **Develop a fundamental understanding of the mechanism of the corrosion reaction occurring under these conditions**
   - **identify the sulfur species participating in the corrosion reaction**
   - **identify the rate limiting step in this reaction**

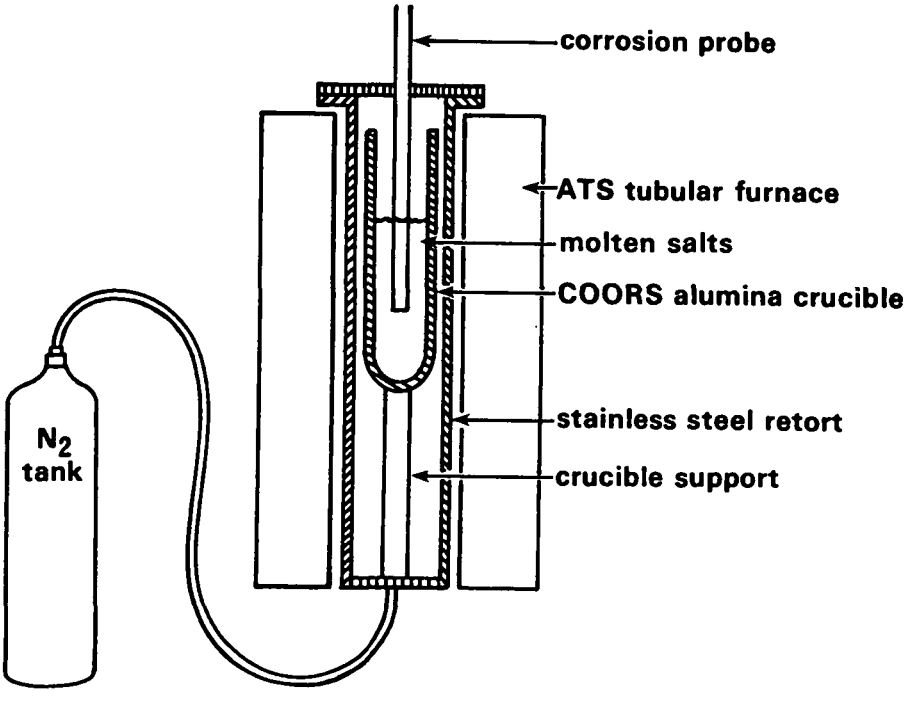
corrosion probe
ATS tubular furnace
molten salts
COORS alumina crucible
stainless steel retort
crucible support
N_2 tank

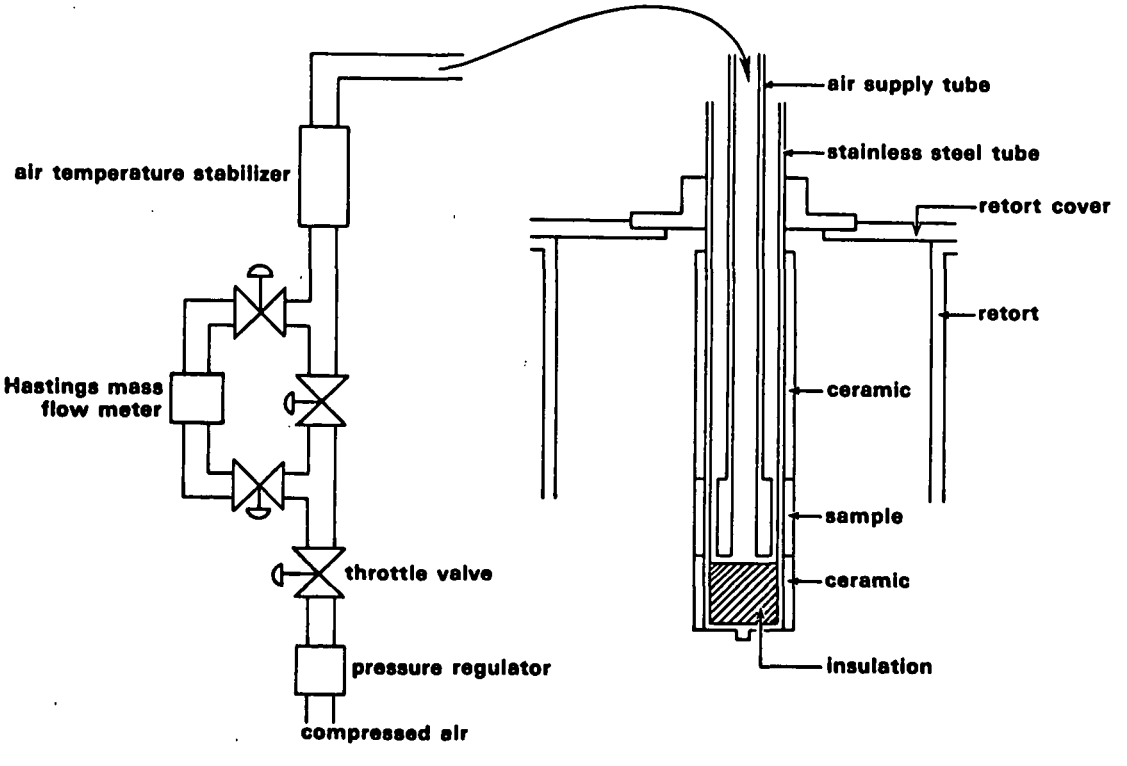
air supply tube
stainless steel tube
retort cover
retort
ceramic
sample
ceramic
insulation
air temperature stabilizer
Hastings mass flow meter
throttle valve
pressure regulator
compressed air

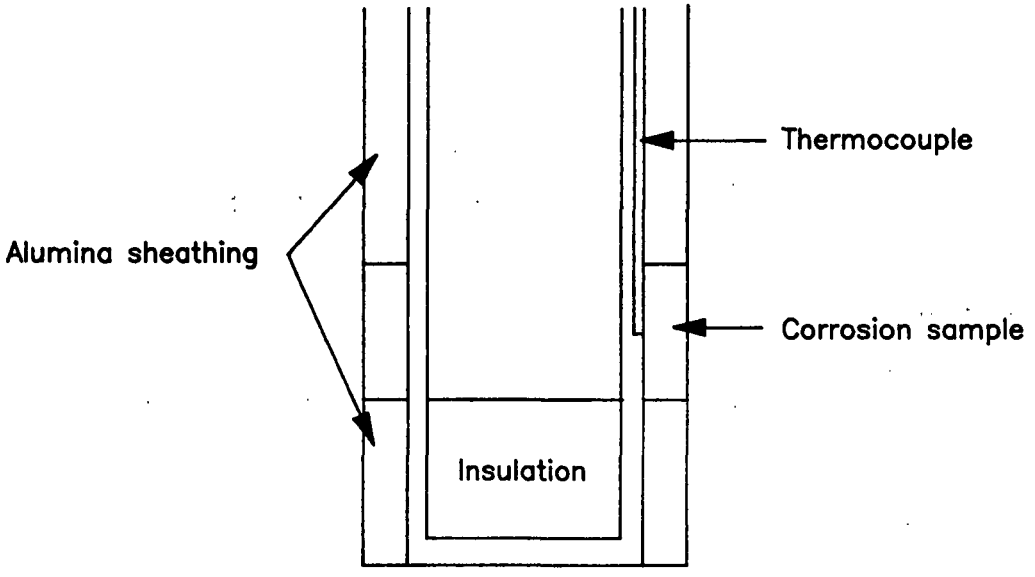
Thermocouple
Alumina sheathing
Corrosion sample
Insulation

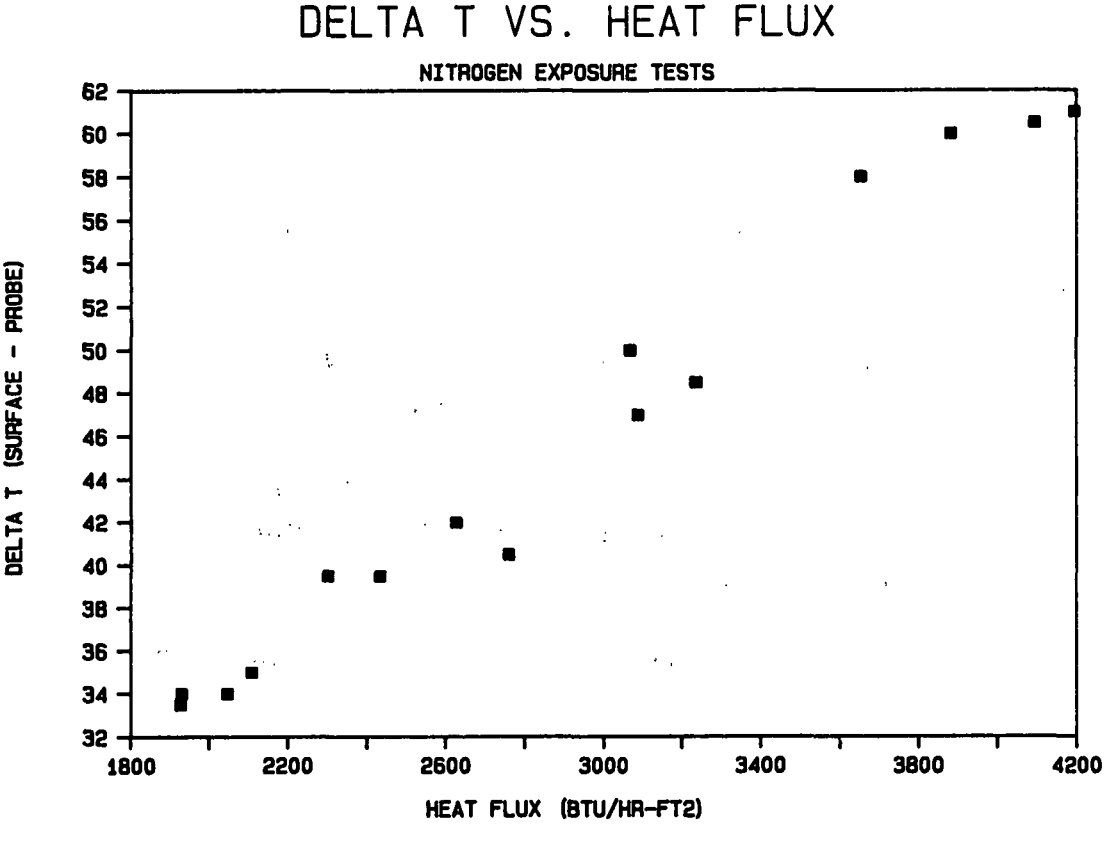
DELTA T VS. HEAT FLUX
NITROGEN EXPOSURE TESTS
DELTA T (SURFACE - PROBE)
62
60
58
56
54
52
50
48
46
44
42
40
38
36
34
32
1800
2200
2600
3000
3400
3800
4200
HEAT FLUX (BTU/HR-FT2)

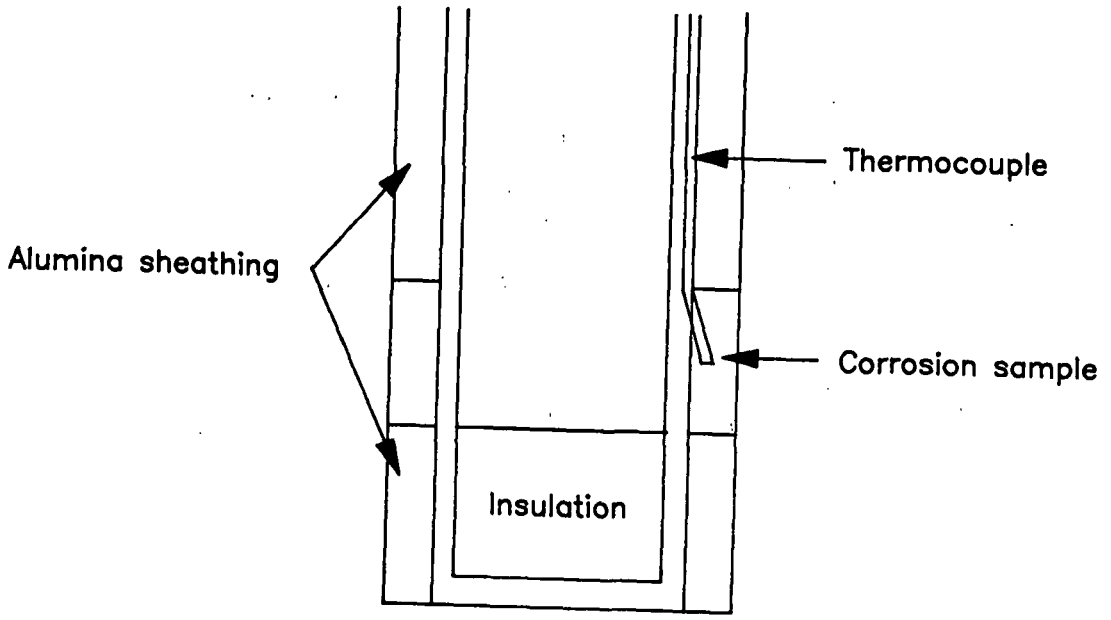

RESULTS

1). An experimental system has been developed and tested

2). A method of measuring the temperature of the corroding metal surface has been developed

3). Corrosion tests have been conducted using sulfide/carbonate smelt and sulfide/sulfate/carbonate smelt

4). Very little corrosion observed at metal temperature < 1000 F

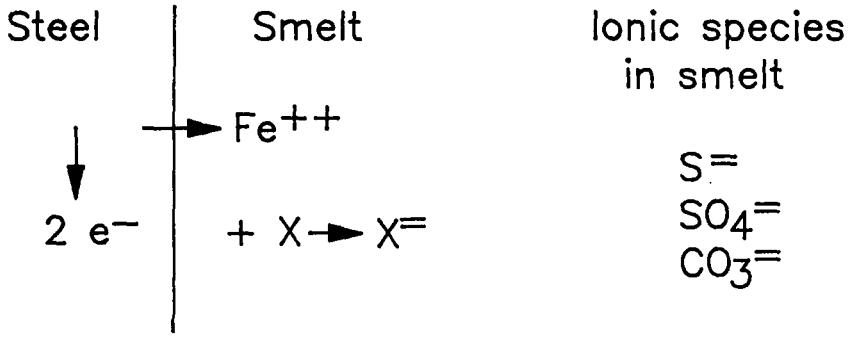

Anodic reaction

$$Fe \longrightarrow Fe^{++} + 2\ e^-$$

Possible cathodic reactions

$$S + 2\ e^- \longrightarrow S^=$$

$$S_2^= + 2\ e^- \longrightarrow 2\ S^=$$

Project 3309

FUNDAMENTALS OF CORROSION CONTROL IN PAPER MILLS

Mark Revall

March 29, 1988

PROJECT 3309

FUNDAMENTALS OF CORROSION CONTROL

IN PAPERMAKING APPLICATIONS

LONG TERM OBJECTIVE

ELIMINATE COSTLY SUCTION ROLL FAILURES

SHORT TERM OBJECTIVE

DEVELOP A LABORATORY TEST THAT PREDICTS SERVICE PERFORMANCE

- ALLOY RANKING
- MECHANISM OF FAILURE
- ALLOY DEVELOPMENT

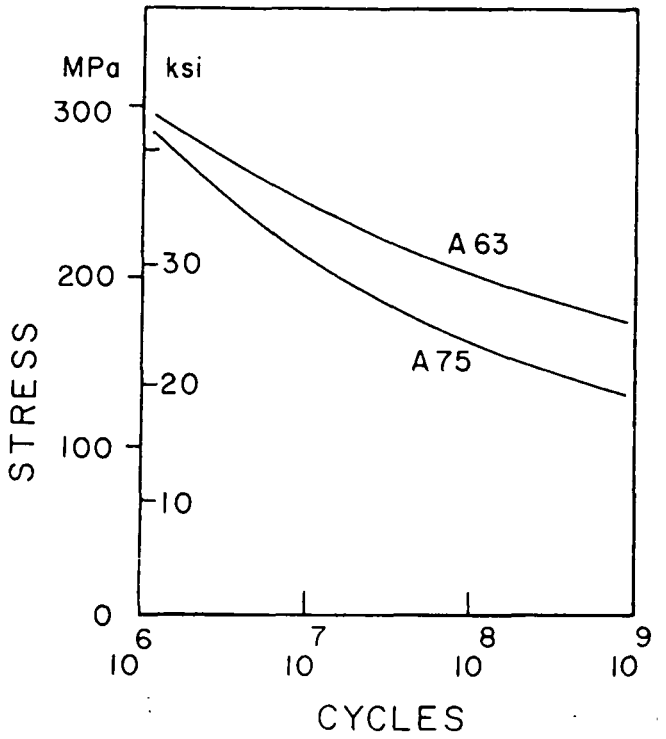
MPa
ksi
300
200
100
0
30
20
10
A 63
A 75
STRESS
10^6
10^7
10^8
10^9
CYCLES

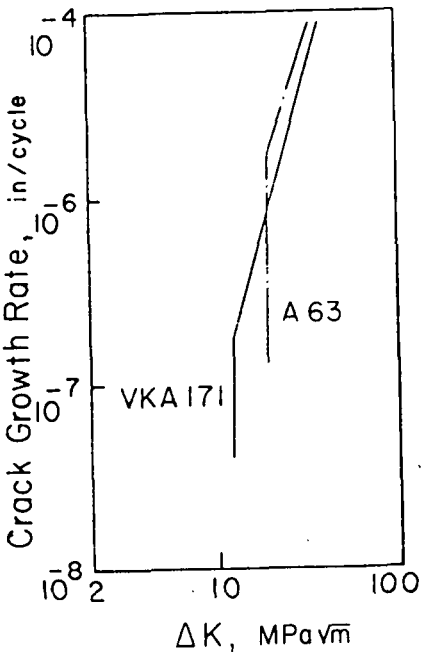
10^{-4}
10^{-6}
10^{-7}
10^{-8}
Crack Growth Rate, in/cycle
A 63
VKA 171
2
10
100
ΔK, MPa√m

PREDICTIVE TEST DEVELOPMENT

INITIATION VS. PROPAGATION

NEAR-THRESHOLD FATIGUE CRACK GROWTH

STRESS INTENSITY CONCEPT

$$\text{DRIVING FORCE FOR GROWTH} = \begin{cases} \text{NOMINAL STRESS} \\ \text{CRACK LENGTH} \\ \text{GEOMETRY} \end{cases}$$

$$\Delta K = (\text{STRESS RANGE})\ (\text{CRACK LENGTH})^{\frac{1}{2}}\ (\text{GEOMETRY})$$

$$= S_R(a)^{\frac{1}{2}}\ fn\ (a/w)$$

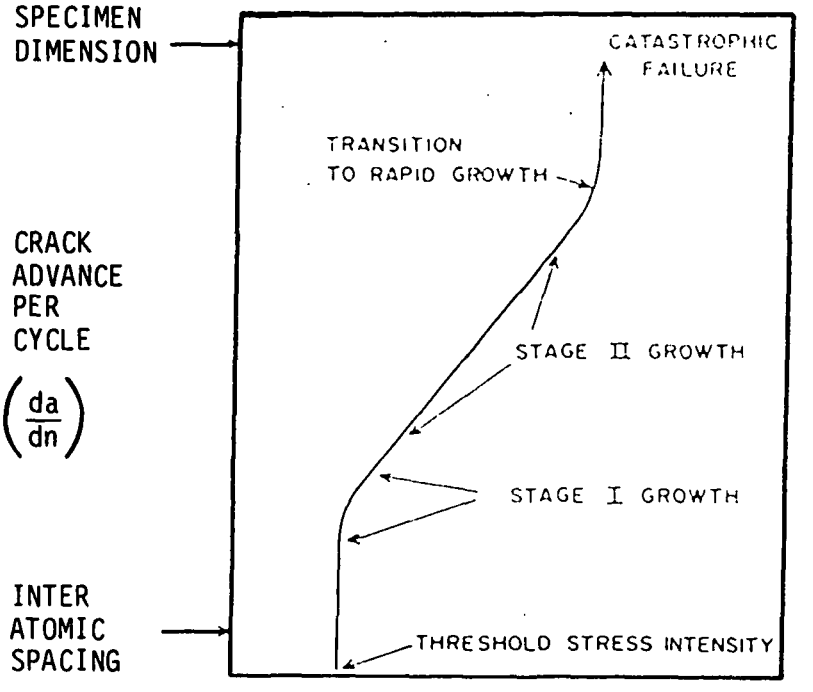

Schematic diagram showing the dependence of crack growth rates on the cyclic stress intensity.

ΔK_{th} DETERMINATION

- CRACK SHARPNESS
- LOAD SHEDDING
- COMPRESSIVE RESIDUAL STRESSES

SIMULATED WHITE WATERS

ENVT	Cl^- ppm	SO_4^{--} ppm	$S_2O_3^{--}$ ppm	pH
A	1000	0	0	4.7
B*	100	1000	0	3.5
C**	1000	1000	0	3.5
D	200	500	50	4.0
E	1000	0	0	3.5
F	200	500	10	4.0
G	3000	0	0	1.0
H	200	500	50	1.0
I	10000	0	0	1.0
J	10000	0	50	1.0

* TAPPI 1
** TAPPI 2

RESULTS FOR 1-N BRONZE

- THRESHOLDS IN AIR ONLY HALF THAT OF DUPLEX
- SIGNIFICANT ENVIRONMENTAL EFFECT IN SOLUTION (pH 3.5, 1000 ppm Cl^-)
- A LARGE ENVIRONMENTAL EFFECT IN HIGHLY AGGRESSIVE SOLUTIONS
- CONSISTENT WITH SERVICE PERFORMANCE

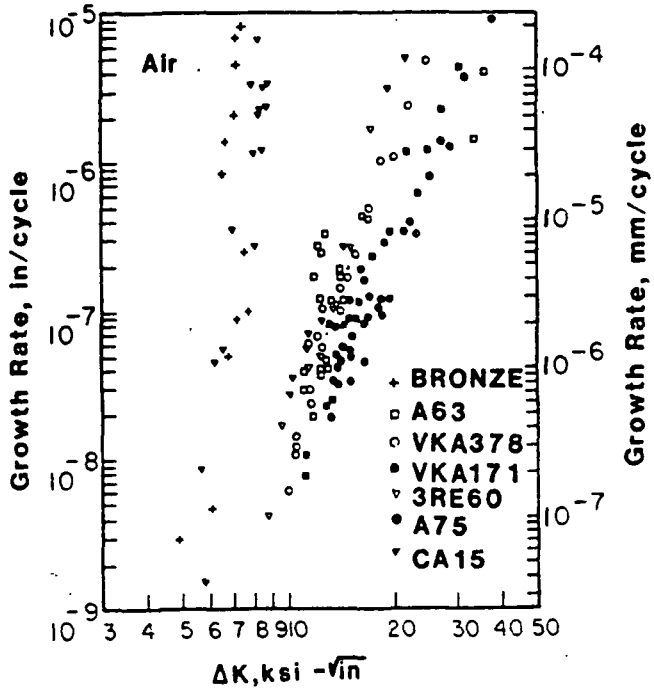
Air
BRONZE
A63
VKA378
VKA171
3RE60
A75
CA15
Growth Rate, in/cycle
Growth Rate, mm/cycle
ΔK, ksi -√in

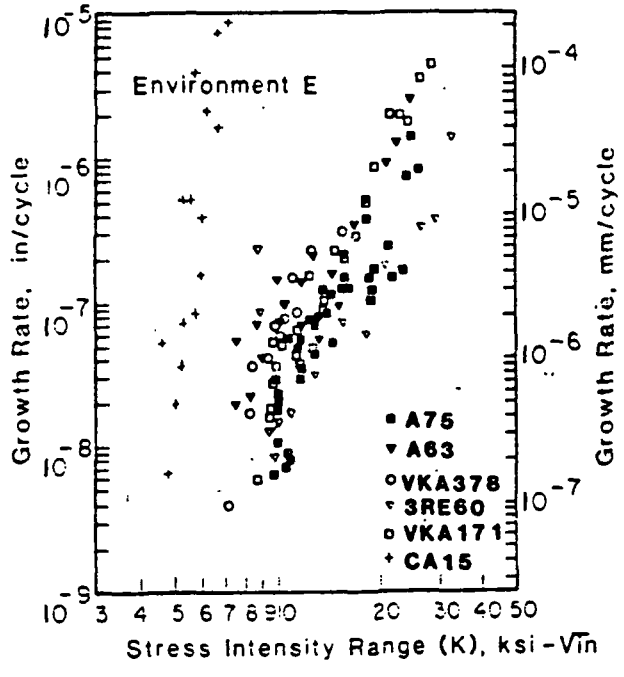
Environment E
A75
A63
VKA378
3RE60
VKA171
CA15
Growth Rate, in/cycle
Growth Rate, mm/cycle
Stress Intensity Range (K), ksi -√in

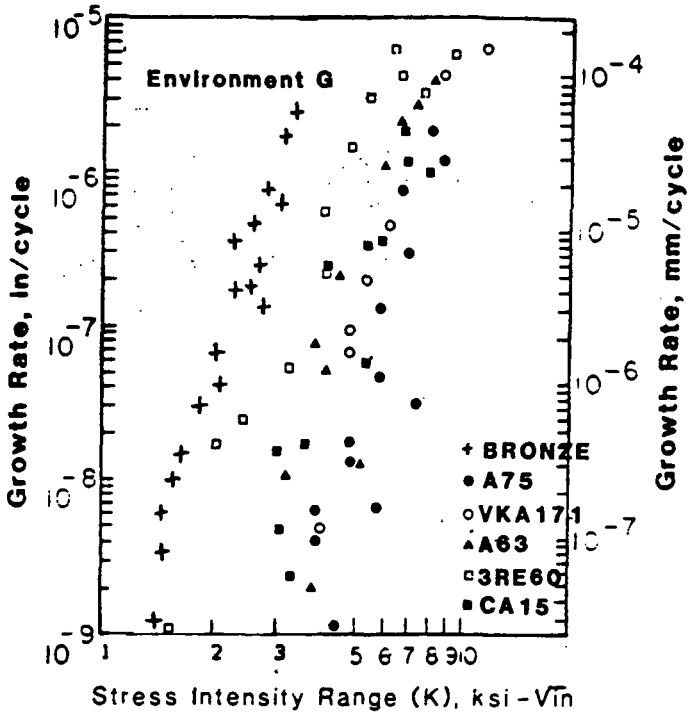

METALLOGRAPHY

- TRANSGRANULAR GROWTH
- IMPORTANCE OF MICROBRANCHING
- GRAIN COMPOSITION
- GRAIN SIZE

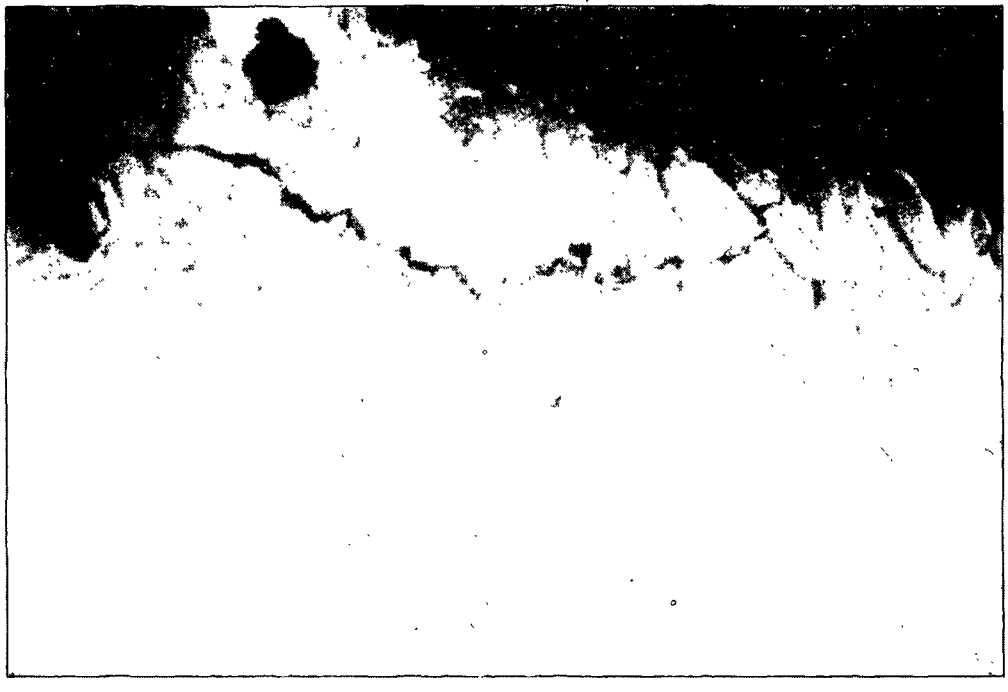

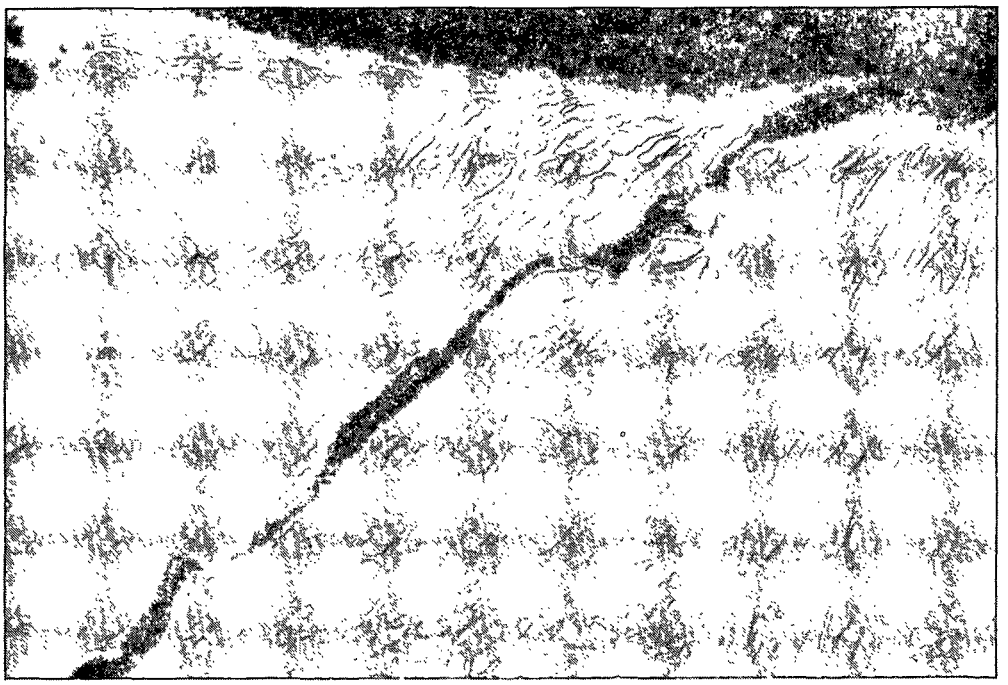

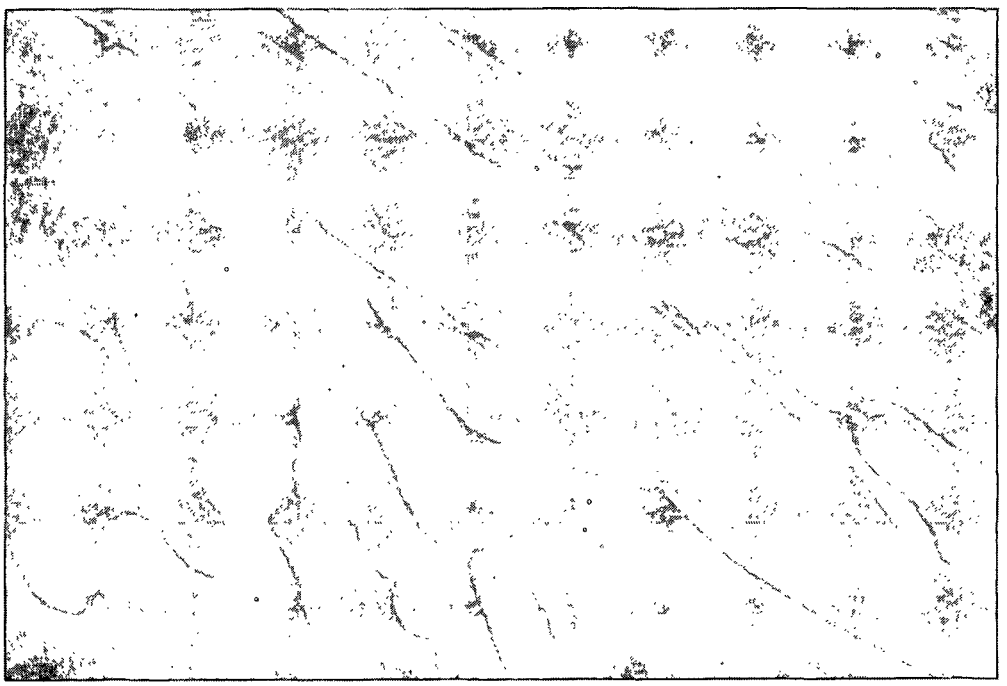

IRON

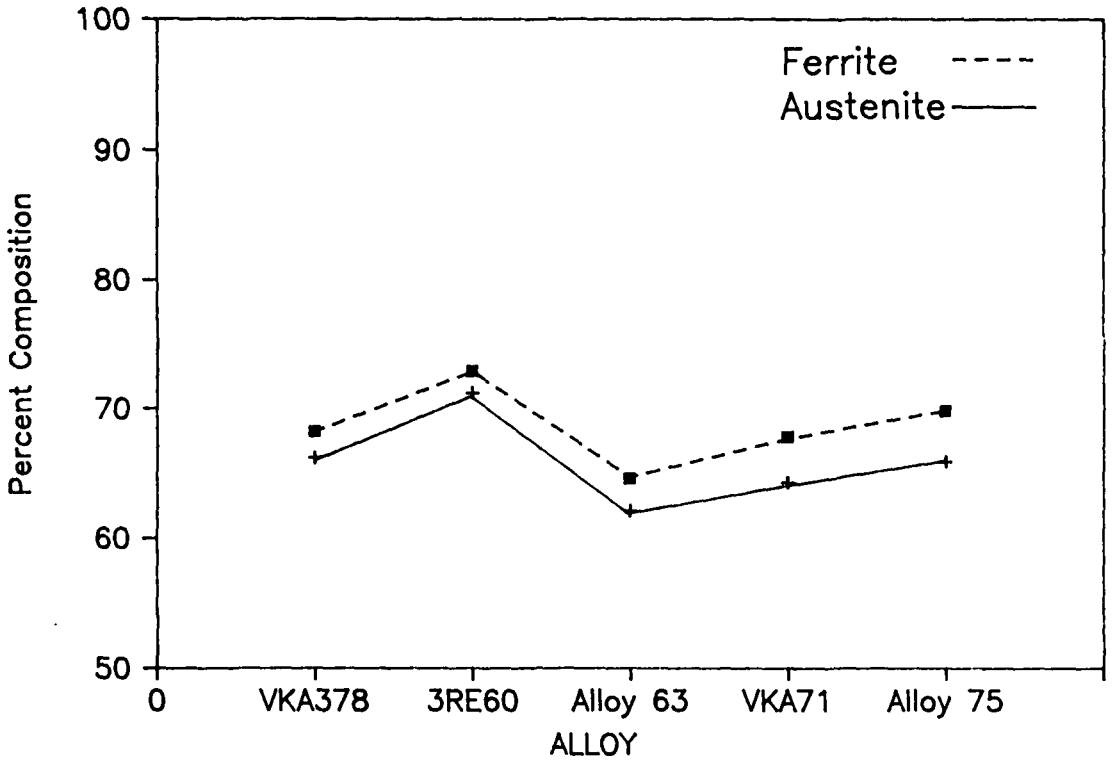

CHROMIUM

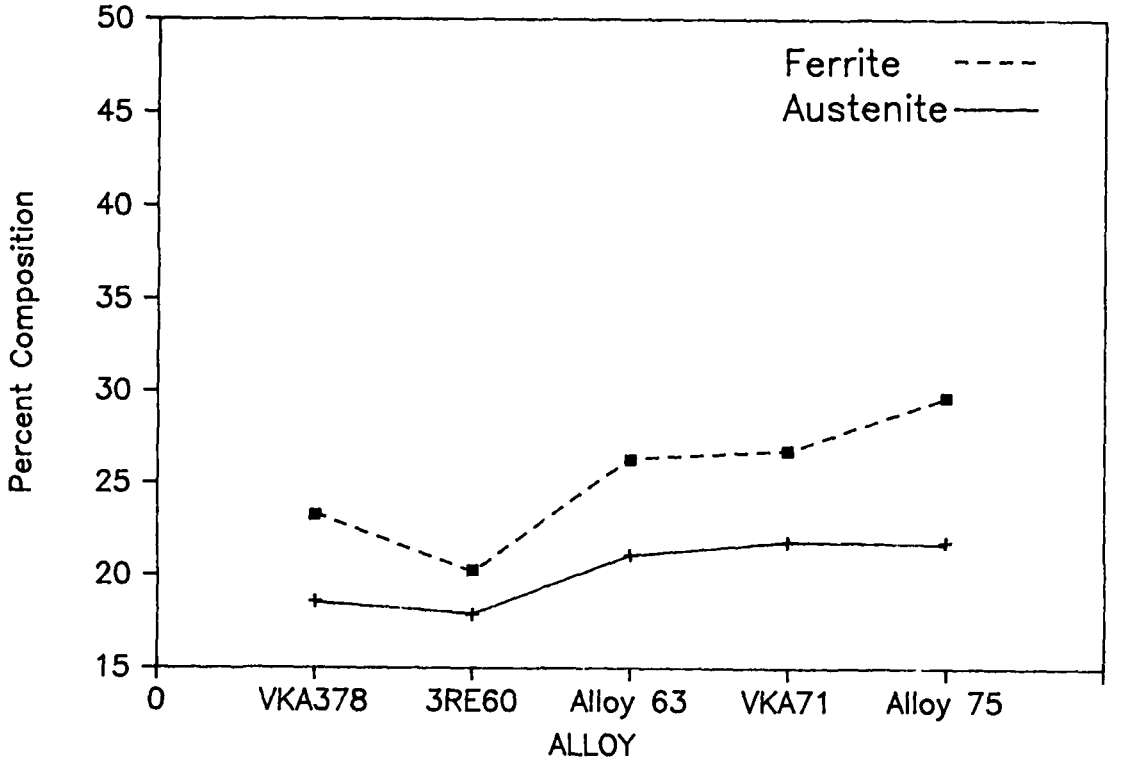

MOLYBDENUM

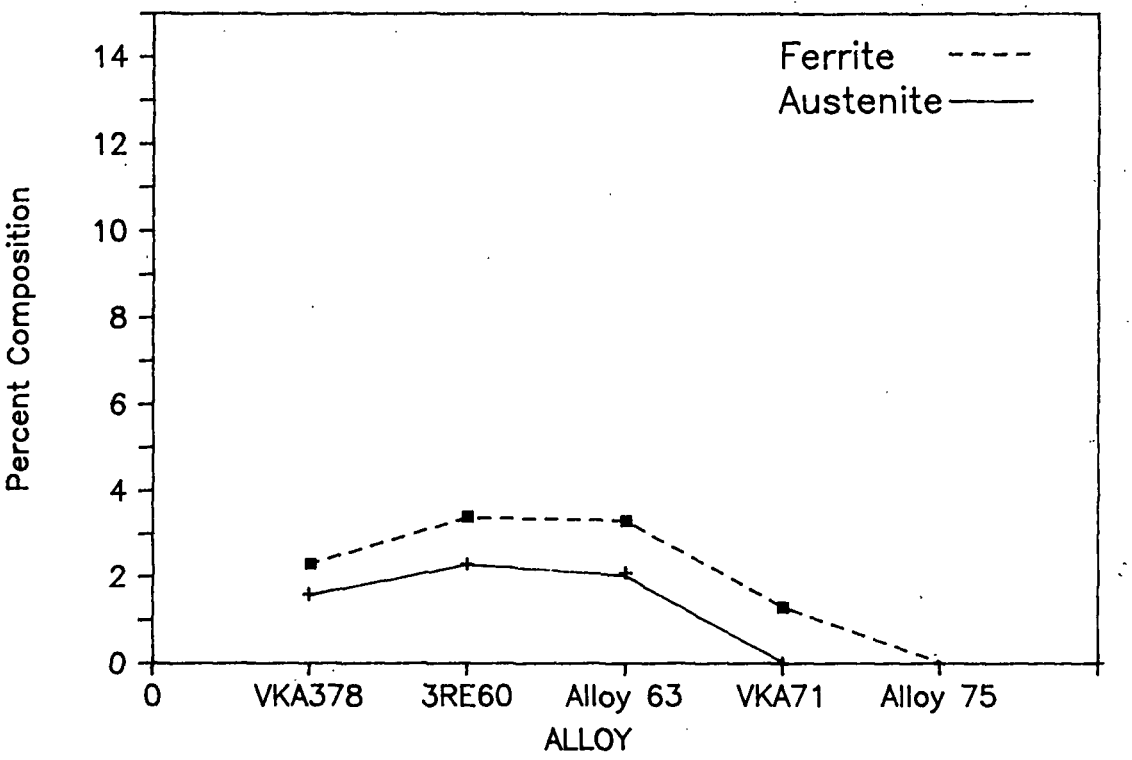

SILICON

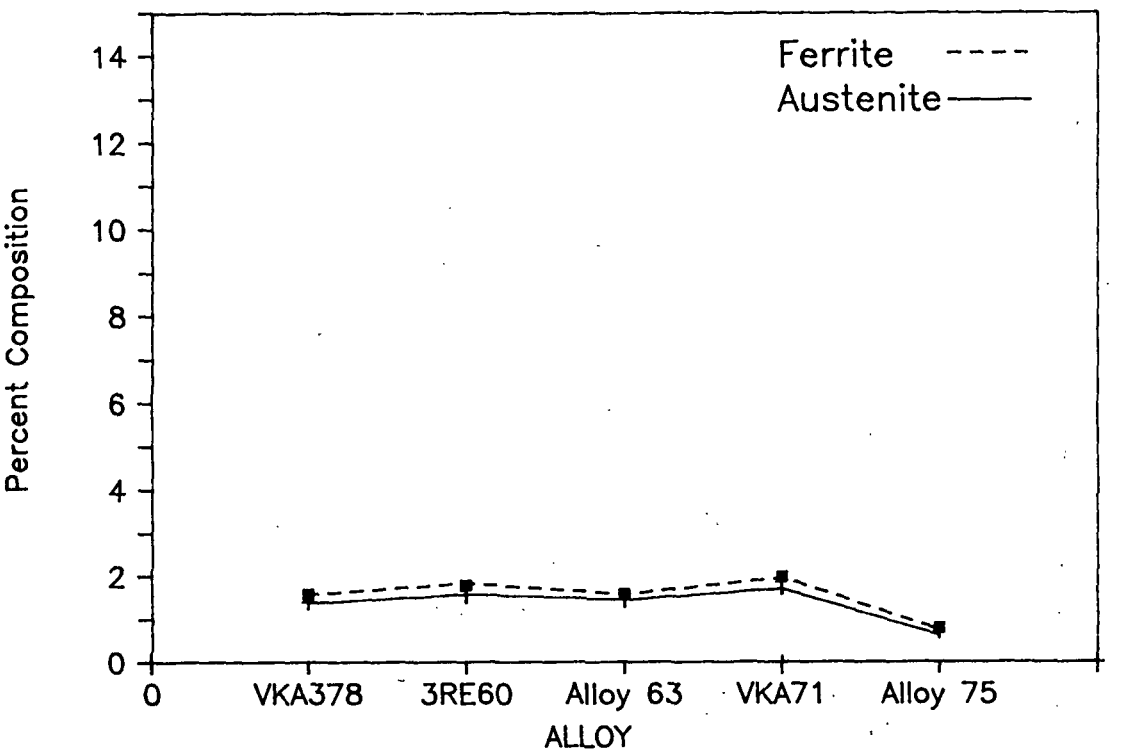

NICKEL

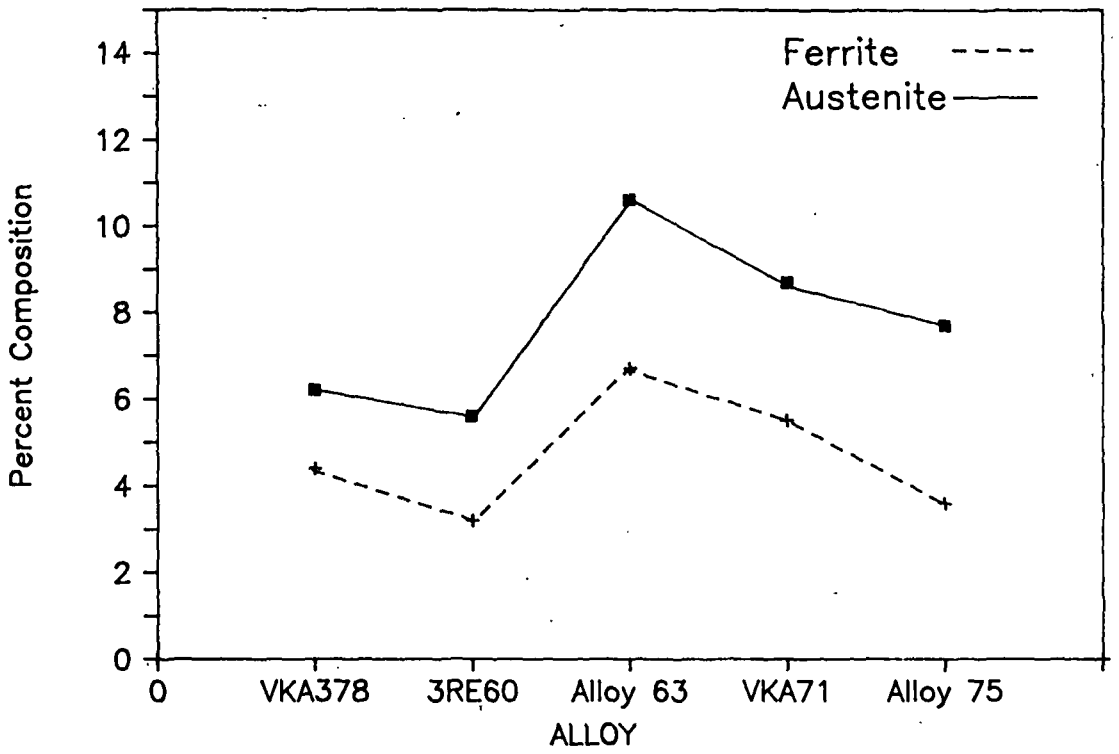
Ferrite
Austenite
Percent Composition
14
12
10
8
6
4
2
0
0
VKA378
3RE60
Alloy 63
VKA71
Alloy 75
ALLOY

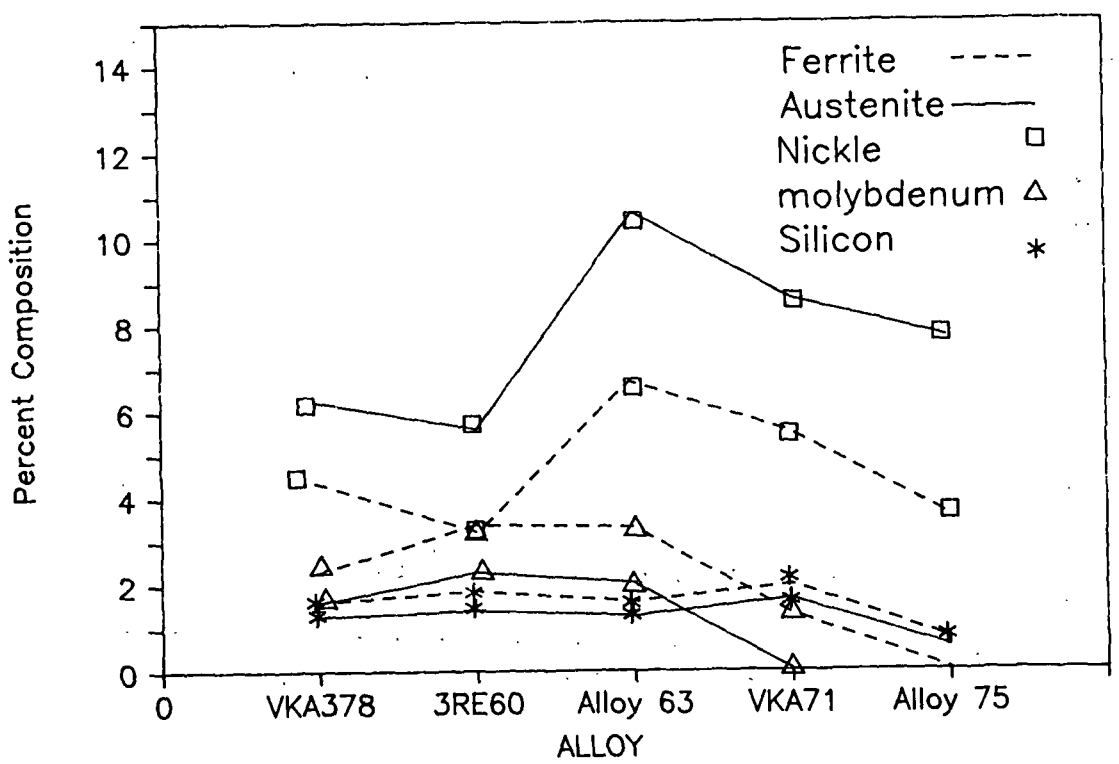
Ferrite
Austenite
Nickle
molybdenum
Silicon
Percent Composition
14
12
10
8
6
4
2
0
0
VKA378
3RE60
Alloy 63
VKA71
Alloy 75
ALLOY

CORROSION FATIGUE LIFETIME

S - N TESTS

- SMOOTH SPECIMEN, ROTATING BENDING
- NOTCHED SPECIMEN, ALTERNATING BENDING

S-N TESTING

- CONTINUE TO FIND NO DIFFERENCE BETWEEN ALLOYS 63 AND 75

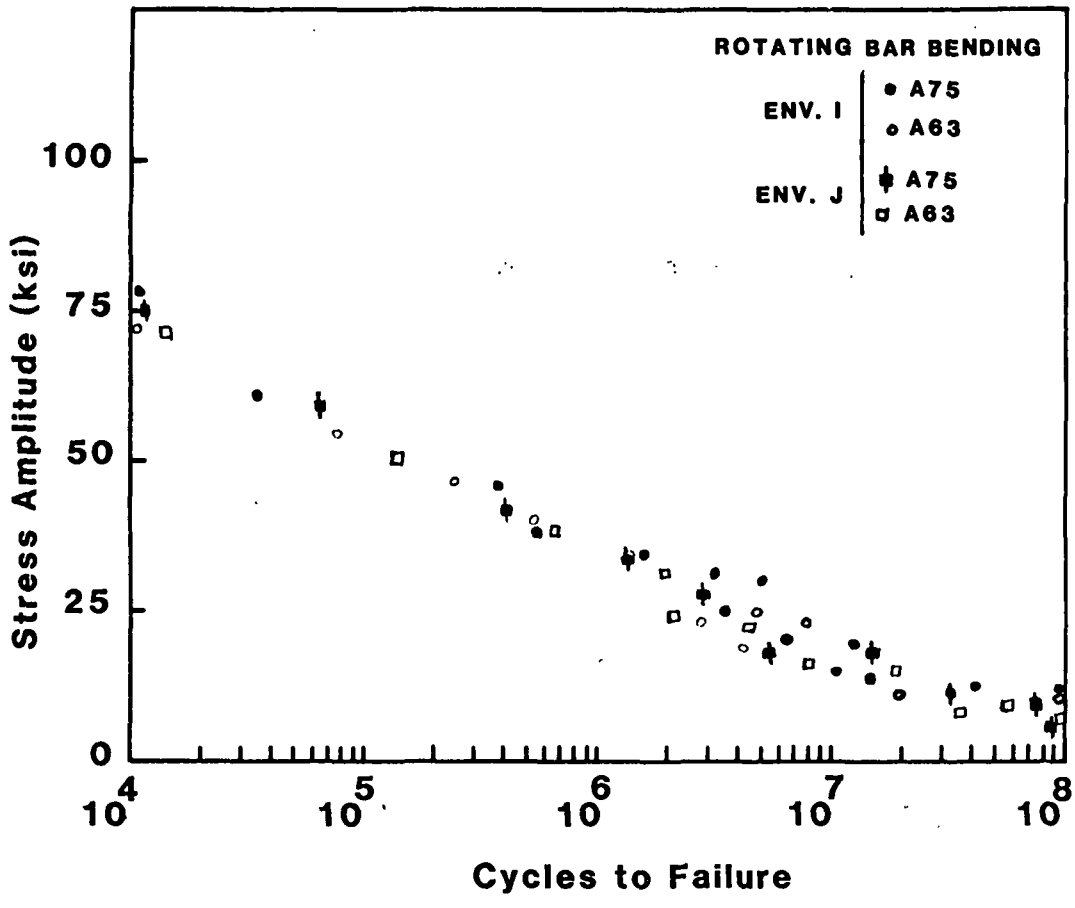

CORROSION FATIGUE LIFETIME

- REDUCTION IN 10^8 CYCLE ENDURANCE LIMIT WITH pH DECREASE
- NO RELATION TO SERVICE PERFORMANCE YET DETECTED

STRESS CORROSION CRACKING

- RESIDUAL STRESSES
- WELDED COUPON EXPOSURE

RESIDUAL STRESS MEASUREMENTS

- HOLE DRILLING METHOD
- RING WELD MORPHOLOGY
- HIGH TENSILE RESIDUAL STRESSES NEAR WELDS
- EXPOSURE OF WELD COUPONS TO SIMULATED WHITE WATERS

WELDED COUPONS

- HIGH RESIDUAL STRESS IN ALL WELDED COUPONS (90 ksi)
- SIGNIFICANT RELAXATION BY STRESS RELIEF ANNEAL
- SIGNIFICANT REDUCTION IN CORROSION BY STRESS RELIEF ANNEAL

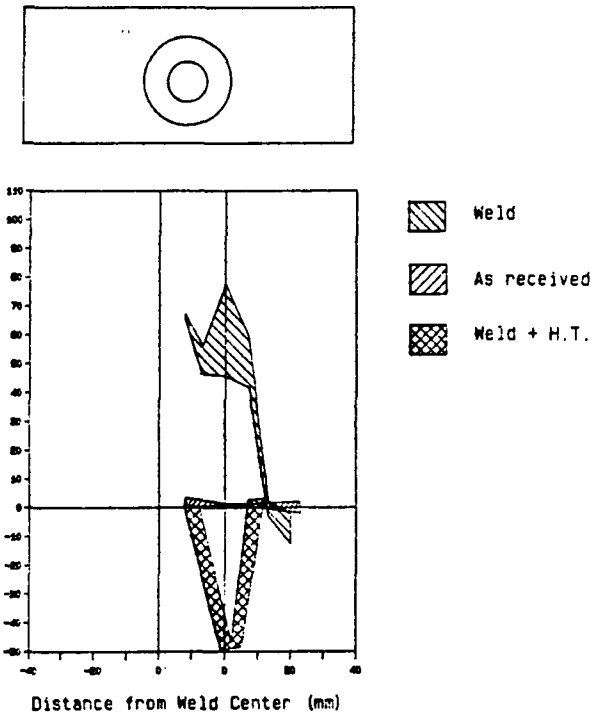

EFFECTS OF WELDS AND POST WELD ANNEALING ON CORROSION

Alloy	No Weld	Weld	Weld + Anneal	Corrosion
VK-A171		X		/
VK-A171		X		/
VK-A378	X			
VK-A378		X		X
VK-A378			X	
3RE60	X			
3RE60		X		X
3RE60			X	
A 75	X			
A 75		X		X
A 75			X	
A 63	X			
A 63		X		
A 63			X	

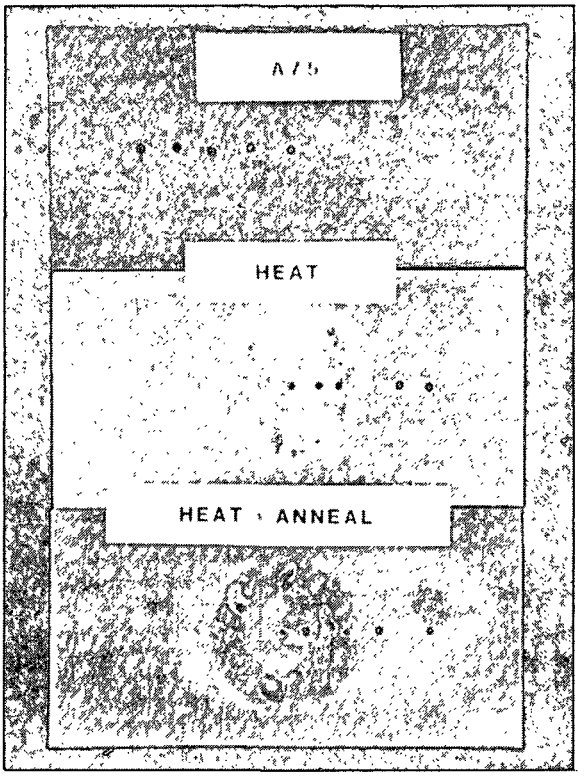
A/5
HEAT
HEAT + ANNEAL

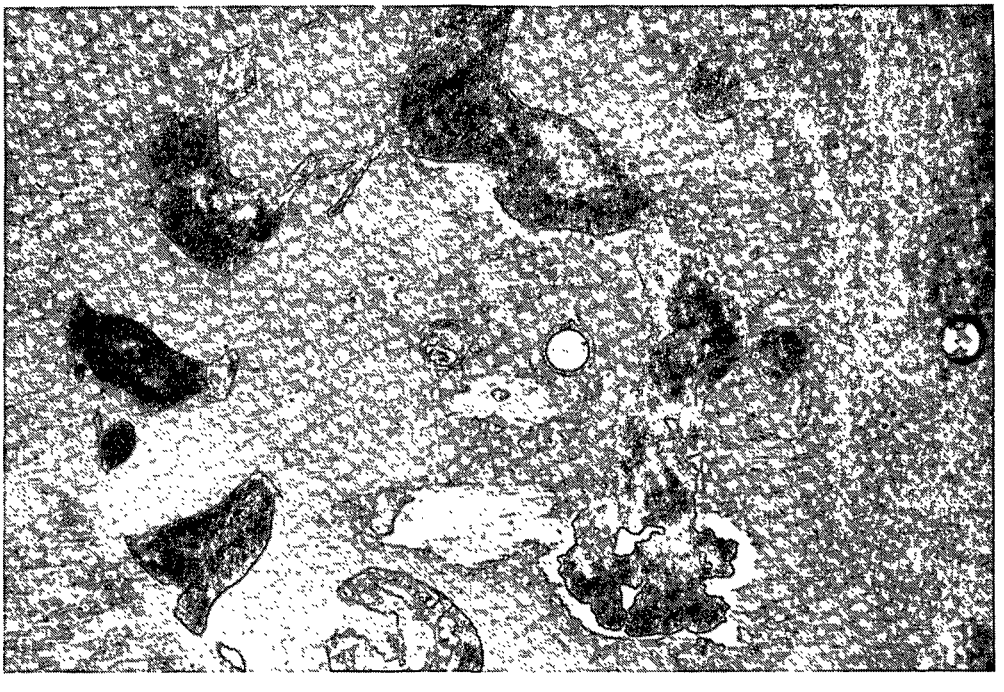

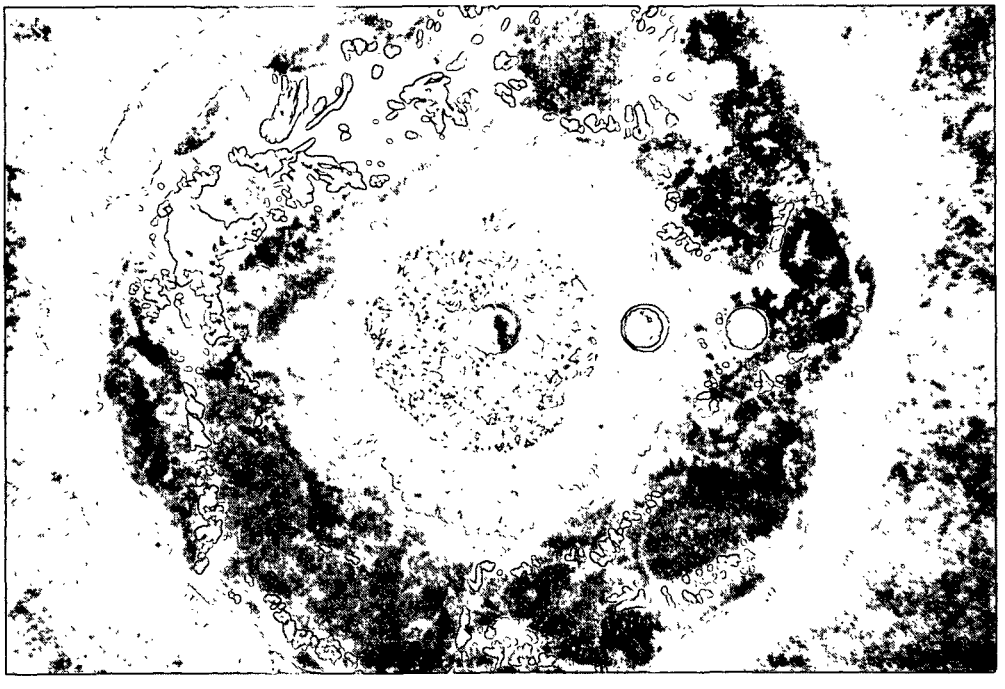

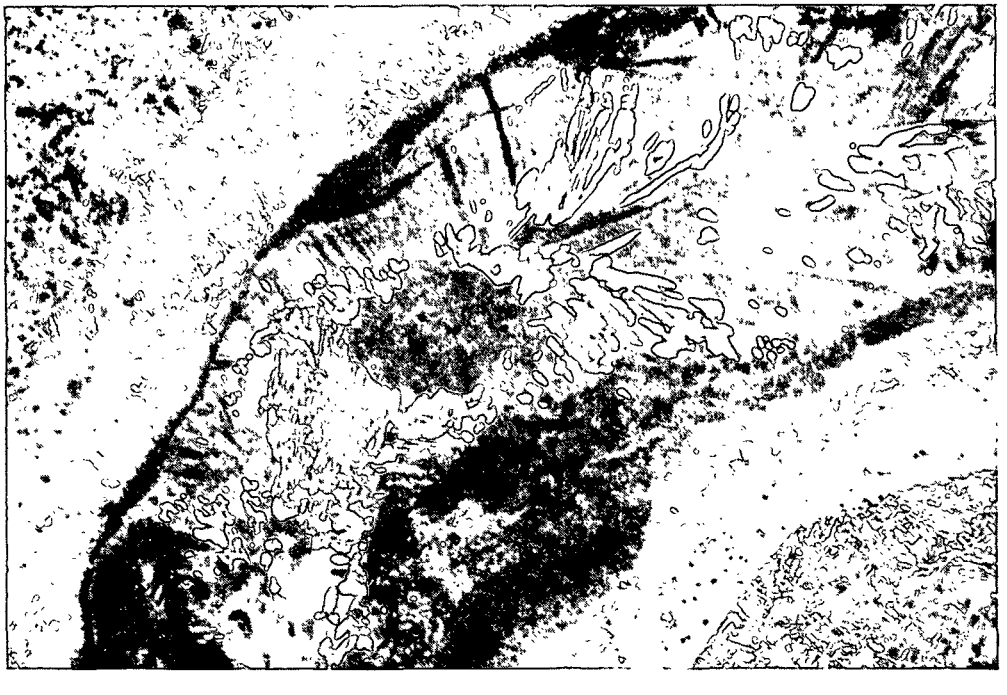

PLANS FOR NEXT PERIOD

- CONTINUED METALLOGRAPHY
- CONTINUED S-N TESTING - OTHER ENVIRONMENTS
  - MEAN STRESS
- RESIDUAL STRESS MEASUREMENTS ON ACTUAL SUCTION ROLLS
- CONTINUE NEAR THRESHOLD FATIGUE TESTING USING A TEST ENVIRONMENT THAT SIMULATES THE ELECTROLYTE IN CREVICE

SIGNIFICANCE TO THE INDUSTRY

- PROGRESS IN IDENTIFYING A PREDICTIVE LABORATORY TEST
- RESOLUTION OF CONCERNS OVER COSMETIC WELDING
- CONFIRMATION OF INADEQUACY OF S-N TESTING AS A PREDICTIVE TECHNIQUE

Project 3556

FUNDAMENTALS OF KRAFT LIQUOR CORROSIVITY

David Crowe

March 29, 1988

PROJECT 3556

FUNDAMENTALS OF KRAFT LIQUOR CORROSIVITY

David C. Crowe

OBJECTIVE

UNDERSTAND CAUSES OF CORROSION OF CARBON STEEL IN KRAFT LIQUOR, AS THE BASIS FOR DEVELOPING METHODS FOR REDUCING CORROSION DAMAGE.

PREVIOUS RESULTS

- QUALIFICATION OF MONITORING METHODS
- DEVELOPMENT OF MICROPROCESSOR BASED DATA ACQUISITION SYSTEM
- LIQUOR CORROSIVITY IS MORE IMPORTANT THAN GRADE OF CARBON STEEL
- FLUCTUATION OF CORROSION RATE COULD NOT BE CORRELATED WITH LIQUOR COMPOSITION CHANGES
- LIQUOR LEVEL CYCLING INCREASED CORROSION RATES
- EFFECTS OF VARIOUS WHITE LIQUOR CONSTITUENTS

Results Since Last Report:

1. Further investigation of effect of velocity using the rotating cylinder electrode and flow loop.
2. Bench testing of improvements to the corrosion monitoring system.
3. Finalization of study of stress corrosion susceptibility of steel in real mill liquor.

CORROSION MONITORING SYSTEM

Objective: Reliability
Ease of Operation
Remote Control

Technique: Microprocessor-based
Linear Polarization Resistance Method

Previous Work: System was designed and used to collect data.

Recently: New hardware and programming have been added so that the system can make measurements, too.

Presently: The system is being tested in the lab.

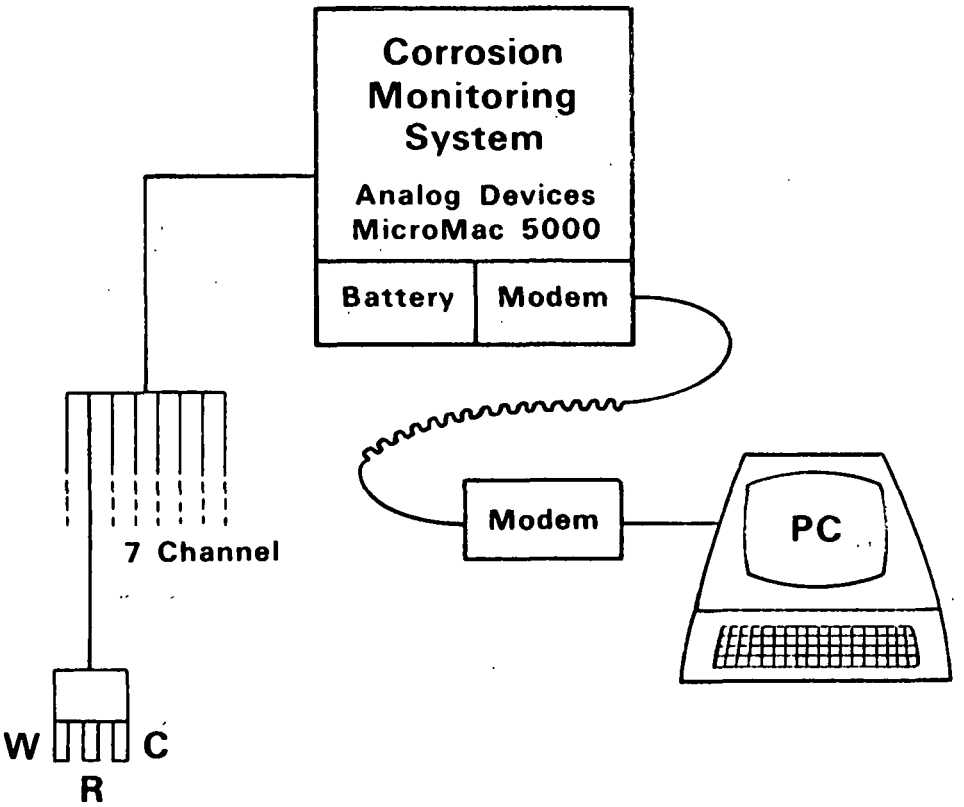

Estimate of Cost for Commercialized Corrosion Monitoring Systems.

Hardware: 7 channel system including MicroMac hardware, modem, card cage, external batteries & NEMA enclosure. $5,000.

Assembly, Software, Initial Support: $10,000.

Total Cost: **$15,000.**

LIQUOR VELOCITY EFFECTS

Objective: To relate corrosion rates to hydrodynamic factors eg. shear, Reynolds number.

Technique: Measure corrosion rates under controlled conditions.

Rotating Cylindrical Electrode

- uniform velocity at surface
- has been demonstrated in corrosion studies
- fluid dynamics established

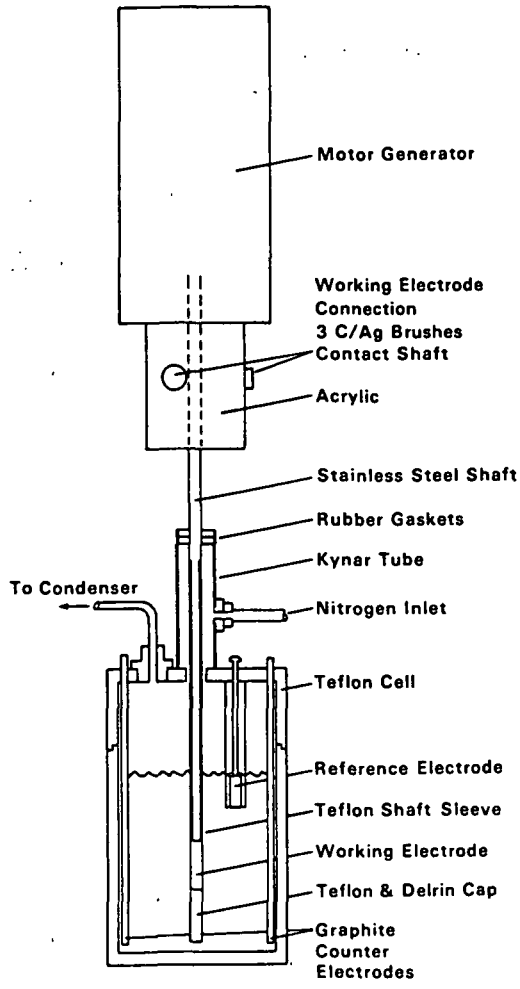

$Re = Vd/\gamma$	A ratio of velocity & viscous forces.
$Sc = \gamma/D$	Diffusion layer thickness.
$Sh = kd/D$	Dimensionless mass transfer.

Fluid Mechanics of the Rotating Cylinder

Three regimes:

Laminar: Very little mass transfer.

Vortex: Intermediate.

Turbulent: $Sh = 0.079\ Re^{0.7}\ Sc^{0.356}$

$$\tau = (f/2)\ \rho\ \omega^2\ r^2$$

Correlation of Rotating Cylinder and Pipe Loop.

$$\log Re_{tube} = 0.67 + 0.833 \log Re_{cyl}$$

Equate the shear, τ

Equate the mass transfer.

Applications to Corrosion Studies

Problems:

- may not be diffusion controlled.
- erosion

Previous Applications:

- inhibitors for pipelines
- steels in sulfuric acid
- Cu/Ni in seawater
- corrosion of ships' hulls

Rotating Cylinder Electrode

Experimental Approach:

1. Measure kinematic viscosity (γ). Calculate Re, τ
2. Measure corrosion rates over a range of potentials.
3. Determine repeatability of tests.
4. Relate corrosion rates to velocity.
5. Compare results with the flow loop.

Results Since Last Report:

1. Tests were performed in 100 g/L NaOH + 30 g/L Na_2S at 1000 rpm over a range of exposure time and temperature. Variations in the corrosion potential confounded the effects of velocity, temperature and time.

Table 1
Results of Preliminary Tests

Exposure time, h	Temperature, C	Wt loss, mpy
24	60	47.8
	70	14.0
	80	44.7
	90	119.1
48	60	45.6
	70	31.9
	80	77.4
	90	65.9
72	60	94.4
	70	53.8
	80	33.5
	90	284.7

Results Since Last Report (cont'd):

2. Corrosion rates at 1000 rpm, at a range of control potentials, showed a dramatic effect of corrosion potential.

Table 2
Corrosion Rate vs. Potential

Corrosion Potential	Corrosion rate
100 mV(SSSE)	7.8 mpy
50	30.5
0	118.0
-50	1786.1
-100	1761.8
-150	196.4
-200	57.5
-250	23.2

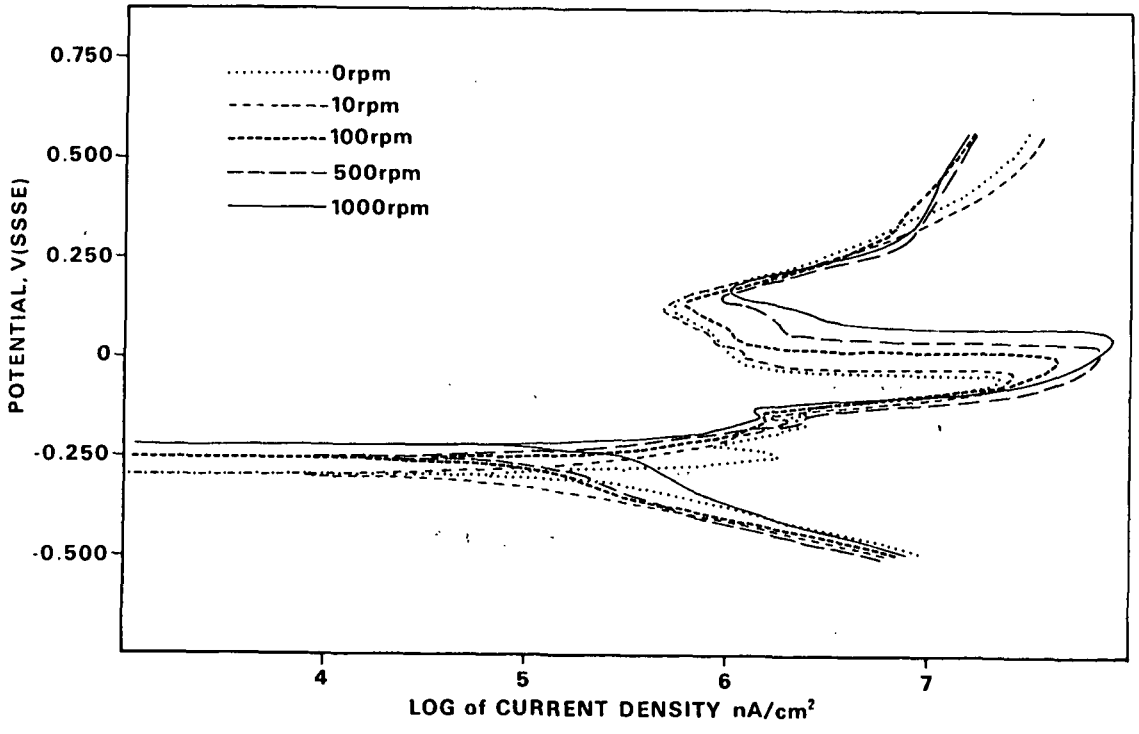

Plans for Next Period:

1. Compare corrosion rates measured with the rotating cylinder electrode and pipe loop.
2. Begin tests of stainless steels (304, 316).

Pipe Flow Loop:

- duplicates flow in mill pipe systems.
- fluid dynamics established.
- must be carefully controlled, cumbersome.

Results Since Last Report:

1. Flow loop has been constructed.
2. Preliminary tests have been run.

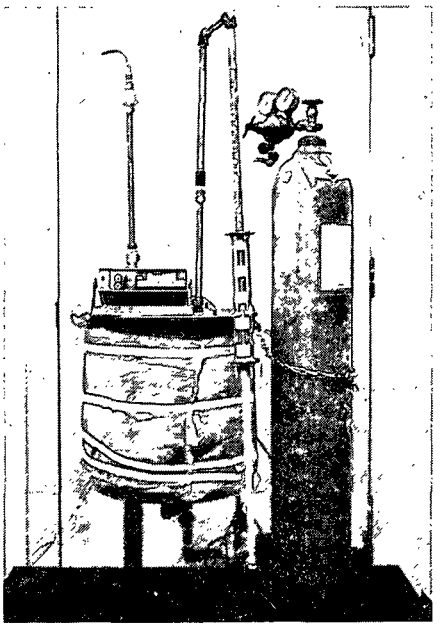

Construction of the flow loop has been completed.

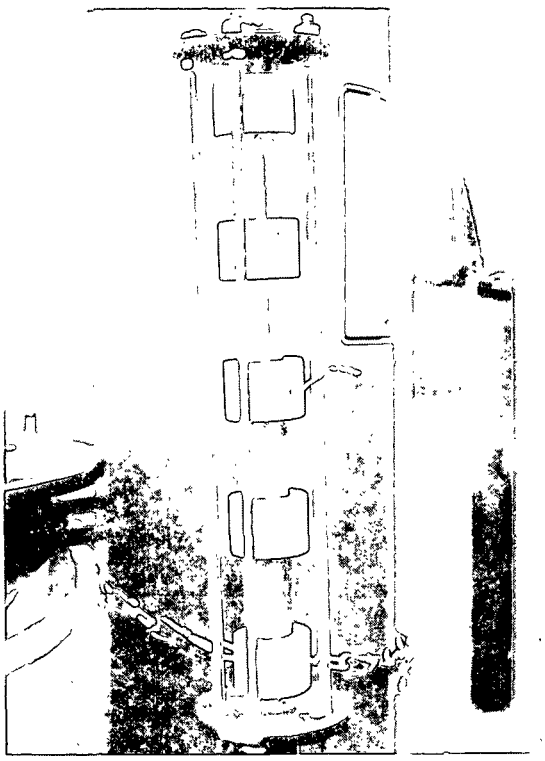

The test section showing the test pieces and the Teflon spacers.

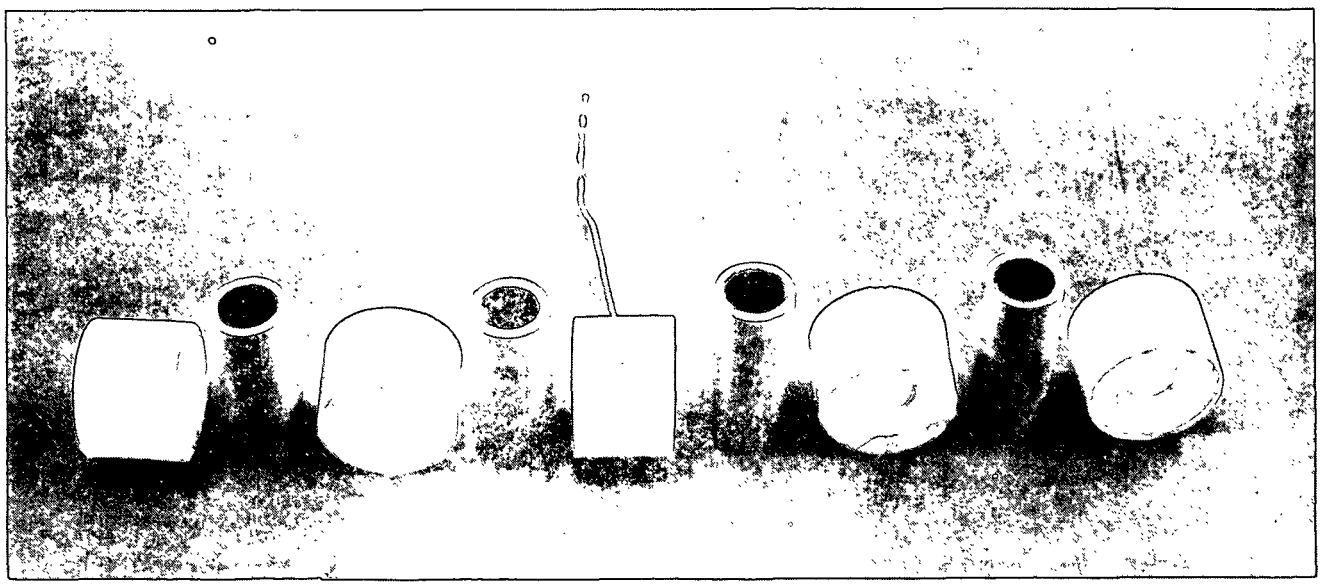

Short pipe sections will be used in the flow loop to measure corrosion rates by weight loss.

Pipe Flow Loop

Future Work

Determine whether corrosion on rotating cylindrical electrodes correlates with pipe flow corrosion.

STRESS CORROSION CRACKING

Objective: To determine the reasons for differences in susceptibility to stress corrosion cracking between digesters.

Technique: Slow strain rate tests of carbon steel in liquors sampled from mills.

The slow strain rate technique:

- Waisted cylindrical tensile specimens are pulled slowly to failure in the environment of interest
- The result:
  Cracking: short test; little reduction in X-section, extensive cracking

  No cracking: long test, ductile failure

The susceptibility to cracking depends on the corrosion potential.

Result - The potential range for cracking varied from mill to mill.

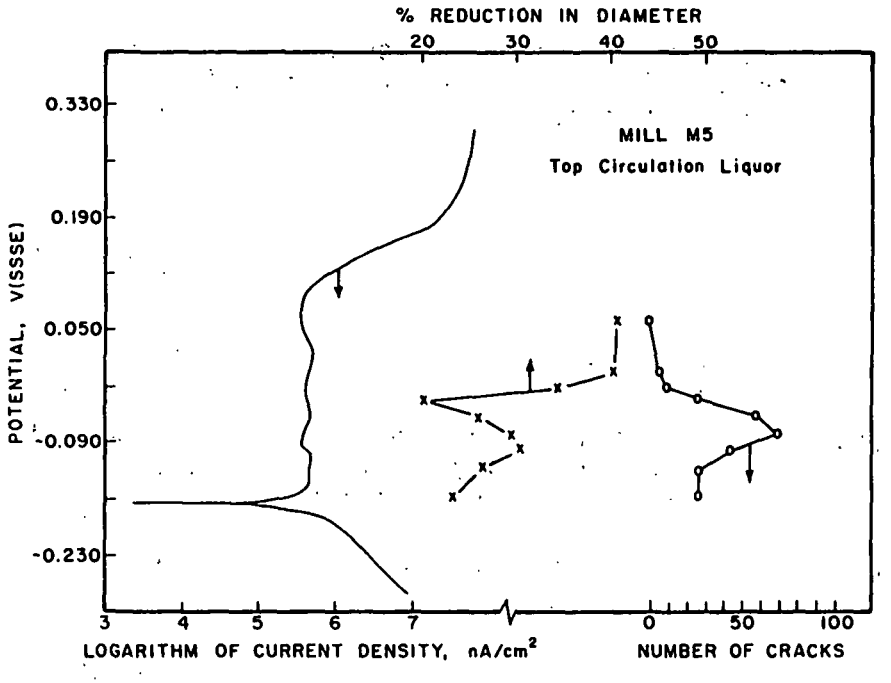
% REDUCTION IN DIAMETER
20
30
40
50
MILL M5
Top Circulation Liquor
0.330
0.190
0.050
-0.090
-0.230
POTENTIAL, V(SSSE)
3
4
5
6
7
0
50
100
LOGARITHM OF CURRENT DENSITY, nA/cm²
NUMBER OF CRACKS

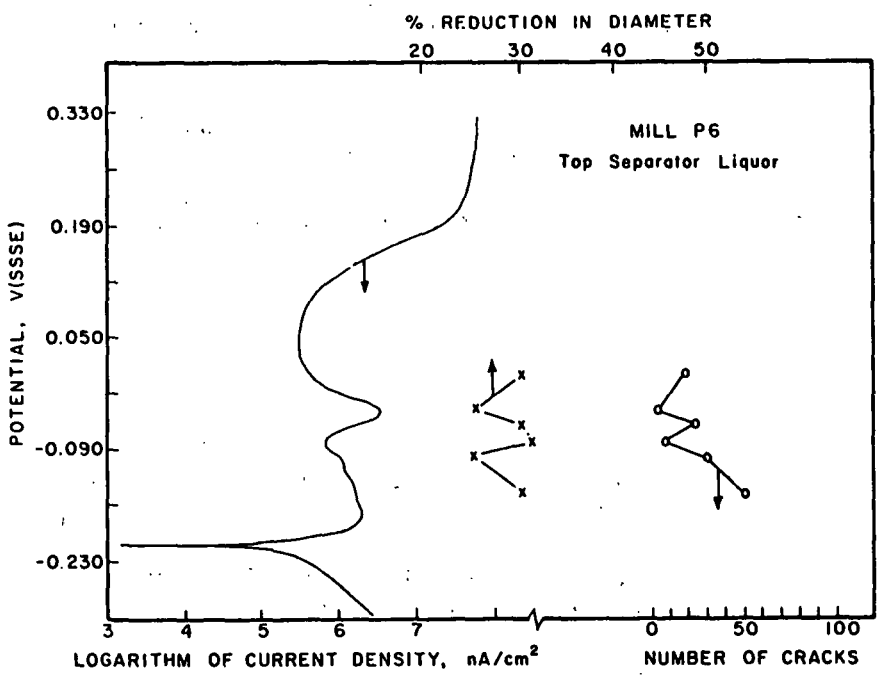
% REDUCTION IN DIAMETER
20
30
40
50
MILL P6
Top Separator Liquor
0.330
0.190
0.050
-0.090
-0.230
POTENTIAL, V(SSSE)
3
4
5
6
7
0
50
100
LOGARITHM OF CURRENT DENSITY, nA/cm²
NUMBER OF CRACKS

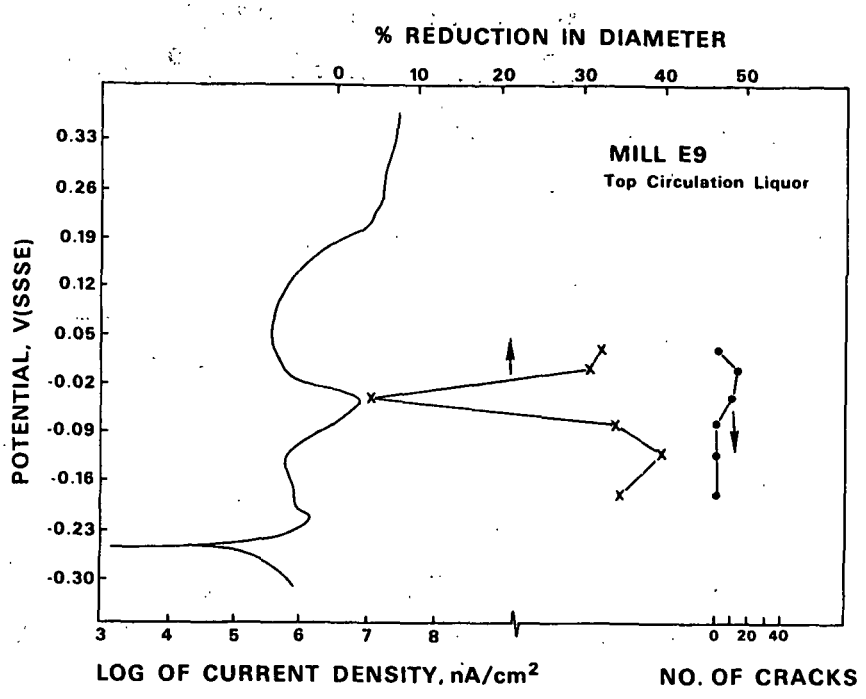
% REDUCTION IN DIAMETER
0
10
20
30
40
50
MILL E9
Top Circulation Liquor
POTENTIAL, V(SSSE)
0.33
0.26
0.19
0.12
0.05
-0.02
-0.09
-0.16
-0.23
-0.30
3
4
5
6
7
8
0
20
40
LOG OF CURRENT DENSITY, nA/cm²
NO. OF CRACKS

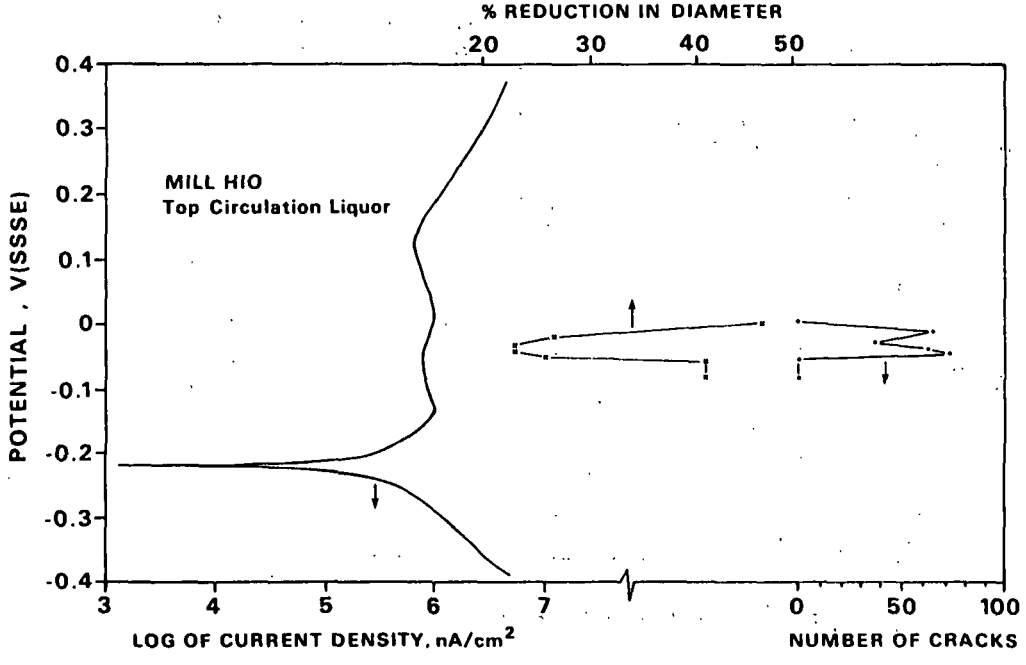
% REDUCTION IN DIAMETER
20
30
40
50
MILL HIO
Top Circulation Liquor
POTENTIAL , V(SSSE)
0.4
0.3
0.2
0.1
0
-0.1
-0.2
-0.3
-0.4
3
4
5
6
7
0
50
100
LOG OF CURRENT DENSITY, nA/cm²
NUMBER OF CRACKS

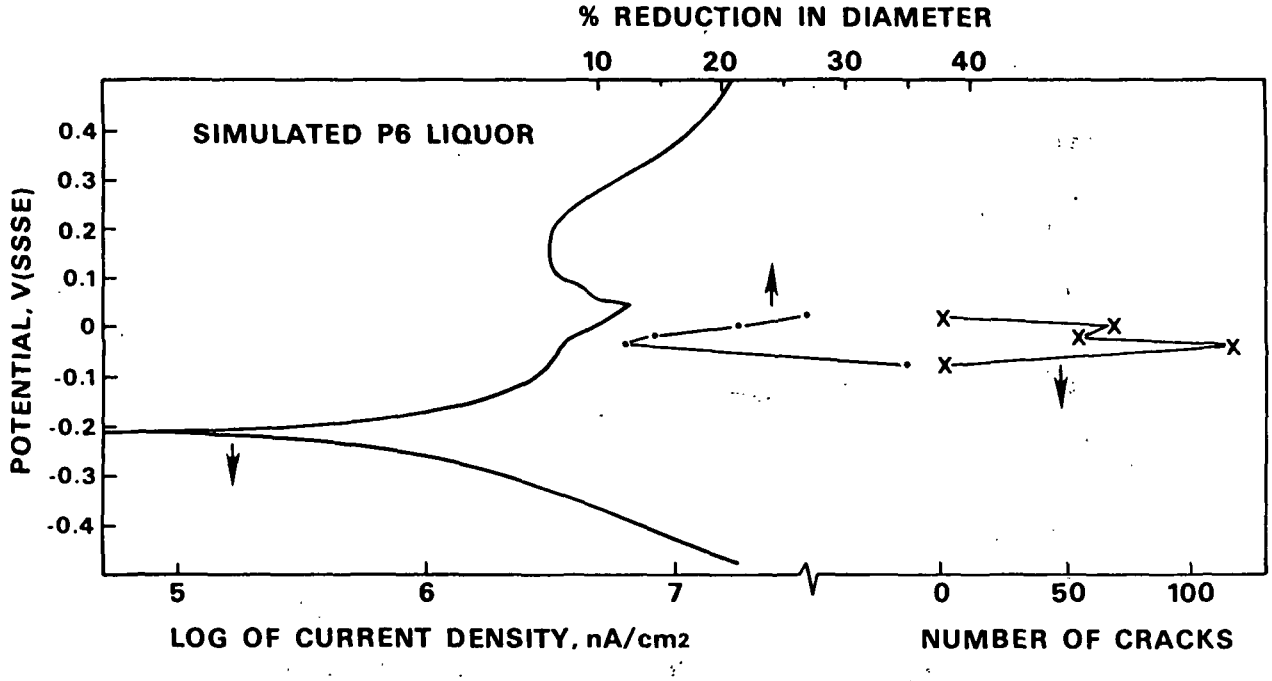
% REDUCTION IN DIAMETER
10
20
30
40
SIMULATED P6 LIQUOR
POTENTIAL, V(SSE)
0.4
0.3
0.2
0.1
0
-0.1
-0.2
-0.3
-0.4
5
6
7
0
50
100
LOG OF CURRENT DENSITY, nA/cm2
NUMBER OF CRACKS

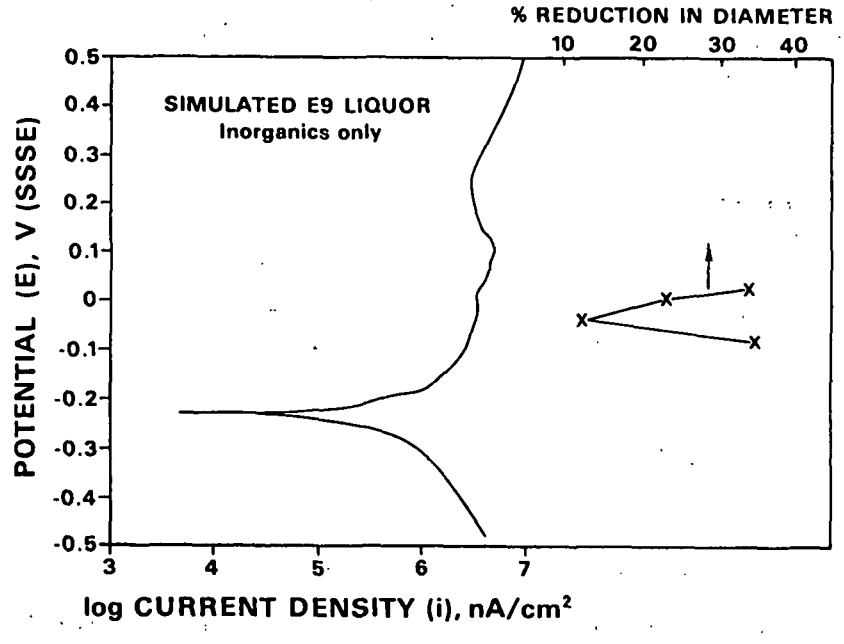
% REDUCTION IN DIAMETER
10
20
30
40
SIMULATED E9 LIQUOR
Inorganics only
POTENTIAL (E), V (SSE)
0.5
0.4
0.3
0.2
0.1
0
-0.1
-0.2
-0.3
-0.4
-0.5
3
4
5
6
7
log CURRENT DENSITY (i), nA/cm²

SLOW STRAIN RATE TESTS:

- Organics in real liquor may have inhibited SC crack initiation.
- Major inorganic species determine the range for cracking, but not necessarily the severity.
- Higher NaOH, Na_2S and $Na_2S_2O_3$ concentrations increase SCC susceptibility and narrow the cracking range.

SIGNIFICANCE TO THE INDUSTRY

- CORROSION MONITORING METHODS MAY BE APPLIED RELIABLY IN WHITE LIQUOR SYSTEMS.
- EFFECTS OF MAJOR LIQUOR CONSTITUENTS ON CORROSIVITY OF WHITE LIQUOR HAVE BEEN DETERMINED.
- SOME OPERATING PARAMETERS WHICH INCREASE CORROSION RATE HAVE BEEN IDENTIFIED.

Project 3470

FUNDAMENTALS OF DRYING

Clyde Sprague

March 29, 1988

Fundamentals of Drying

IMPULSE DRYING

Project 3470
Project 3595

Clyde Sprague

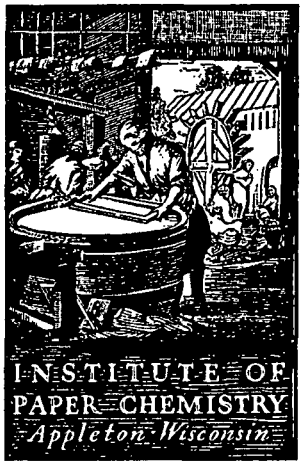

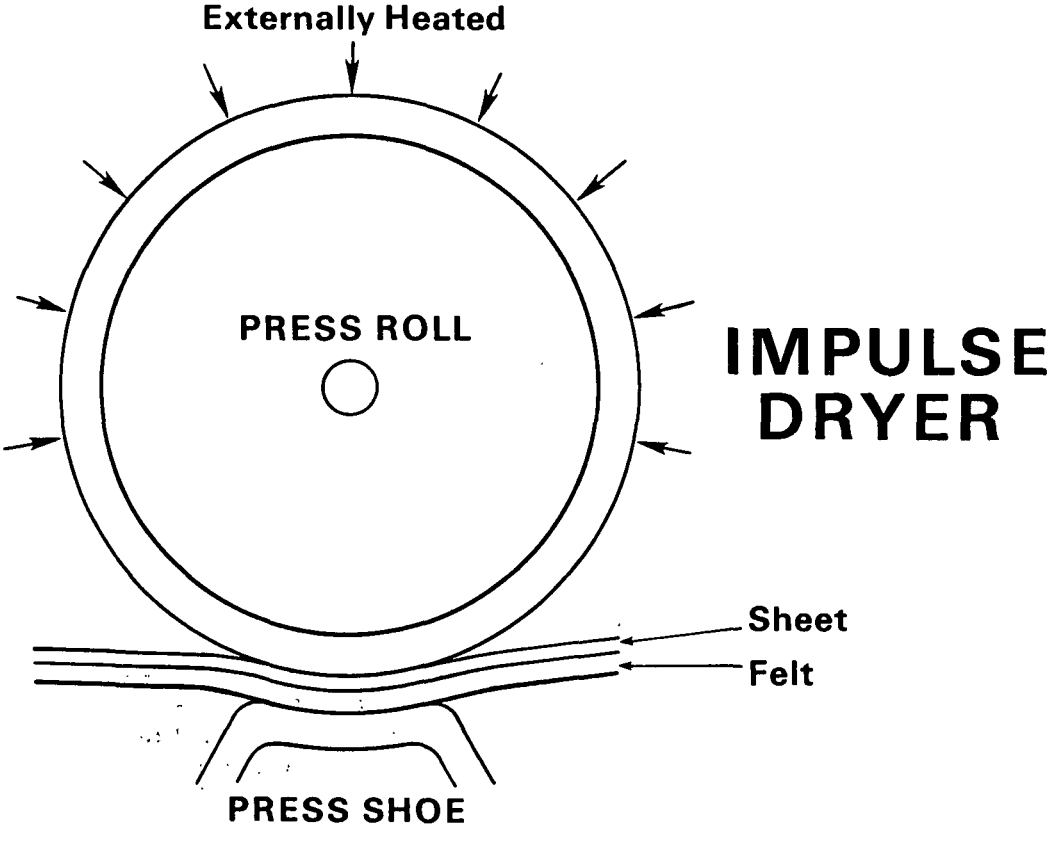

DISCUSSION TOPICS

- OVERALL PROJECT PLAN
- STUDENT WORK
- ROLL DRYER START UP
- ROLL DRYER - 2ND NIP
- CONTRACT WORK
- CONVERSION ISSUES
- FUNDAMENTALS - DELAMINATION

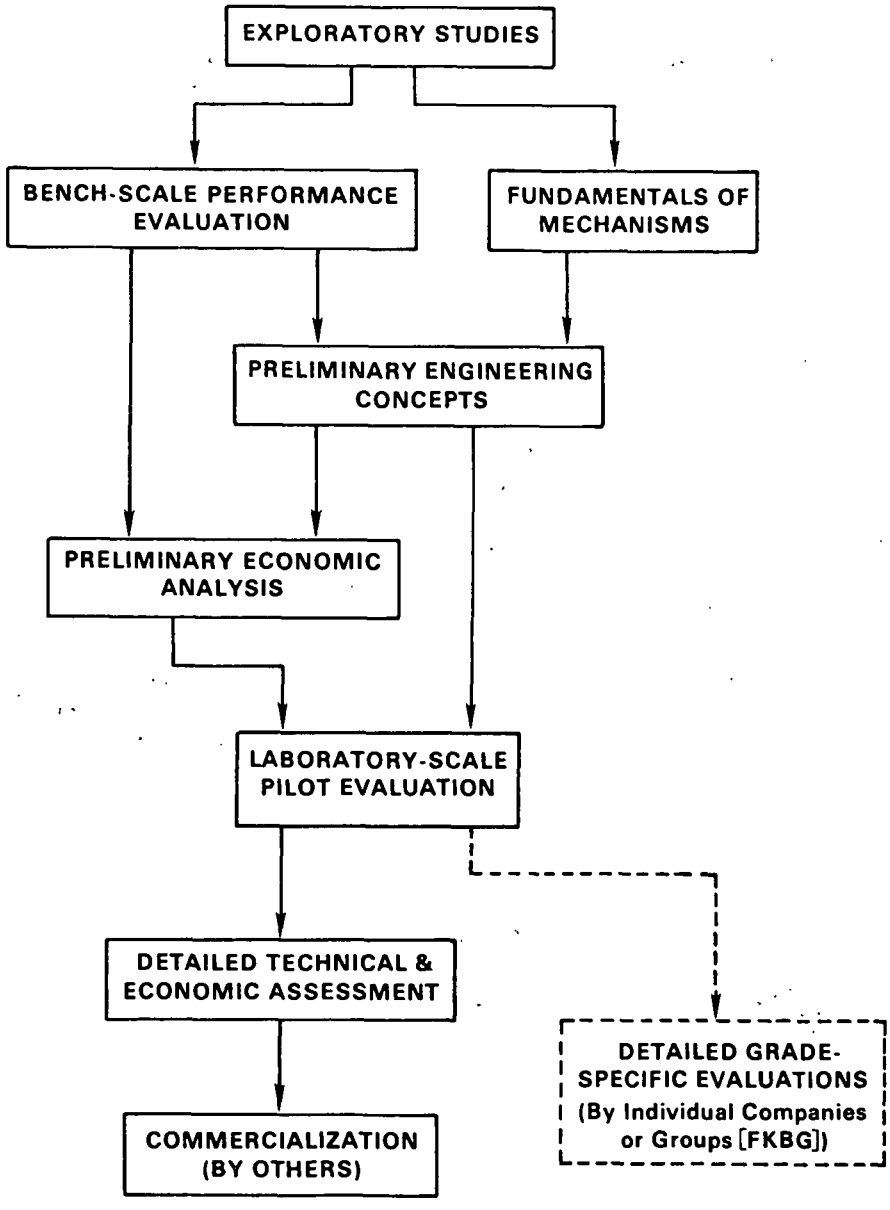

IMPULSE DRYING PROJECT PLAN

STUDENT CONTRIBUTIONS

- RUDEMILLER - BOILING HEAT TRANSFER
- BURNS - EXPANSION PROCESSES

- BARTZ - ECONOMICS
- ARNOLD - DENSITY PROFILES

- SANTKUYL - DELAMINATION
- WADSWORTH - TWO-SIDEDNESS
- ZAVAGLIA - FLASH X-RAYS

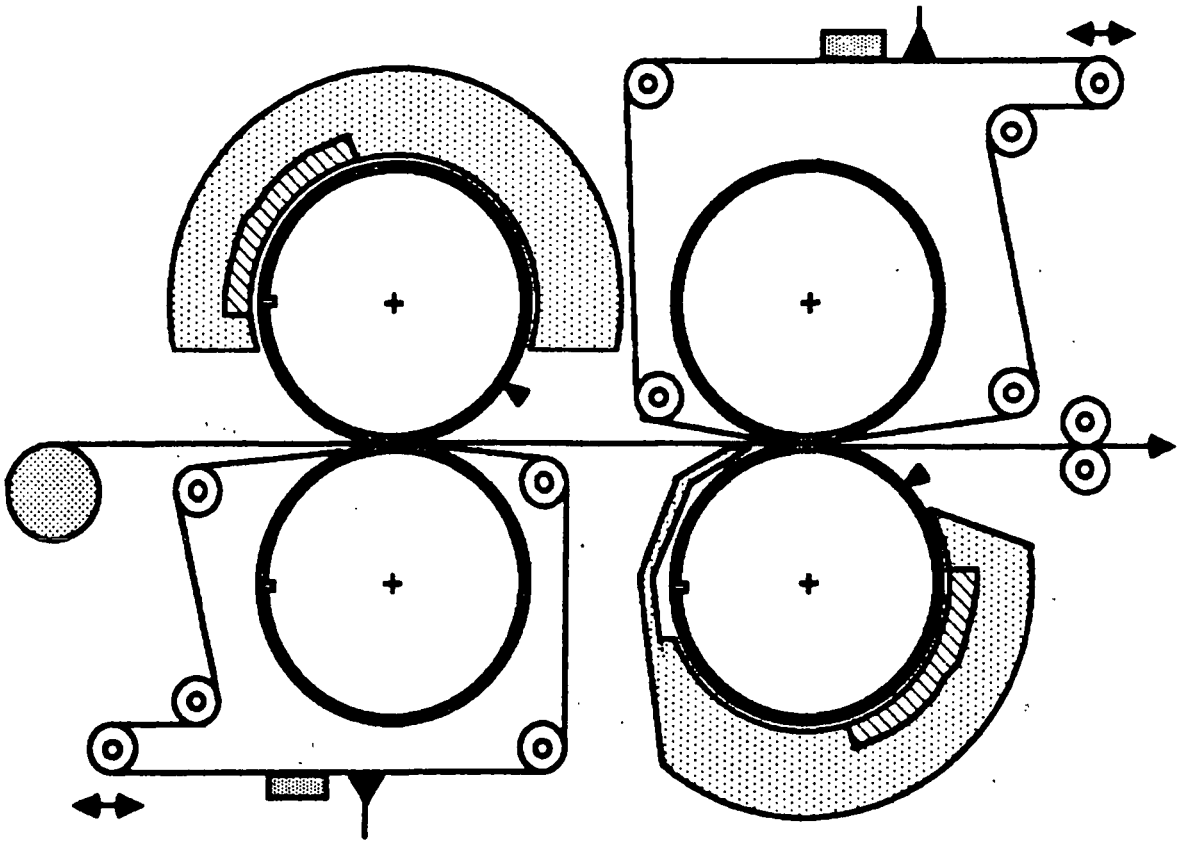

PURPOSES

- DEMONSTRATE CONTINUOUS OPERATION
- ADDRESS ENGINEERING ISSUES
- REALISTIC TWO-SIDED DRYING
- DRYING UNDER TENSION
- MORE REALISTIC SAMPLES FOR PROPERTY TESTS

The laboratory pilot impulse dryer, the next major step in this project, will operate on a continuous basis to provide confidence and valuable information for the commercialization step.

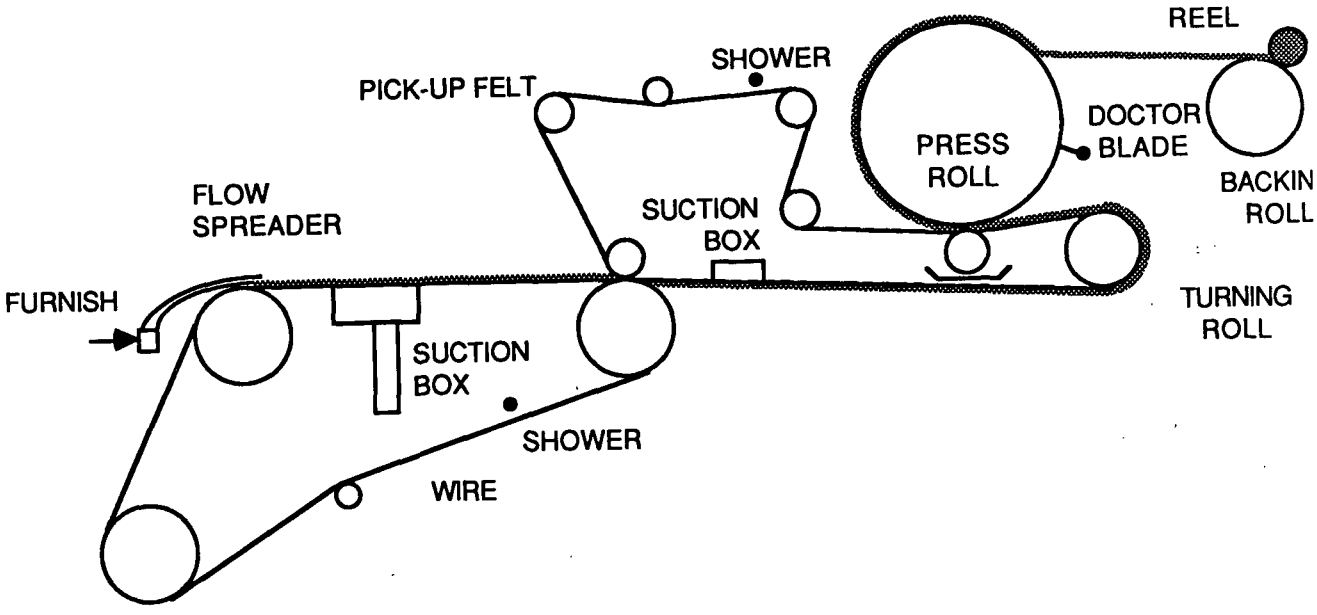

PILOT ROLL IMPULSE DRYER

a - heated roll
b - unheated roll
c - infrared heaters
d - felt drive roll
s - felt guide roll
t - felt tension roll
u - vacuum box
w - water shower
x - paper test sample roll
r - reel
p - unwind drive roll

sl - slitter
wt - web tension sensing roll
sc - sheet sample catch tray

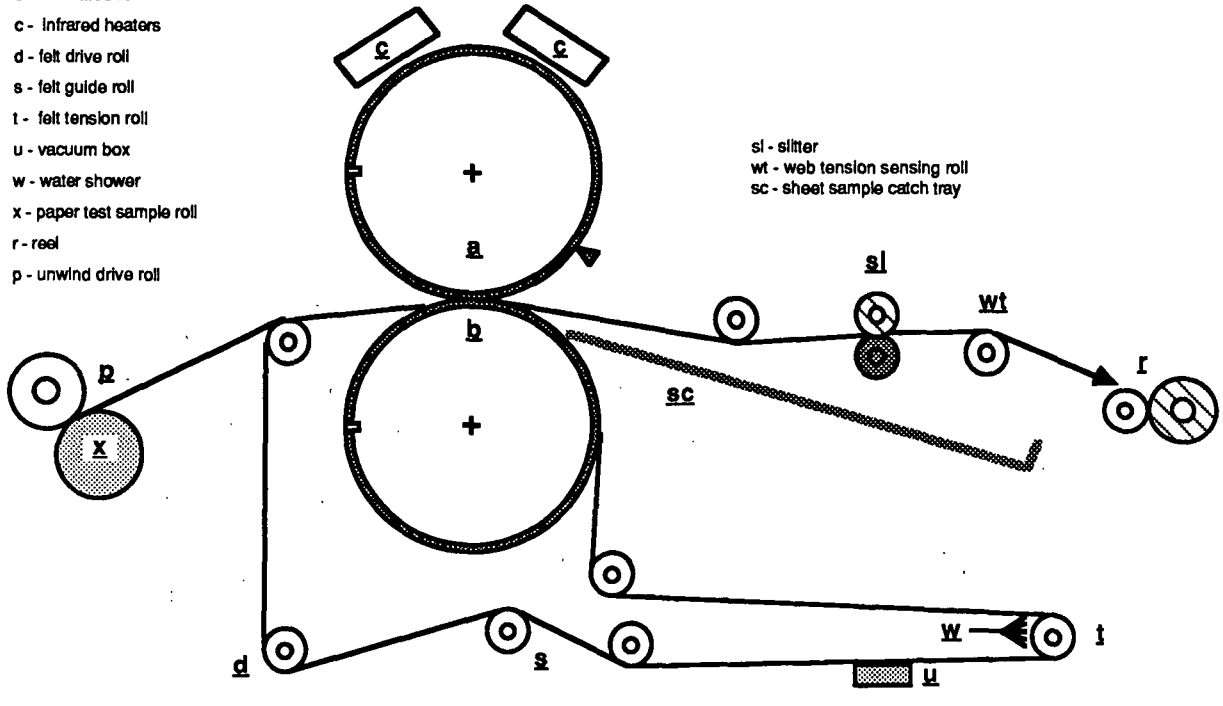

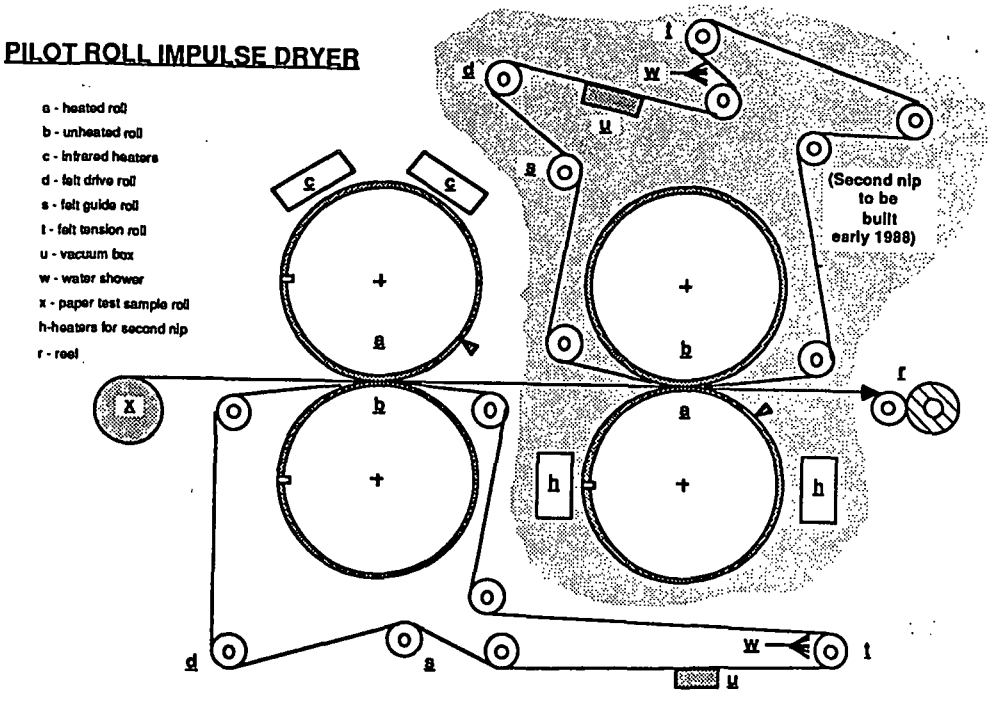

IMPULSE DRYING OF LINERBOARD AND MEDIUM

FKBG PROJECT 2926-11

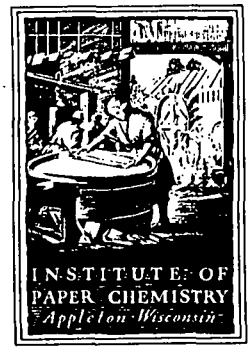

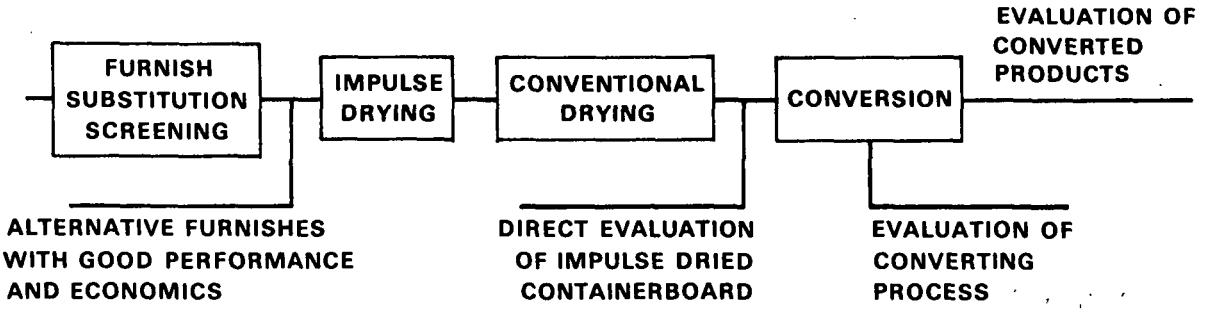

FKBG PROJECT: PHASE II

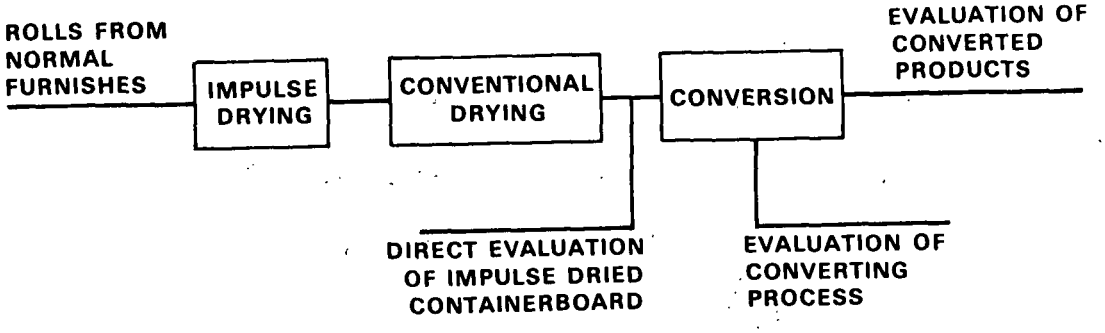

FKBG PROJECT: PHASE I

		MEDIUM		
		Control	50 ms NRT	100 ms NRT
LINER	Control	X	X	X
	50 ms NRT		X	X
	100 ms NRT		X	X

FUTURE SURFACE QUALITY RELATED EXPERIMENTS

MEDIUM: GLUEABILITY

NEWSPRINT: PRINTING QUALITY TESTS

UNCOATED PRINTING PAPER: PRINTING QUALITY

LIGHTWEIGHT COATING RAWSTOCK:
COATING PERFORMANCE
PRINTING QUALITY

(All grades will have water removal, strength performance evaluation as in previous studies)

DELAMINATION

HISTORY OF DELAMINATION OBSERVATIONS

- BURTON'S MS WORK
- ARENANDER - WAHREN
- BURTON'S PhD WORK
- DEVLIN'S PhD WORK
- IPC BENCH-SCALE WORK
- IPC ROLL PRESS WORK
- CONTRACT WORK

IMPLEMENTATION

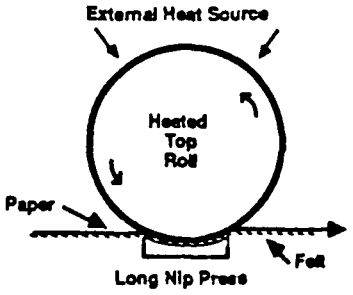

IMPULSE DRYING

MECHANISMS IN NIP

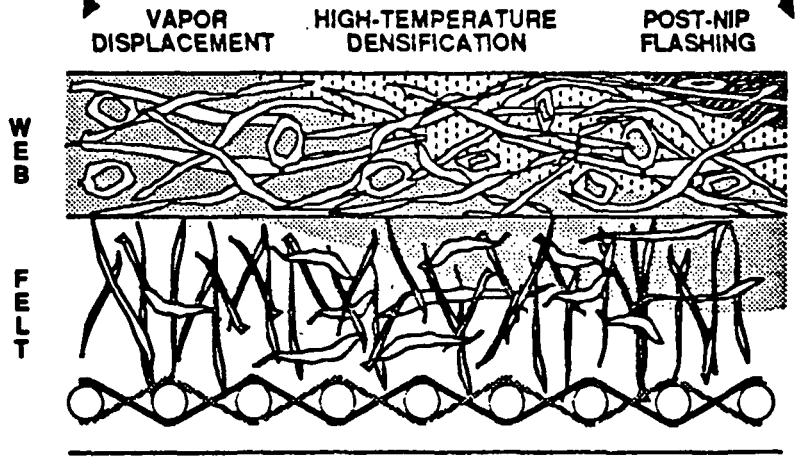

POSSIBLE CONTRIBUTING MECHANISMS

- FLASHING
- ADHESION
- CENTRIFUGAL FORCES

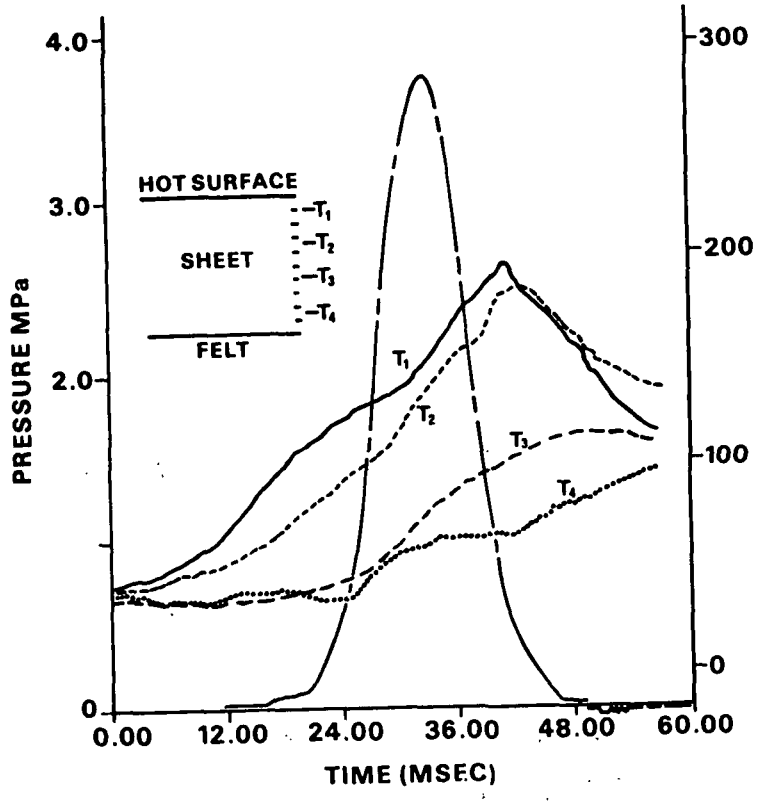

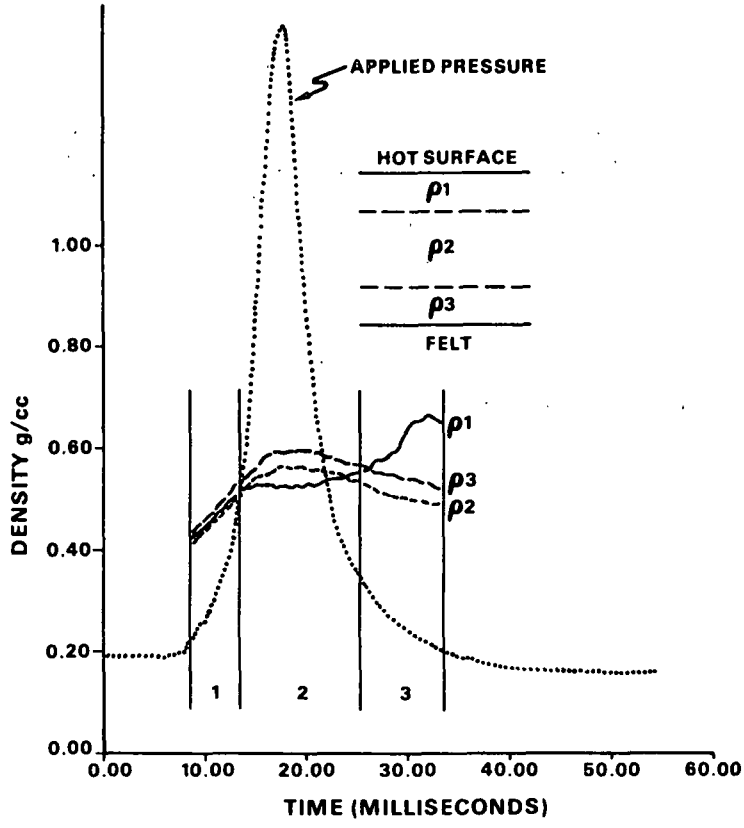

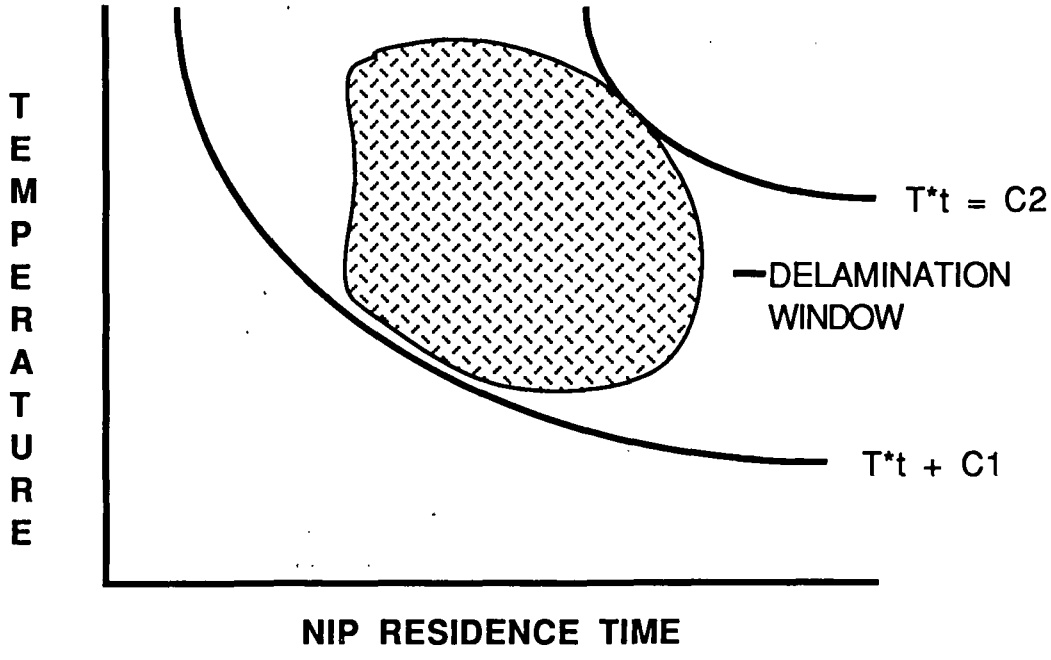

THE CONCEPT OF A DELAMINATION WINDOW

GRADES TESTED TO DATE

LIGHTWEIGHT COATING

WRITING

NEWSPRINT

TISSUE

CORRUGATING MEDIUM

LINERBOARD — VIRGIN KRAFT

— RECYCLED FIBER (100%)

— CMP (74 & 88% YIELD)

HEAT FLUX CONTROL

- HOT SURFACE TREATMENTS
- HOT SURFACE TEMPERATURE
- HOT SURFACE MATERIAL
  - HOMOGENEOUS
  - LAYERED
  - BLENDED
  - GRADIENT

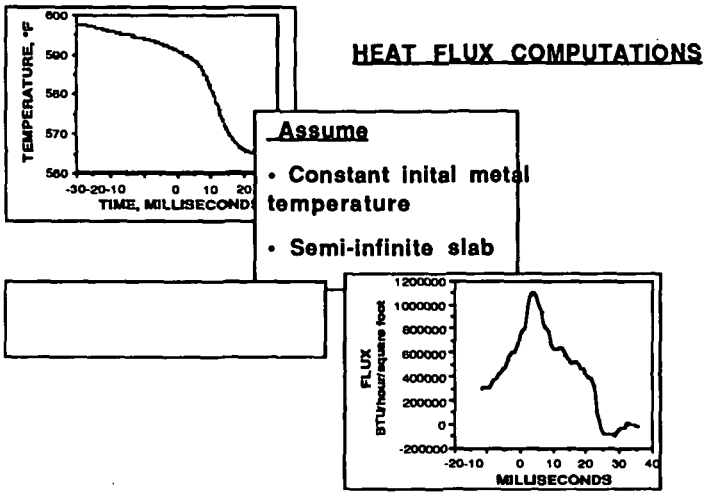
HEAT FLUX COMPUTATIONS
Assume
• Constant inital metal temperature
• Semi-infinite slab
TEMPERATURE, °F
TIME, MILLISECONDS
FLUX BTU/hour/square foot
MILLISECONDS

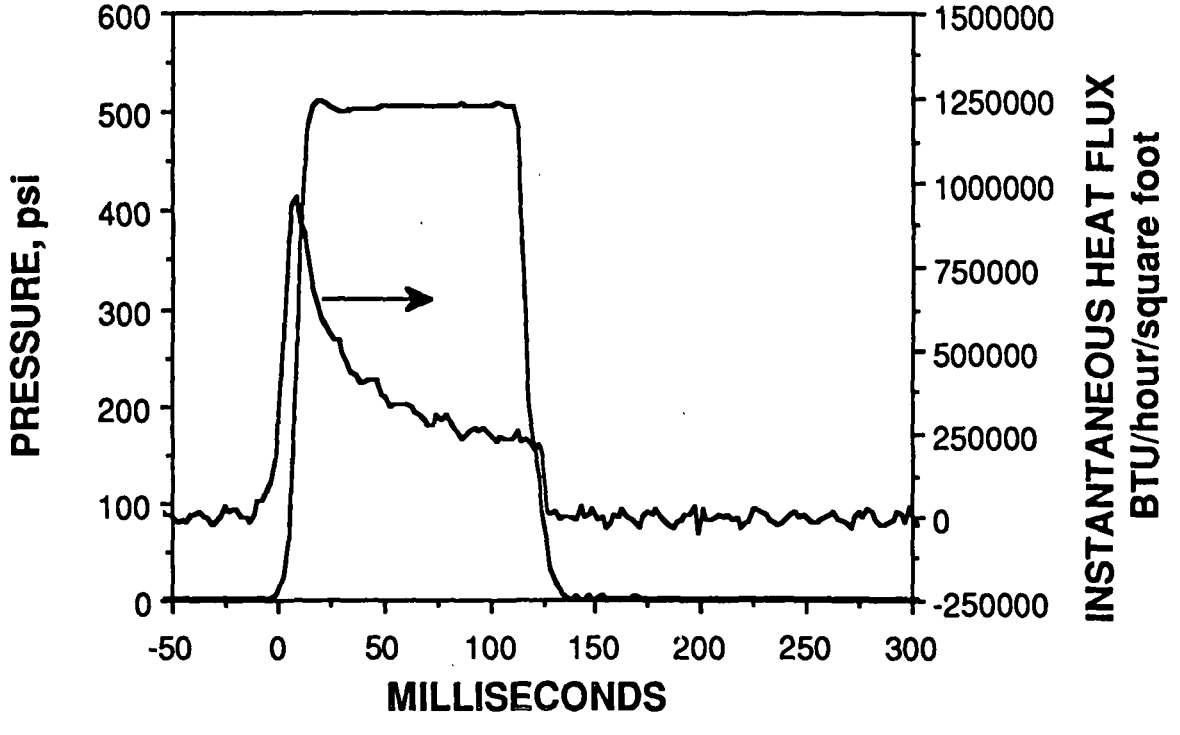
PRESSURE, psi
INSTANTANEOUS HEAT FLUX BTU/hour/square foot
MILLISECONDS
600
500
400
300
200
100
0
1500000
1250000
1000000
750000
500000
250000
0
-250000
-50
0
50
100
150
200
250
300

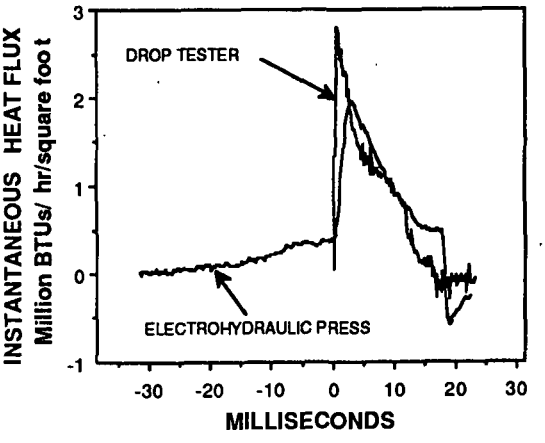
INSTANTANEOUS HEAT FLUX
Million BTUs/ hr/square foot
3
2
1
0
-1
DROP TESTER
ELECTROHYDRAULIC PRESS
-30 -20 -10 0 10 20 30
MILLISECONDS

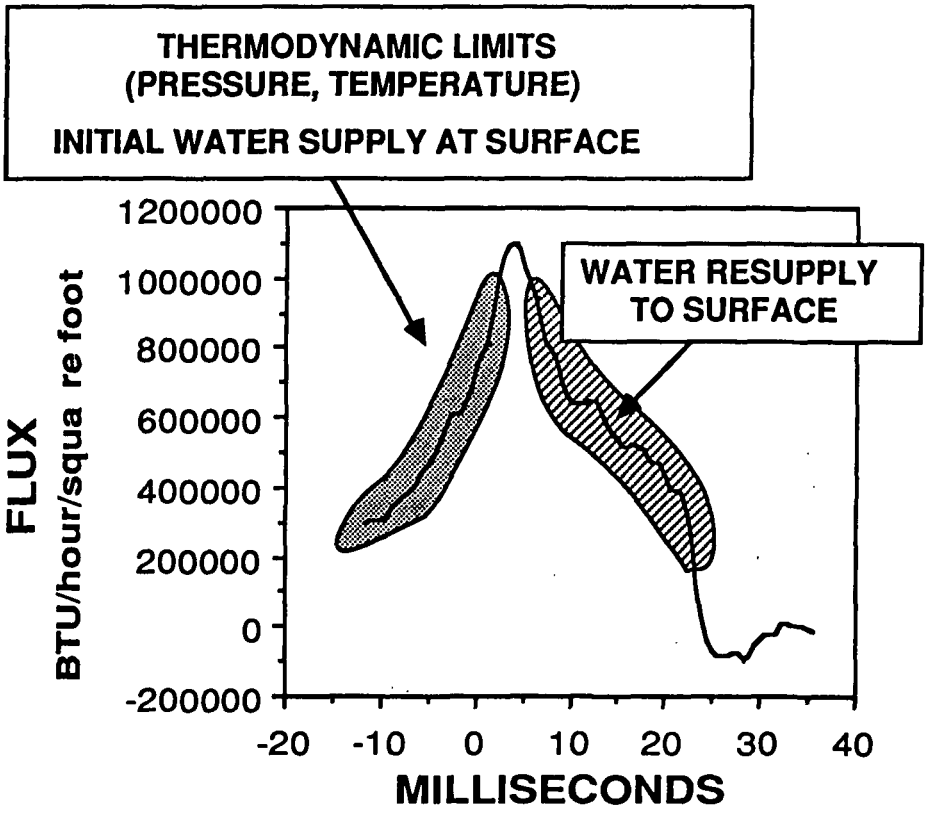
THERMODYNAMIC LIMITS
(PRESSURE, TEMPERATURE)
INITIAL WATER SUPPLY AT SURFACE
WATER RESUPPLY
TO SURFACE
FLUX
BTU/hour/squa re foot
1200000
1000000
800000
600000
400000
200000
0
-200000
-20 -10 0 10 20 30 40
MILLISECONDS

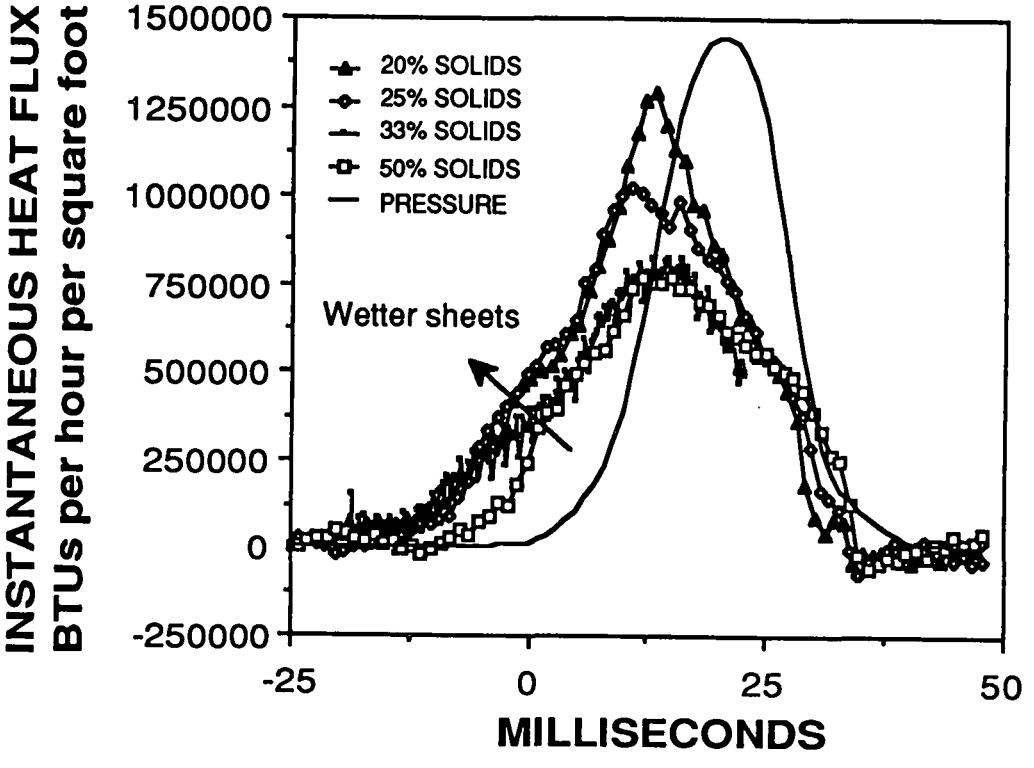

VAPOR RELEASE

- VENTING

RELEASE

- SURFACE TREATMENTS
  - ONE SHOT
  - CONTINUOUS

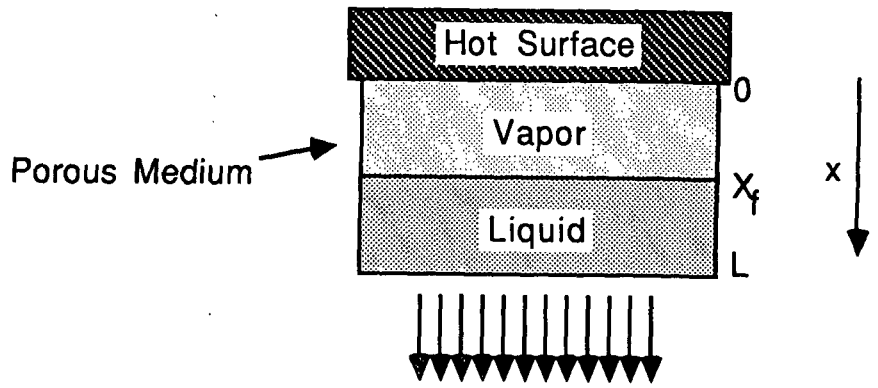

FURNISH EFFECTS

ON

DELAMINATION

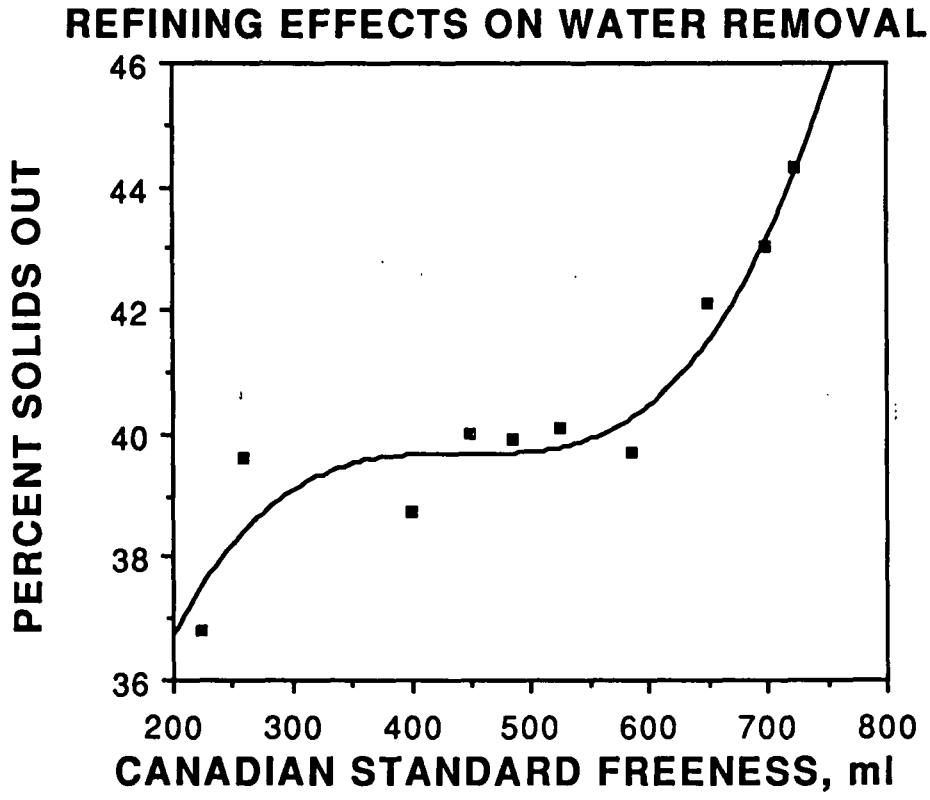
REFINING EFFECTS ON WATER REMOVAL
PERCENT SOLIDS OUT
46
44
42
40
38
36
200
300
400
500
600
700
800
CANADIAN STANDARD FREENESS, ml

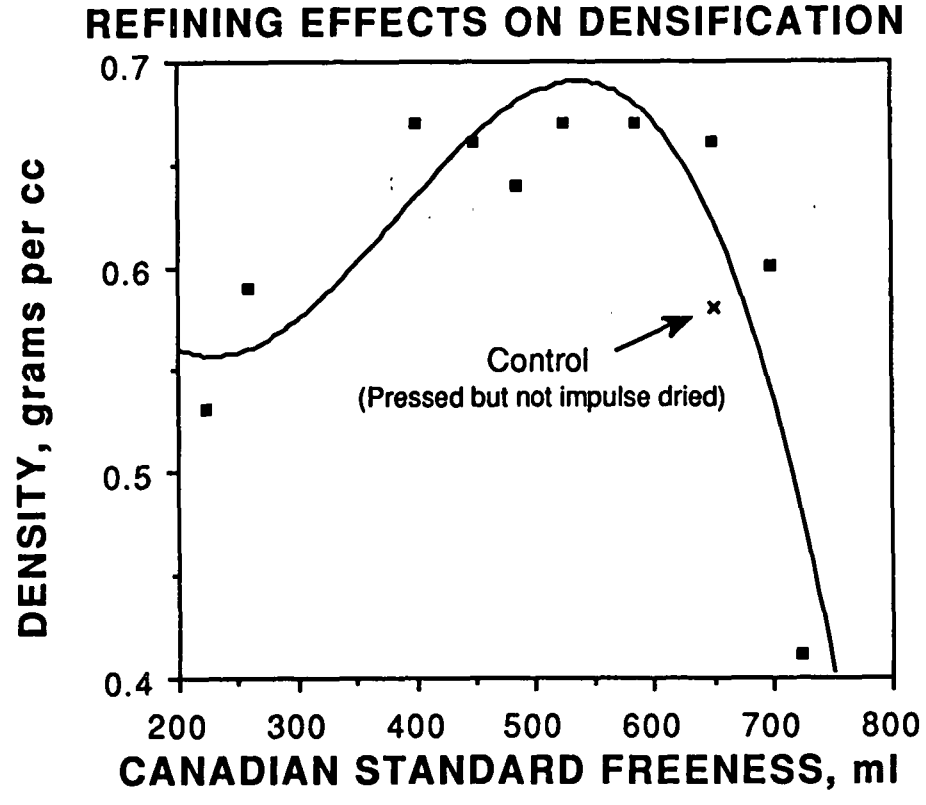
REFINING EFFECTS ON DENSIFICATION
DENSITY, grams per cc
0.7
0.6
0.5
0.4
Control
(Pressed but not impulse dried)
200
300
400
500
600
700
800
CANADIAN STANDARD FREENESS, ml

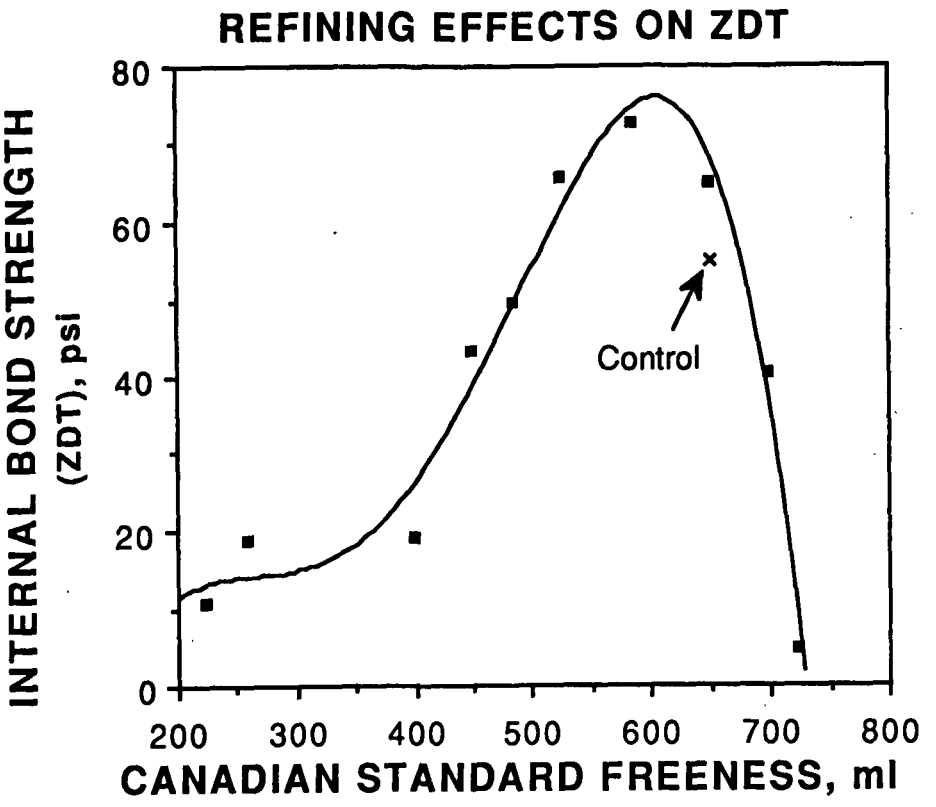
REFINING EFFECTS ON ZDT
INTERNAL BOND STRENGTH (ZDT), psi
80
60
40
20
0
Control
200
300
400
500
600
700
800
CANADIAN STANDARD FREENESS, ml

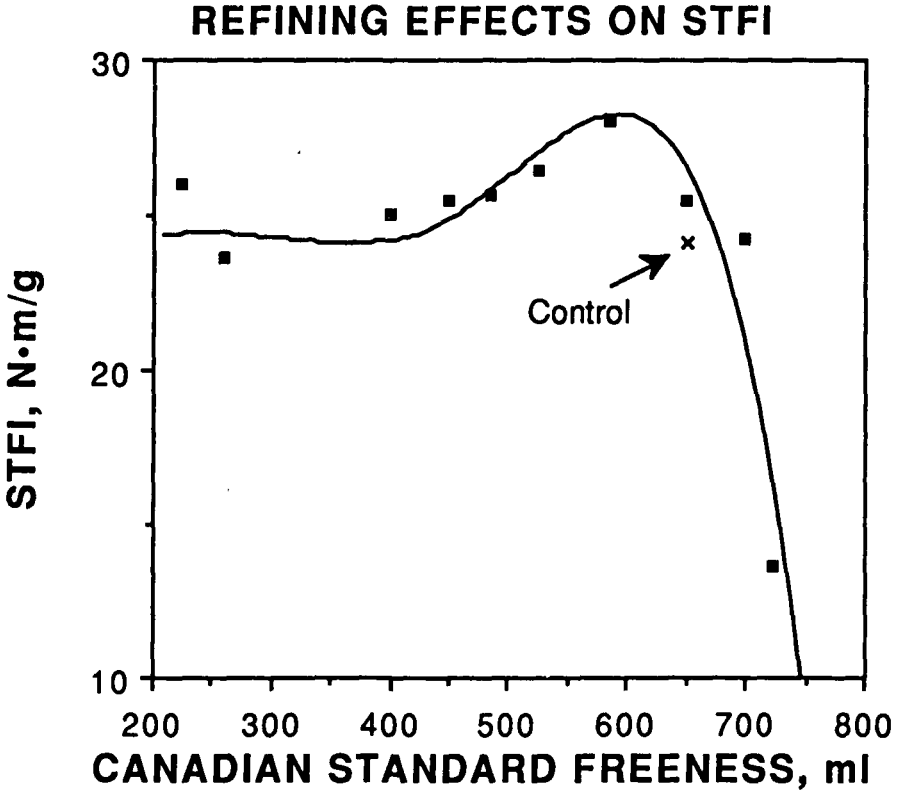
REFINING EFFECTS ON STFI
STFI, N•m/g
30
20
10
Control
200
300
400
500
600
700
800
CANADIAN STANDARD FREENESS, ml

FACTORS TO BE INVESTIGATED

- HEAT FLUX CONTROL
- VAPOR RELEASE
- ADHESION - RELEASE
- FURNISH ISSUES
    - FURNISH TYPE
    - FURNISH CHARACTERIZATION
    - REFINING - FINES RETENTION
    - BASIS WEIGHT
- OPERATING CONDITIONS

MEASUREMENTS

- STFI - AS A DETECTOR
- OTHER SHEET PROPERTIES
- WATER REMOVAL
- HEAT FLUX
- INTERNAL TEMPERATURES
- INTERNAL COMPRESSION
- X-RAY RADIOGRAPHY
- PERMEABILITIES
- WRV

PLANS FOR NEXT SIX MONTHS

- CONCENTRATE ON DELAMINATION
- FINISH SECOND NIP
- BEGIN TWO-SIDED TESTS
- CONTINUE CONVERSION TESTS
- REDUCE CONTRACT LOAD

Project 3480

DISPLACEMENT DEWATERING

Jeff Lindsay

March 29, 1988

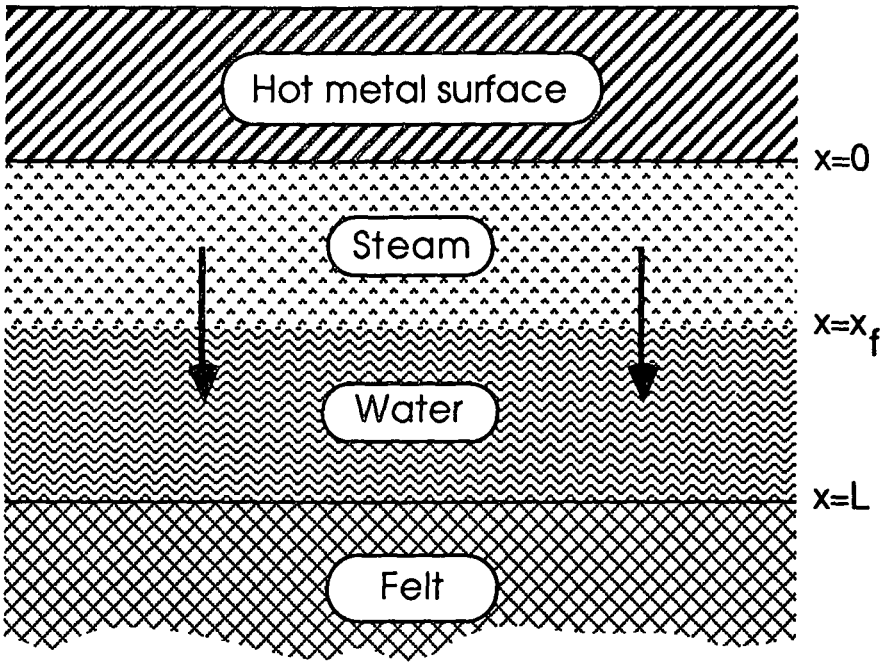

Displacement in paper during impulse drying.

Moving Interface Problems in Porous Systems

- MIPPS -

Unusual Features:

- Transient flow with changing physical properties
- Simultaneous heat, mass, and momentum transfer
- Expanding gas phase (compressible flow)
- Two phases coupled with a moving interface
- Interface location changes with each time step
- Interface temp., pressure, and velocity are unknown
- Wicking allowed to occur: heat pipe mechanism

Moving Interface Problems in Porous Systems
- MIPPS -

Numerical Approach:

- Fully implicit
- Staggered grid structure
- Moving, nonuniform grids (denser near interface)
- Cubic spline interpolation
- Compressible form of SIMPLE pressure corrections
- Under-relaxation on variables and interface conditions
- Gas and liquid phases solved sequentially
- Coupling achieved iteratively
- Interface equilibrium maintained at each time step

MODIFICATIONS TO MIPPS:
REVIEW OF THE SHARP FRONT APPROXIMATION

1. While often used in displacement studies, the sharp front approximation is not rigorously correct. Smooth curves of variable saturation exist.

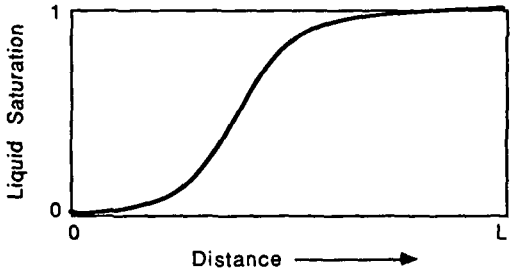

2. For phase-change processes in porous media, the sharp front approximation becomes realistic at high values of heat flux.

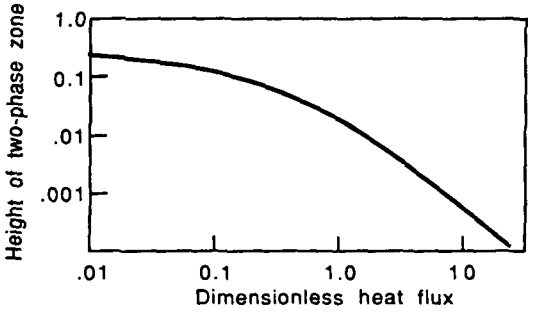

Dimensionless height of two-phase zone versus heat flux. From experimental data of Udell, 1983.

3. For displacement with low rates of heat transfer, MIPPS must account for a broad two-phase region without a sharp moving boundary. This is now being done.

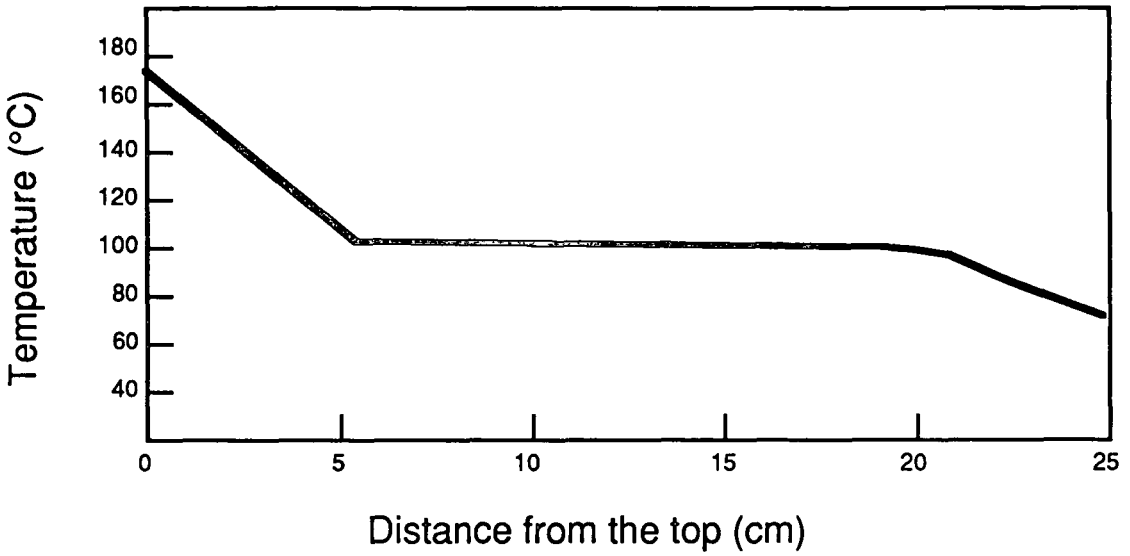

Temperature profile of 65-100 mesh Ottawa sand: porosity of 0.38, average saturation on 0.51, heat flux of 1510 W/m^2. From K. S. Udell, J. Heat Transfer, 105: 485-492 (1983).

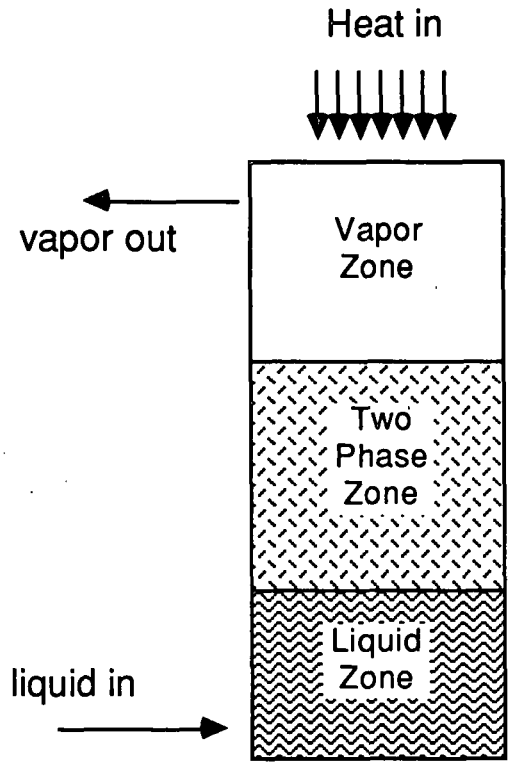

Udell's experimental apparatus showing various zones.

MIPPS Predictions

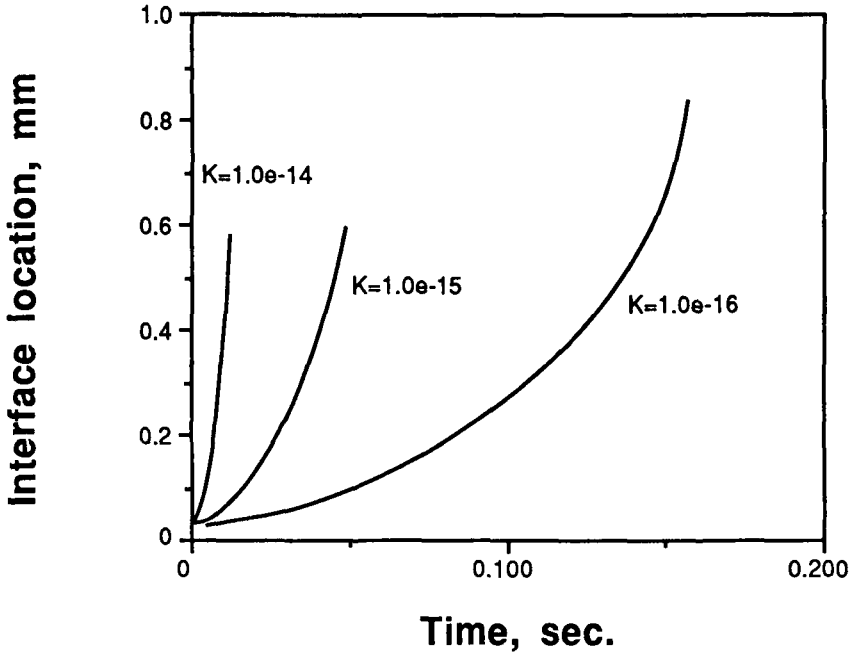

Interface movement in three MIPPS predictions with different permeabilities. Each case used a surface temperature of 600°K, an effective pore radius of 5.0μm, a sheet thickness of 1 mm, and a water resupply rate of 0.5 kg/sm^2.

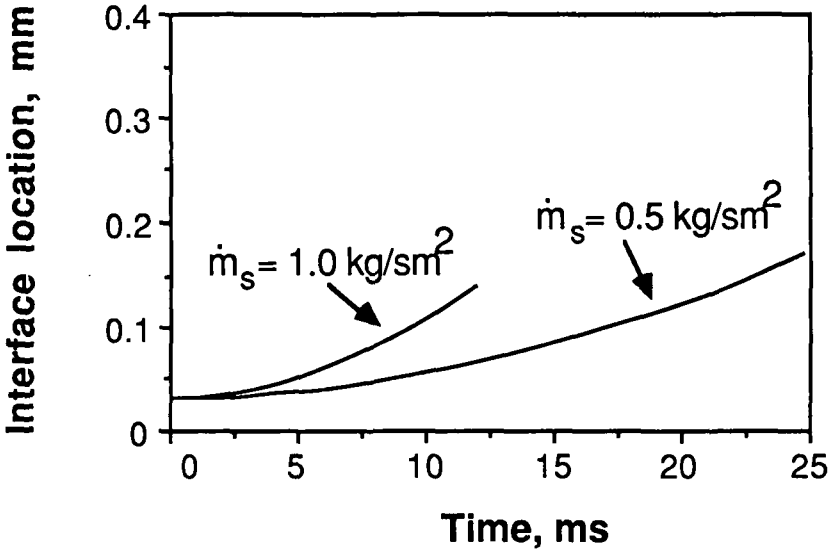

Effect of water resupply rate to surface on interface motion in MIPPS predictions. Permeability was 1.0x10^{-15}m^2; surface temperature was 600°K; and the effective pore radius was 5.0 μm.

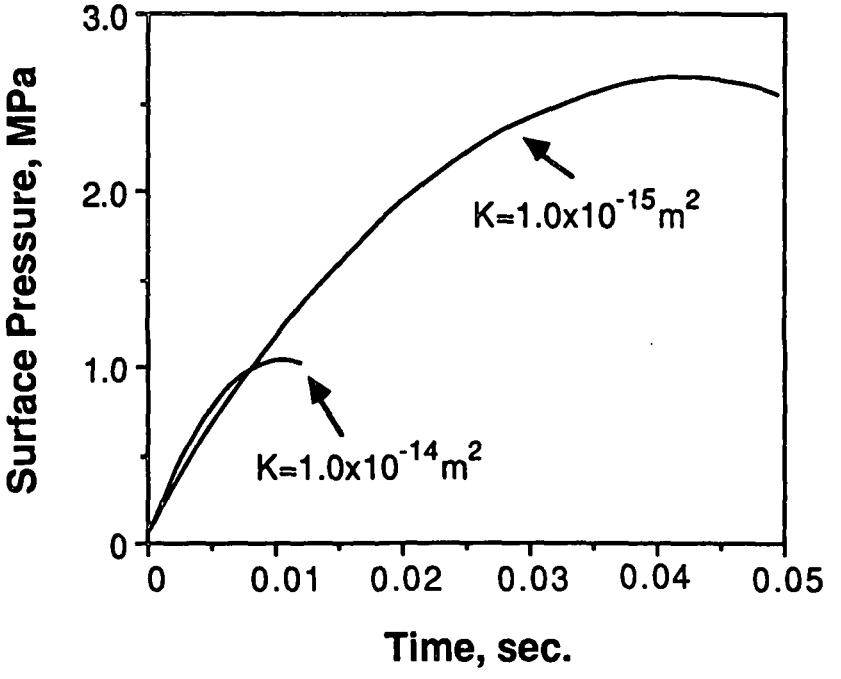

Effect of permeability on gas-phase pressure development. Reflux ratio was 0.5 kg/sm^2, and the effective pore radius was 5µm.

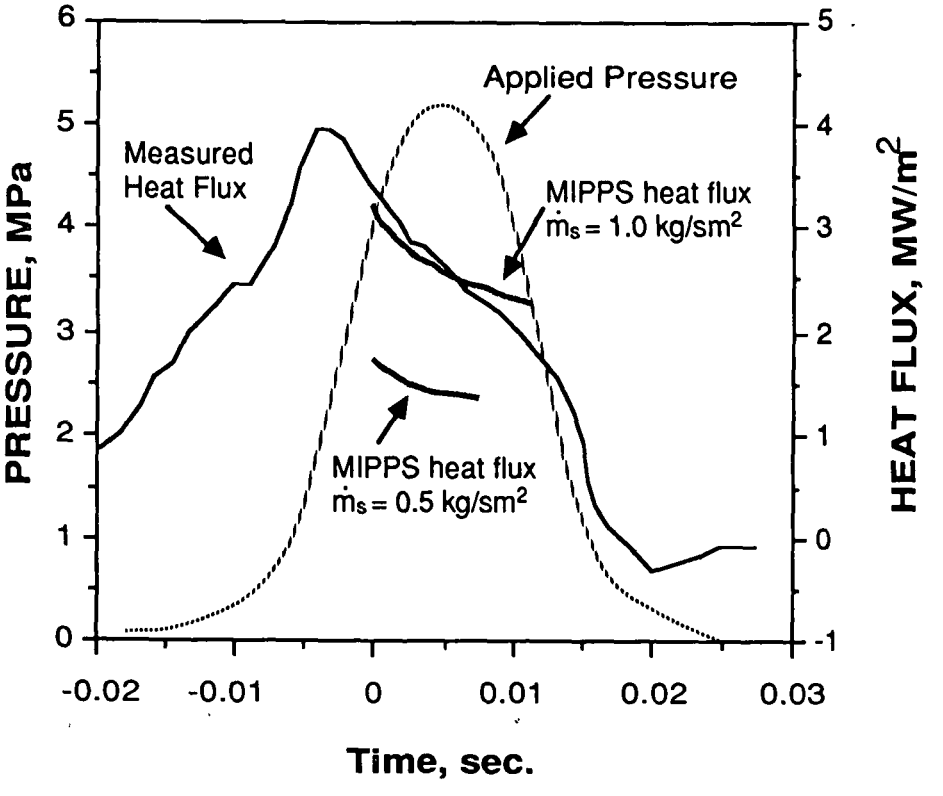

Comparison of experimental heat flux data from Burton [2] with two MIPPS predictions. MIPPS predictions used K=1.0x10^{-15}m^2 and water resupply rates of 0.5 to 1.0 kg/sm^2.

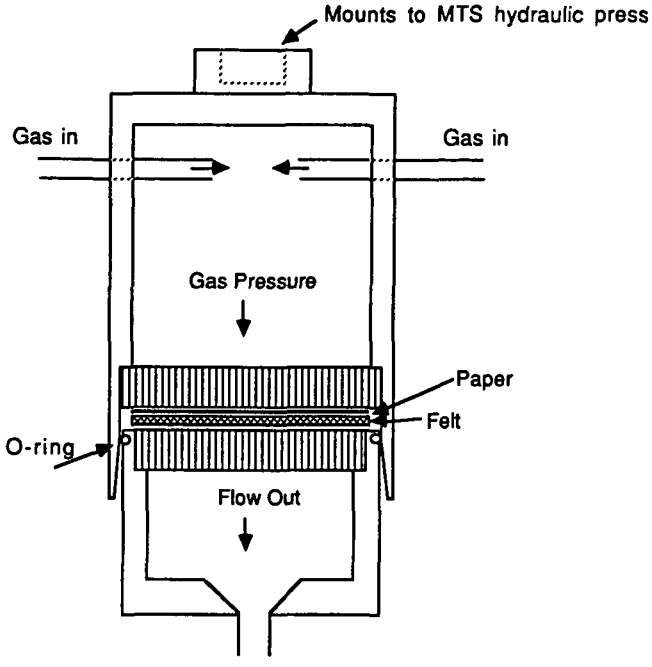

Figure 1. Displacement dewatering equipment (gas supply valves and pressure chamber not shown).

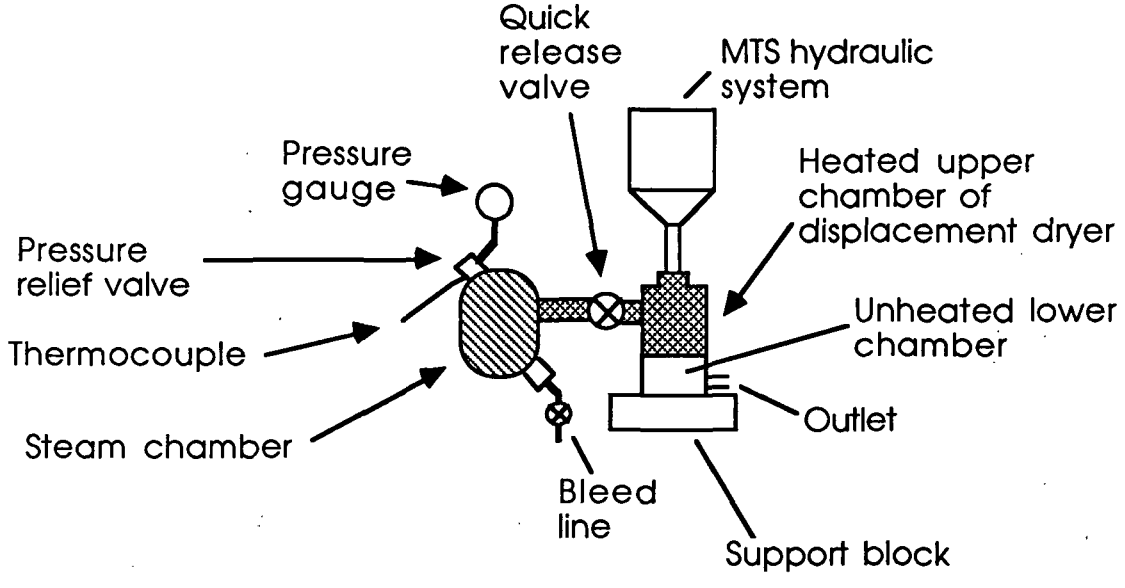

Schematic of the experimental displacement device operating with steam

ANISOTROPIC PERMEABILITY IN PAPER

The new displacement device can be adapted to measure both the x and y components of lateral permeability in paper. The degree of compression can also be controlled.

A round sheet of paper with upper and lower surfaces sealed by contact with platen heads will be used. Dyed fluid will be injected at constant pressure into the center of the sheet. The fluid will move outward towards the edge of the paper. After a specified time, the process is stopped and the shape of the dyed region in the sheet is recorded. The size and shape of the dyed region gives the x and y components of lateral permeability.

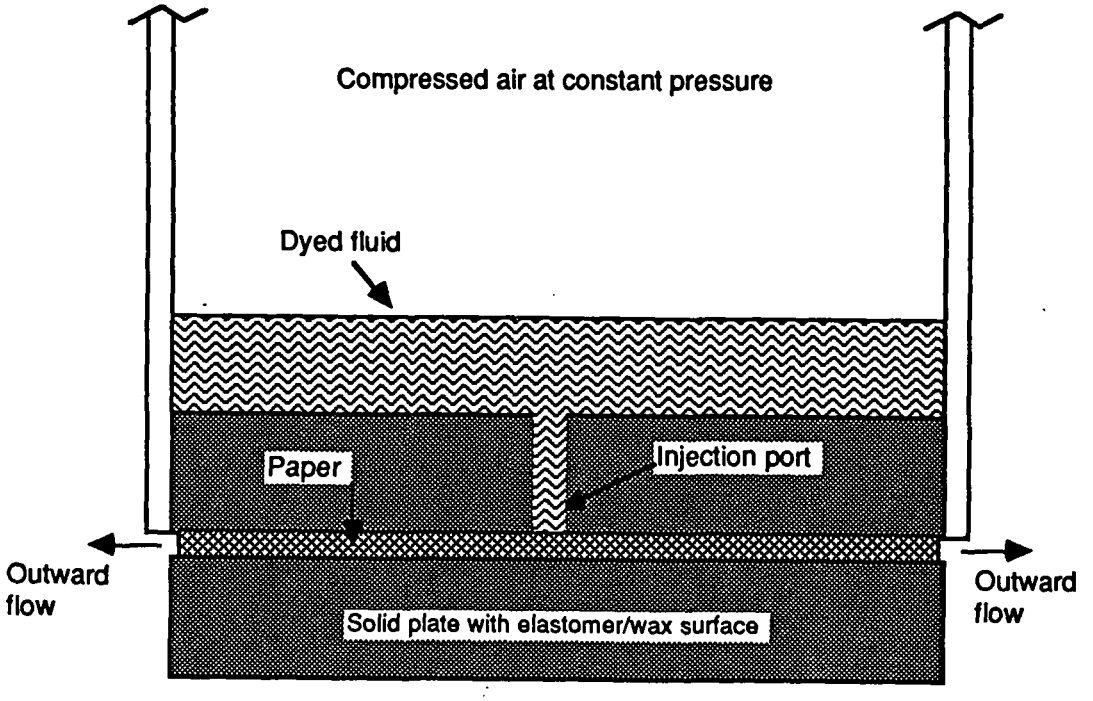

Adaptation of MTS displacement head for measurement of lateral permeability in paper.

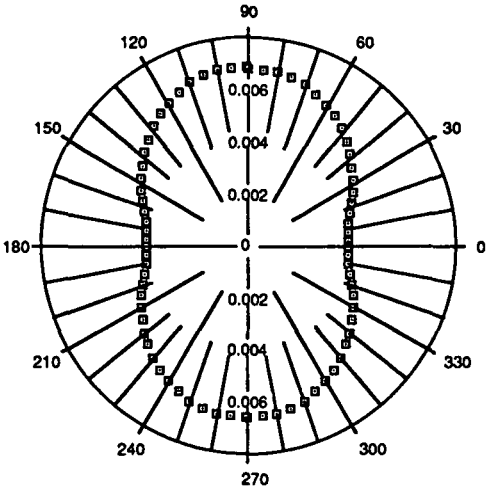

Predicted boundaries of dye after 30 sec. of injection into the center of a saturated sheet with strong anisotropy: $K_y/K_x=3$. The boundaries of the sheet (r = 0.05m) exceed the outer circle shown. (Test problem from A247.)

RESEARCH OF A190 STUDENTS

Joseph Zavaglia - interface motion in impulse drying

James Burkhead - sheet density in impulse drying

Toshihiko Fukushima - felt flows

RESEARCH OF DOCTORAL CANDIDATES

James Burns: wet pressing dynamics

Gary Rudemiller: boiling heat transfer in porous media

John McKibben: free-surface black liquor flows

Nick Triantafillopoulos: instabilities in a short dwell coater

FLUENT
AS A TOOL FOR THE PULP AND PAPER INDUSTRY

FLUENT, a computaional fluid mechanics code by Creare, Inc., has been used extensively during the last six months to solve a variety of fluid flow problems related to the paper and pulp industry. It has also been helpful in the recent course "Flow Through Porous Media" (A247).

RECENT APPLICATIONS OF FLUENT AT THE IPC:

- Study of flows in lateral permeability measurements in paper.
- Extensive analysis of flows in a short dwell coater (Nick Triantafillopoulos and Gary Rudemiller)
- Free surface flows in black liquor sprays (research in progress: John McKibben)
- Reacting flows in a recovery boiler (Dan Sumnicht, Allan Walsh, Andy Jones)
- Heat conduction in an experimental device for the study of impulse drying mechanisms (Gary Rudemiller)

Project 3479

MEDIUM CONSISTENCY PROCESSING

Dennis Spencer

March 29, 1988

OBJECTIVES

- TO DETERMINE TO WHAT EXTENT THE FIBER ORIENTATION CAN BE ACHIEVED DURING HIGH SPEED FLOW OF A CONCENTRATED FIBER SUSPENSION IN CERTAIN CONVERGING FLOWS
- TO COMPARE THE RESULTS OBTAINED IN THIS CASE WITH THE BEST POSSIBLE, BOTH EXPERIMENTALLY AND THEORETICALLY
- TO ASCERTAIN THE RELATIVE IMPORTANCE OF FIBER-FIBER INTERACTIONS AND TURBULENT FLUCTUATIONS IN DETERMINING FIBER ORIENTATION DISTRIBUTION

EXPERIMENTAL PLAN

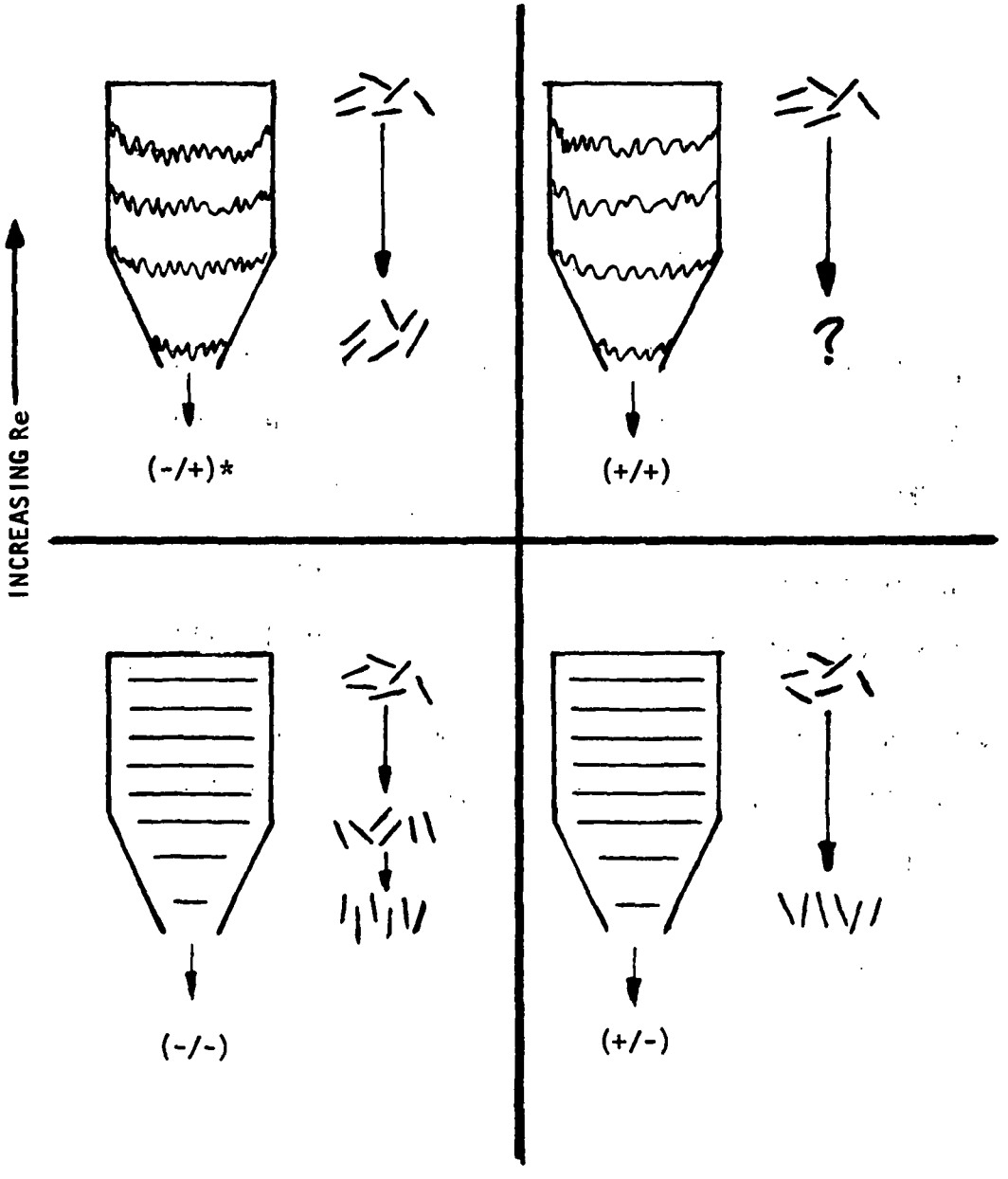

*(CONCENTRATION/SPEED)

EXPERIMENTAL PLAN

QUADRANT (Fig. 2)	% CONSISTENCY	VELOCITY	FIBER-FIBER INTERACTION	Re #	IMAGING
1	HIGH	HIGH	+	+	FXR
2	LOW	HIGH	-	+	OPTICAL
3	LOW	LOW	-	-	OPTICAL
4	HIGH	LOW	+	-	FXR

EFFECTIVE ENERGIES
THROUGH-WATER

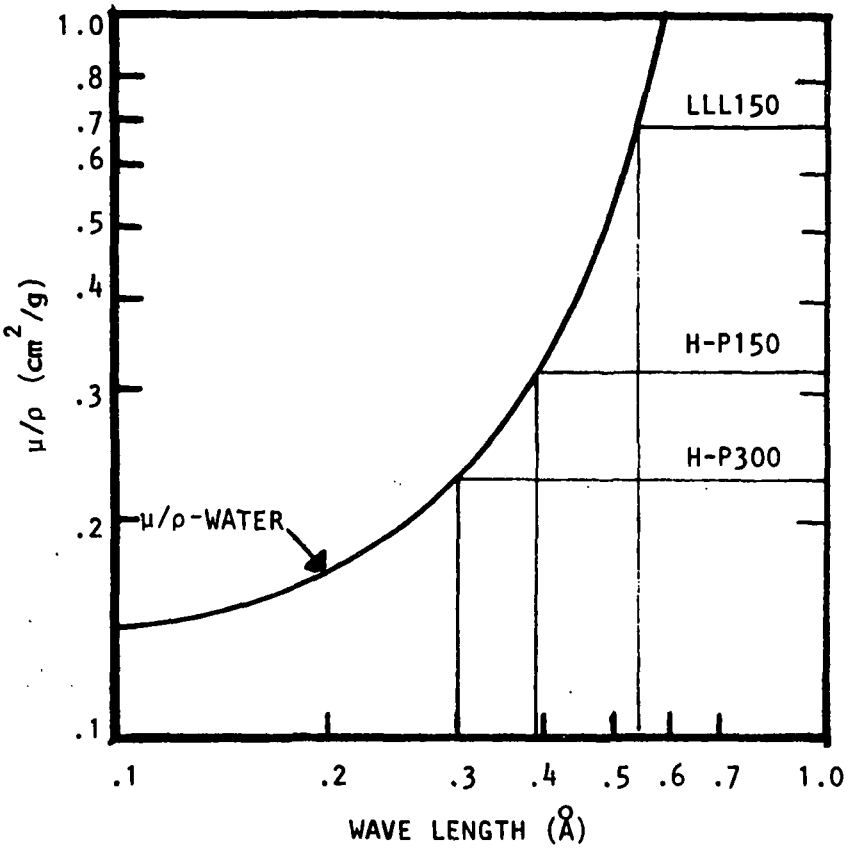

EQUIVALENT ENERGIES THROUGH WATER

	μ/ρ	λ(Å)	KeV
LLL (150kVp)	.69	.54	23
H-P 150kVp	.32	.38	33
H-P 300 kVp	.23	.30	41

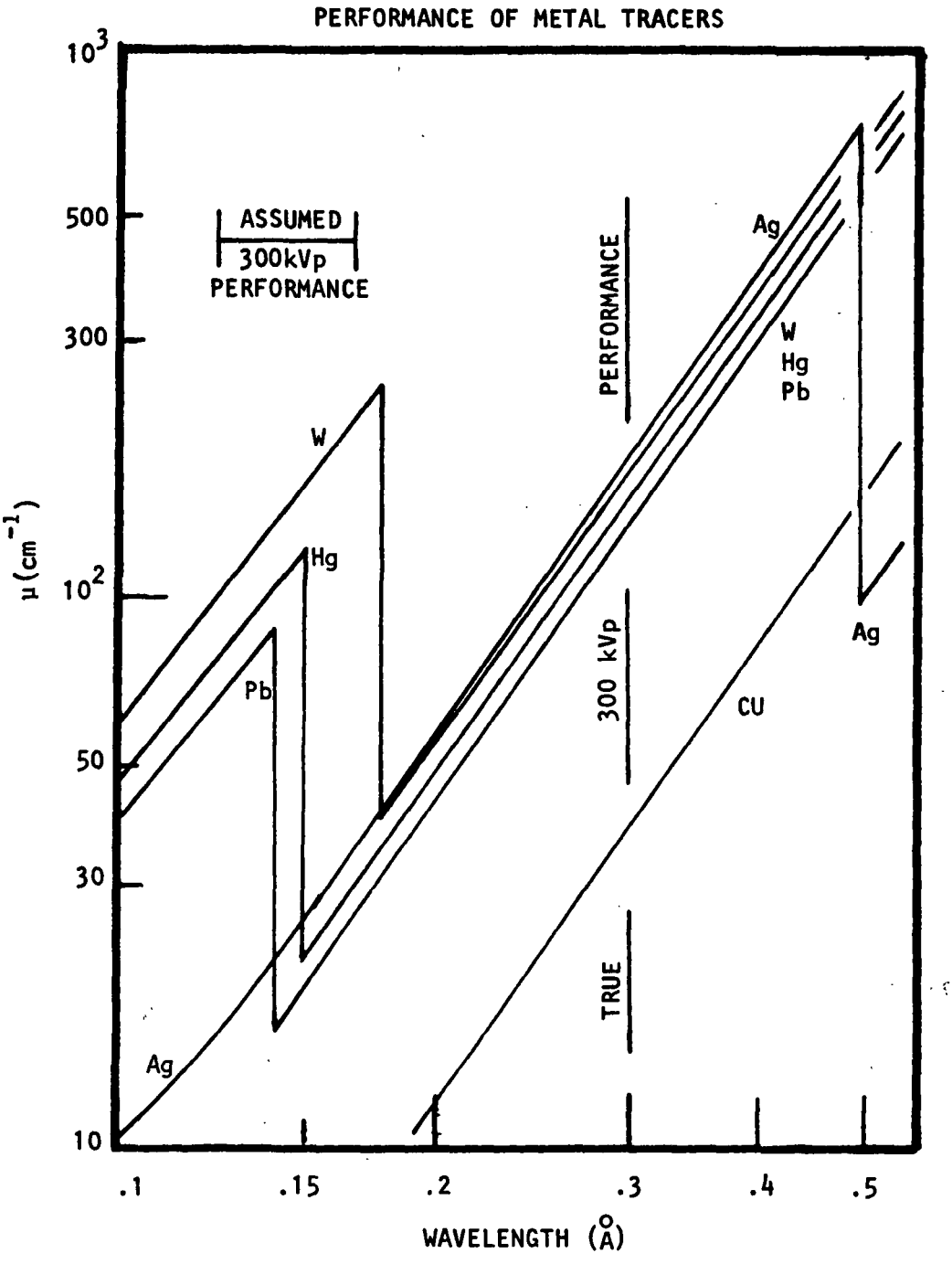
PERFORMANCE OF METAL TRACERS
10^3
500
300
10^2
50
30
10
$\mu(cm^{-1})$
ASSUMED
300kVp
PERFORMANCE
W
Hg
Pb
Ag
PERFORMANCE
W
Hg
Pb
Ag
300 kVp
CU
Ag
TRUE
.1
.15
.2
.3
.4
.5
WAVELENGTH (Å)

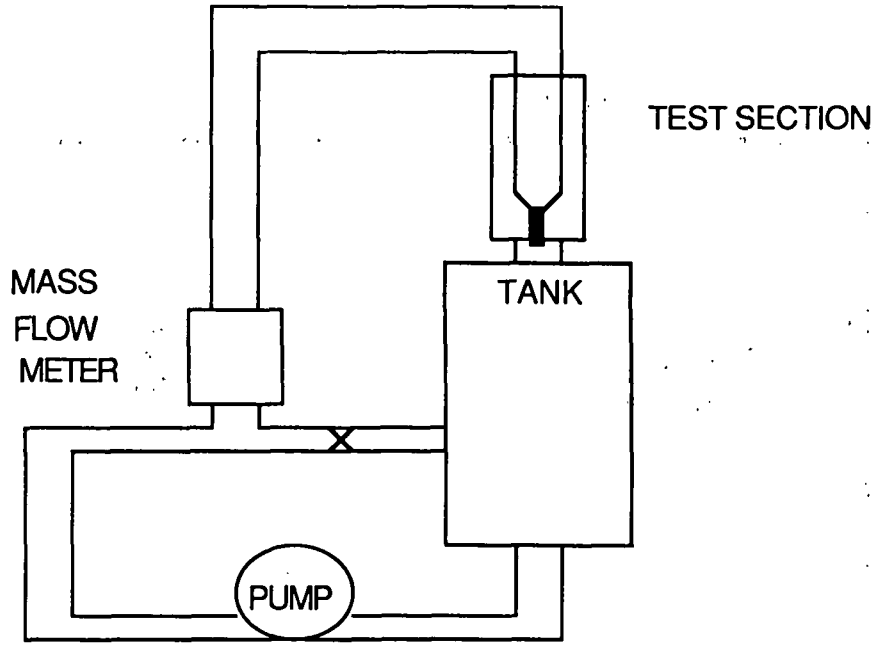
TEST SECTION
MASS
FLOW
METER
TANK
PUMP

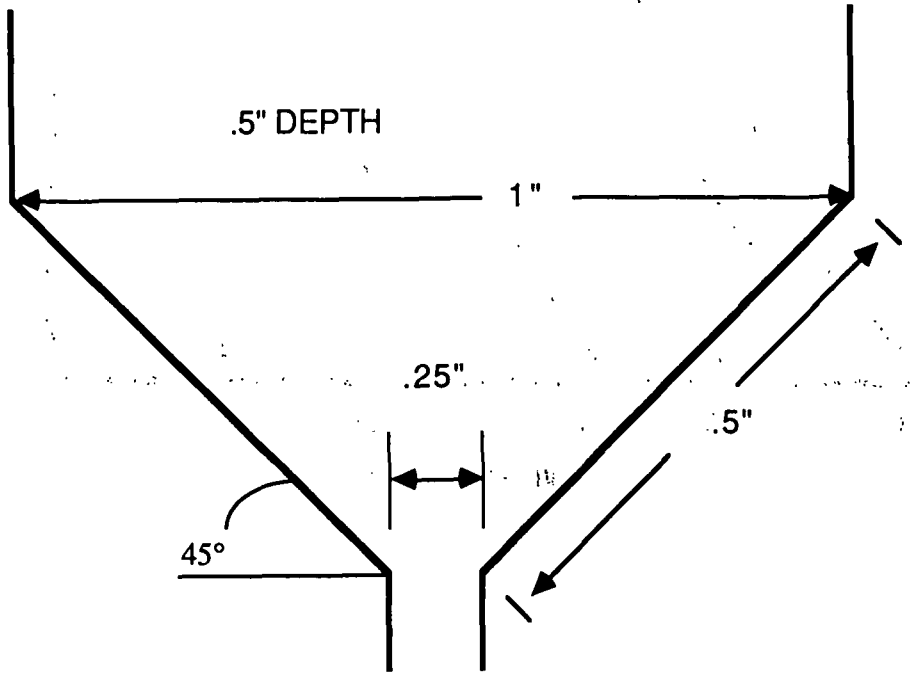
.5" DEPTH
1"
.25"
.5"
45°

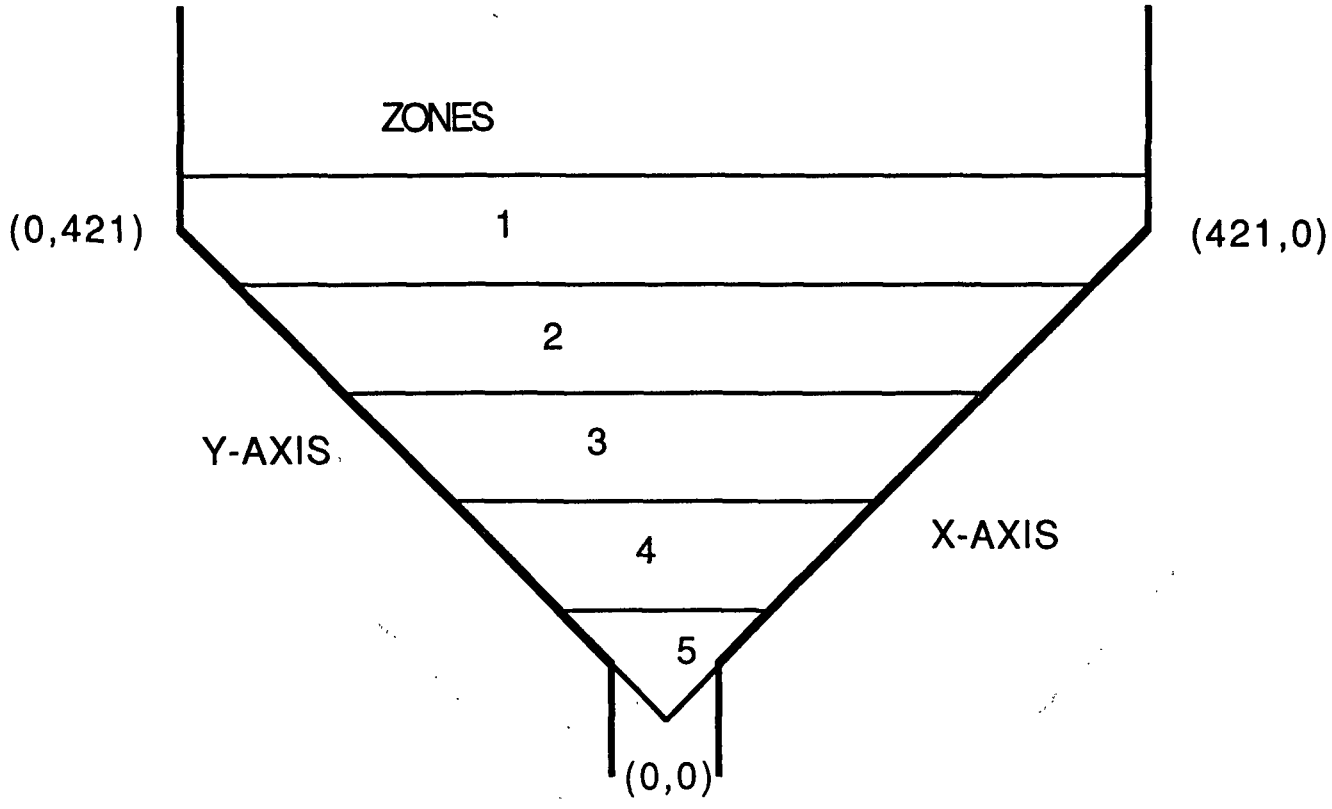

FIBER LENGTH	VOLUMETRIC CONSISTENCY	VELOCITY
1MM	9.8 %	7.5 & 15 m/s
1MM	6.5 %	7.5 & 15 m/s
2MM	3.68 %	7.5 & 15 m/s
2MM	2.45 %	7.5 & 15 m/s

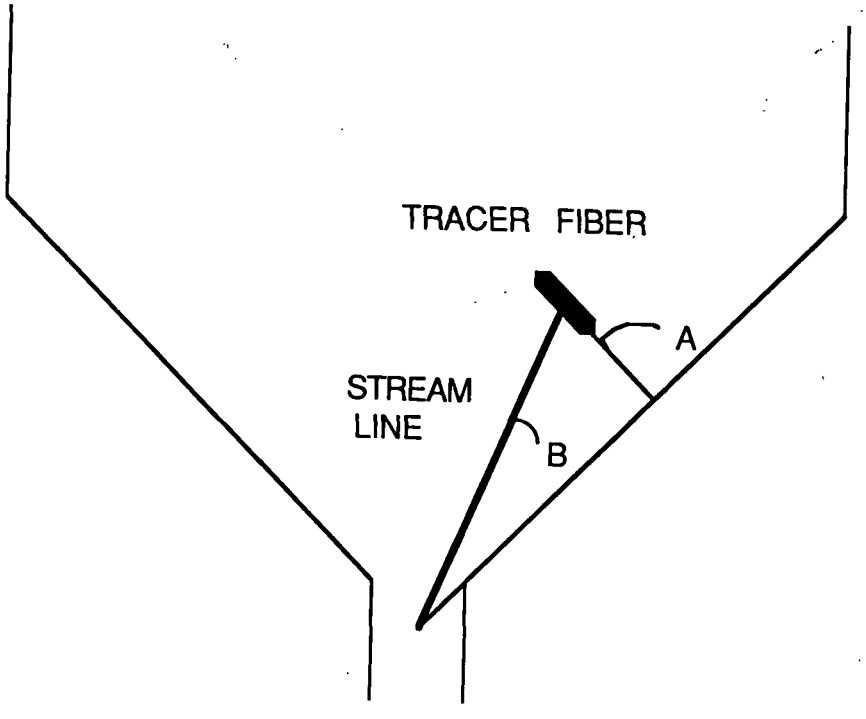
TRACER FIBER
A
STREAM
LINE
B

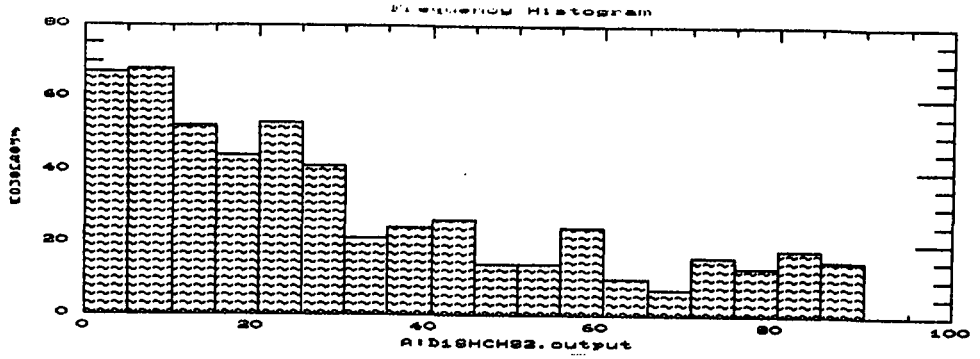
Frequency Histogram
A:D1SHCHS2.output

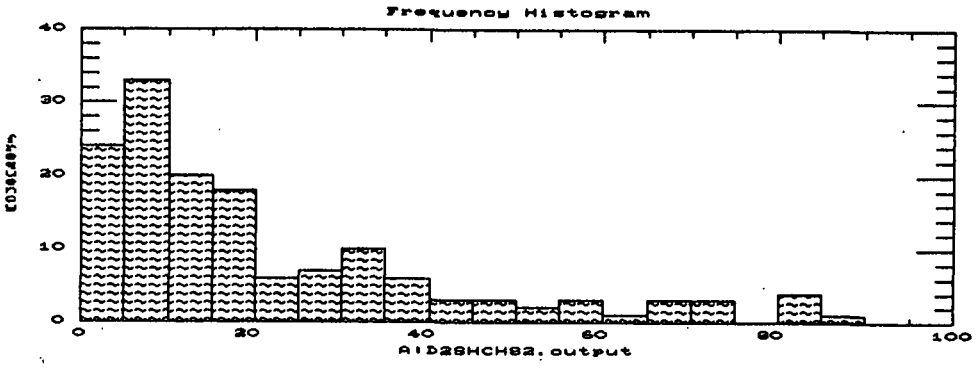
Frequency Histogram
A:D2SHCHS2.output

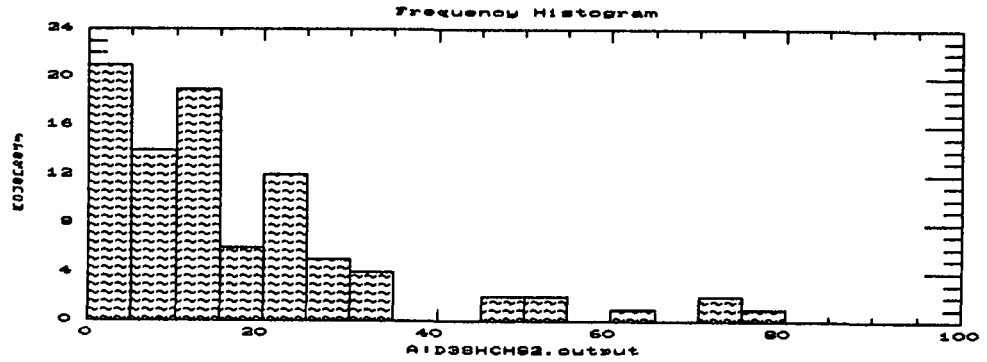
Frequency Histogram
A:D3SHCHS2.output

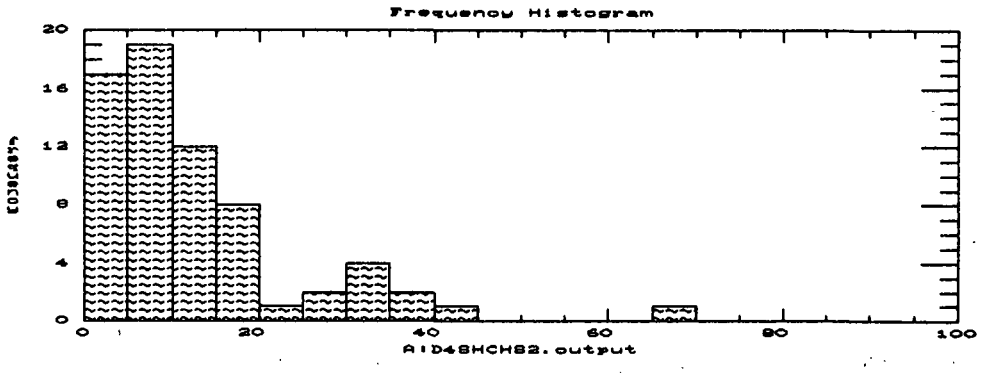
Frequency Histogram
A:D4SHCHS2.output

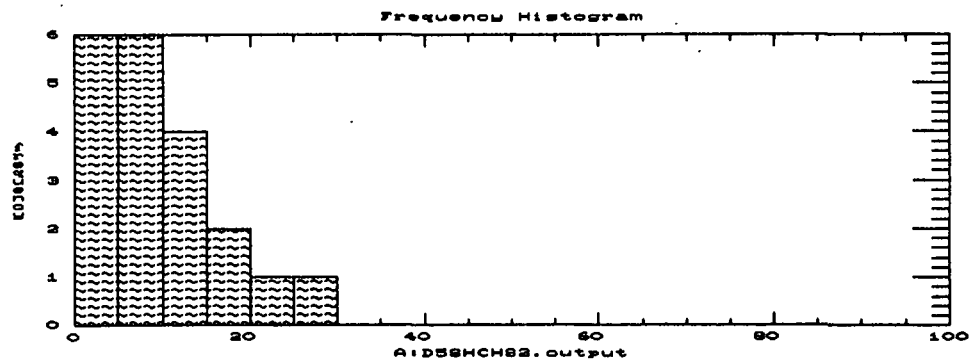
Frequency Histogram
A:D5SHCHS2.output

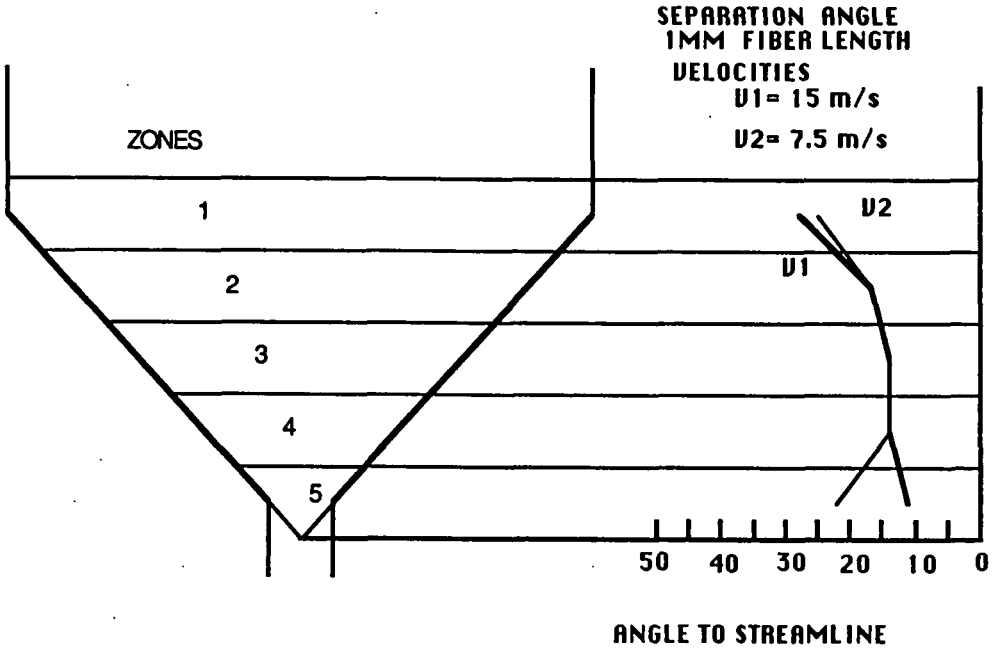
SEPARATION ANGLE
1MM FIBER LENGTH
VELOCITIES
V1= 15 m/s
V2= 7.5 m/s
ZONES
1
2
3
4
5
V2
V1
50 40 30 20 10 0
ANGLE TO STREAMLINE

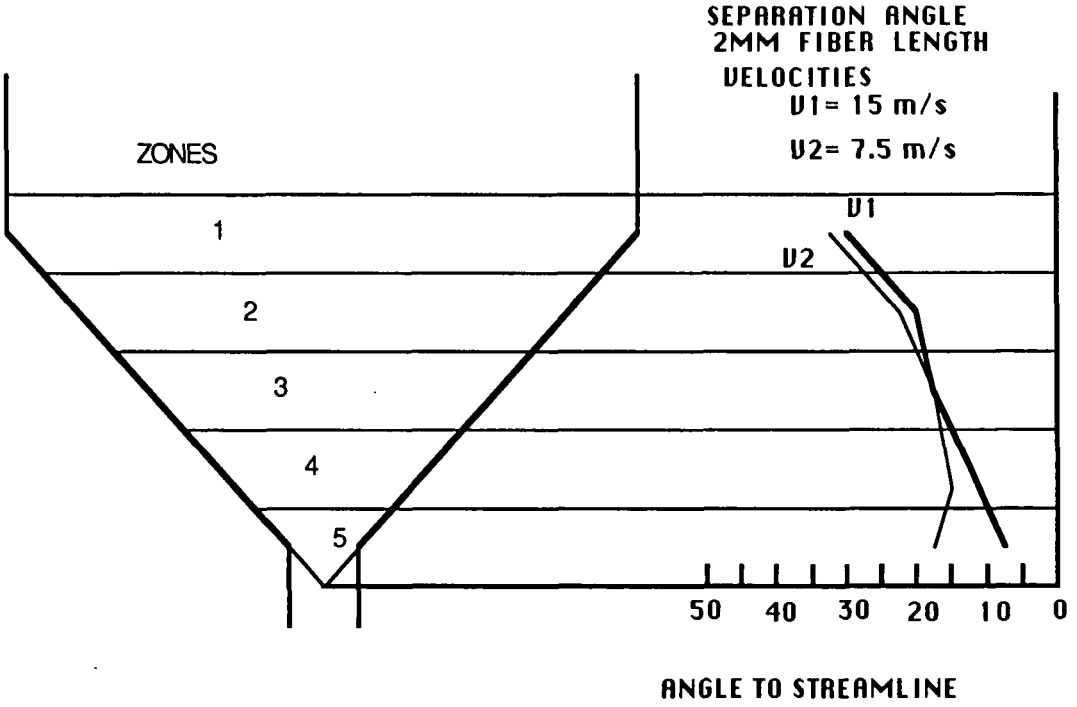
SEPARATION ANGLE
2MM FIBER LENGTH
VELOCITIES
V1= 15 m/s
V2= 7.5 m/s
ZONES
1
2
3
4
5
V1
V2
50 40 30 20 10 0
ANGLE TO STREAMLINE

Project 3471

PROCESS MODELING AND SIMULATION

Gary Jones

March 29, 1988

PERFORMANCE ATTRIBUTE

- MODEL DEVELOPMENT
  - DATA ANALYSIS
  - MODELS
- MODEL VALIDATION
- IMPLEMENTATION

DATA ANALYSIS

ALEXANDER & MARTON	YIELD, CWT, REFINING (CSF), WET PRESSING
TMP MILL	YIELD, REFINING, SCREENING, CLEANING
WMU	CALENDERING, SPECIES MIXTURES, MACHINE CONDITIONS
SETTERHOLM, FLEISCHMAN	ORIENTATION ANGLE, WET STRETCHING
KIBBLEWHITE, CLARK, ETC.	MODEL VALIDATION

ALEXANDER AND MARTON DATA

CONSTANTS
SPECIES, PULPING TYPE, KAPPA NO., BLEACHING

INDEPENDENT VARIABLES

CELL WALL THICKENESS (1.8, 3.5 μ)	CWT
YIELD (48-60%)	Y
REFINING (30-700 CSF)	CSF
WET PRESSING PRESSURE (0-9200 psi)	P

DEPENDENT VARIABLES

SHEET PROPERTIES

DENSITY

MODULUS

BREAKING LENGTH

BURST, TEAR

RUPTURE ENERGY

ELONGATION AT BREAK

SCATTERING COEFFICIENT

SINGLE FIBER PROPERTIES

MODULUS

BREAKING LENGTH

FIBRIL ANGLE

SWELLING

CROSS SECTIONAL AREA

MODELS DEVELOPED FROM A&M DATA

HANDSHEET PROPERTIES:

DENSITY	(JONES)
MODULUS	(PAGE)
BREAKING LENGTH	(PAGE)
BURST	(JONES, VANDENAKKER)
TEAR,	
RUPTURE ENERGY	(JONES)
STRAIN AT BREAK	(JONES)
SCATTERING COEFFICIENT	(MALMBERG)

FIBER PROPERTIES:

EFFECTIVE FIBER	
MODULUS	(JONES)
TENSILE	(JONES)

PROCESS:

- SURFACE AREA VS. CSF
- BONDING COEFFICIENT
- RELATIVE BONDED AREA
- COMPRESSIBILITY COEFFICIENTS

SHEET DENSITY (ρ)

$$\frac{1}{\rho} = \frac{1}{\rho_u} + \left(\frac{1}{\rho_l} - \frac{1}{\rho_u} \right) \frac{1}{S_b 2}$$

$$\rho_u = \frac{1}{.764 + .000477\ CSF + .1146\ (CWT-1.5)}$$

$$\rho_l = \frac{1}{\frac{1}{\rho_u} - .05866\ CSF + .0783\ Y + 43.142}$$

$$\rho_{l_m} = .05\ (CWT - .8) + .002\ (Y - 48)$$

$S_b \approx 1$ at high CSF, low wet pressing thick walled vessels

$\rho_u \sim .8$ to 1.1 g/cc

$\rho_l \sim .06$ to $.3$ g/cc

HYDRODYNAMIC SPECIFIC SURFACE (S_h)

$$S_h = 95.7 - .12\ CSF\ (m^2/g)$$

BONDING AREA

$$S_{bo} = C_i \cdot S_h$$

$$C_1 = .0734 - .00654\ Y \qquad Y\ (\%)$$

WET PRESSING EFFECTS

$$S_b = S_{bo}\, f(\rho)$$

$$f(\rho) = 1 + MP^N$$

$$M = e^{.144 + .00177\ CSF}$$

$$N = .0003\ CSF - .000515\ Y$$

SHEET MODULUS

- CONFIRMED PAGE MODEL

$$E = \left(\frac{E_f}{3}\right)\left(\frac{\rho}{\rho_f}\right)\left(1 - \frac{k}{RBA}\right) \quad \text{(Page/Nissan)}$$

$$k = \frac{W}{L}\left(\frac{E_f}{2G_f}\right)^{\frac{1}{2}}$$

$$RBA = \frac{\rho - \rho_l}{\rho_u - \rho_l}$$

SHEET MODULUS

$$E = \frac{E_f}{3}\left(\frac{\rho - \rho_1}{\rho_u}\right)\left(1 - \frac{k}{RBA}\right) \quad \text{(Modified)}$$

$$E = E_o\,(\rho - \rho_o)$$

$$E_o = \frac{E_f}{3\rho_u}$$

$$\rho_o = \rho_1 + (\rho_u - \rho_1)\left(\frac{W}{L}\right)\left(\frac{E_f}{2G_f}\right)^{\frac{1}{2}}$$

SHEET MODULUS

$E = 10.6\,(\rho - .19)$ LINEAR FORM (MALMBERG) $(R^2 = .95)$

$E = 13.6\left(1 - \frac{.4}{\rho + .4}\right)$ NONLINEAR FORM $(R^2 = .95)$

$$\frac{E_f}{3\rho_u} = E_o = \text{CONSTANT}$$

$$E_f = 3\,E_o\,\rho_u = \frac{31.8}{.746 + .000477\ CSF + .115\ CWT}$$

DID NOT FIT SINGLE FIBER MODULUS DATA

$$\frac{E_f}{3\rho_u CWT} \approx \text{CONSTANT}$$

FIBER MODULUS

$$E_f = 172.4 + 0.55\ (CWT \cdot \rho_u \cdot g)\ \frac{Kg}{mm^2}\ (R^2 = .89)$$

EFFECTIVE FIBER MODULUS IN SHEET E_f^*

$$E_f^* = \frac{58\ (E_f - 172.4)}{CWT\ g}$$

$$\frac{E_f^*}{3\rho_u} = 10.6 = E_o$$

BREAKING LENGTH (Z)

- PAGE MODEL CONFIRMED

$$\frac{1}{Z} = \frac{9}{8Z_f} + \frac{12A\rho_u g}{RBA\ b\ p\ L}\ \text{(PAGE)}$$

$$Z_f = \frac{P_1(\rho - P_3)}{(\rho + P_2)}\qquad (R^2 = .85)$$

$P_1 = 24.51 + .414\ Y - 3.5\ CWT$
$P_2 = 3.37$
$P_3 = .086$

FIBER TENSILE (Z_f)

$$Z_f = \frac{9}{8} P_1 = \frac{9}{8}\ (24.5 + .414\ Y - 3.5\ CWT)$$

-Z_f does not fit single fiber data well

BURST (B)

VAN DEN AKKER MODEL

$$B = C\,(E_1)^{\frac{1}{2}}\,\frac{(T_{MD} + T_{CD})}{2}$$

$$B = 5.1\,(E_1)^{\frac{1}{2}}\,Z \quad (R^2 = 0.90)$$

LINEAR MODEL

$$B = -15.1 + 10.175\,Z \qquad (R^2 = .92)$$

$$C = 5.6 - .127\,CWT\,(1 + .0015\,CSF)$$

STRAIN AT BREAK, (E_1)

$$E_1 = 0.85 + .02677\,Z - .177\,E \quad (R^2 = .85)$$

RUPTURE ENERGY (R.E.)

$$R.E. = 392 - 308E_1(1 - .237\,Z) \qquad (R^2 = .95)$$

TEAR

$$Tear = 296 - 14\,E - B - \frac{20.7}{\rho} \qquad (R^2 = .8)$$

SCATTERING COEFFICIENT (SL)

$$SL_u - SL = SL_k (\rho - \rho_1) \qquad (R^2 = .94)$$

$$SL_u = 874 + .04\ CSF - 77.5\ CWT$$

$$SL_K = 928 - 98\ CWT - 6.6\ Y$$

POROSITY (POR)

$$POR = A_1 + A_2/CSF$$

$$A_1 \approx 0$$

$$A_2 \approx 12000$$

OTHER EFFECTS

- APPARENT FIBER CRUSHING, DAMAGE AT HIGH PRESSURE
- REDUCED DENSITY, MODULUS, TENSILE
- NOT ADEQUATELY ACCOUNTED FOR

FLEISCHMAN DATA (IPC)

- SHEET ANISOTROPY (WET STRETCH, ORIENTATION)
- MODULUS (E_x, E_y, E_z)
- TENSILE (Z_x, Z_y, Z_z)
- COMPRESSIVE STRENGTH (C_x, C_y)
- SINGLE SPECIES

MODULUS

$$E_x/E_y = R + .335 - .583\ WS + 0.708\ WS \cdot OR + 0.6350R^2 \quad (R^2 = .95)$$

$$E_x/\rho = 6.84 + 5.69\ OR + 0.927WS \cdot OR \quad (R^2 = .96)$$

$$E_y/\rho = 14.79 - 4.18\ OR - .2880R \cdot WS \quad (R^2 = .98)$$

E_z - interactions between WS, OR and ρ

$$E_z = .257 + (.124\ WS - 1.106)\ \rho$$

$$+ (1.339\ .02936\ OR - .0241\ WS)\ \rho^2$$

TENSILE

Z_x, Z_y similar to E_x, E_y

or

$$Z_x = -6.97 + 6.56\ E_x \quad (R^z = .90 \text{ con coef. } = .95)$$

$$Z_y = 3.56 + 5.43\ E_y \quad (R^z = .94 \text{ con coef. } = .97)$$

$$Z_z = .220 + 1.86 \cdot E_z \quad (R^2 = .943)$$

COMPRESSIVE STRENGTH

(HABEGER, WHITSITT MODELS)

$$C_x = 3.38 + 5.51\ E_x^{.75}\ E_z^{.25} \quad (R^2 = .95)$$

$$C_y = 3.46 + 4.76\ E_x^{.75}\ Ez^{.25} \quad (R^2 = .92)$$

OTHER MODELS UNDER DEVELOPMENT

- IPC DATA (BRIAN BURGER)
  - EFFECTS OF REFINING, SPECIES
  - ANISOTROPY, MODULUS, TENSILE

- WMU DATA
  - CALENDERING MACHINE EFFECTS
  - PAUL ROZIK (A190 WORK)

BRIGHTNESS

$$C_K = C_{Lig}X_{Lig} + C_{cell}X_{cell} + C_{ext}X_{ext} \quad (cm^2/g)$$

$$C_{cell} = 7.5$$

$$C_{ext} = 1.0$$

$$C_{Lig} = 250 \text{ to } 350$$

$$\text{Brightness} = \frac{C_K}{S_K} + 1 - \left(\left(\frac{C_K}{S_K}\right)^2 + 2\left(\frac{C_K}{S_K}\right) \right)^{\frac{1}{2}}$$

OTHER MODELS

- OTHER COMPRESSIVE PROPERTIES (RING CRUSH, ETC.)
- FORMATION (GRABER & GOTTSCHING)
- LAMINATES
- EFFECTS OF UNUSUAL PULPING CONDITIONS

DENSITY MODEL VALIDATION

- FITS DATA OF

  KIBBLEWHITE - KRAFT 4 NEW ZEALAND BEECH FPEICES (RANDOM)

  FLEISCHMAN - BLEACHED KRAFT - DOUGLAS FIR, SPRUCE MIXTURES

  TMP MILL (ASSUMED 100% YIELD, SPECIES UNKNOWN)

  CLARK BLEACHED SULFITE (SPECIES UNKNOWN)

PERFORMANCE ATTRIBUTES

YIELD

KAPPA

$\bar{L}$

σ_L

$\bar{w}$

σ_w

K-FACTOR

C_K ABSORPTION COEFFICIENT

R ANISOTROPY RATIO

ρ_v COEFFICIENT OF VARIATION IN SHEET DENSITY

ρ_f

CWT

E_f

Z_f

ρ_f

DATABASE DEVELOPMENT

SOURCES:

- ISENBERG DATA
- IPC DATA SUPPLEMENT
- FPL
- LITERATURE

REQUIRE:

SPECIES

E_f

Z_f

ρ_f

BENDING MODULUS

CWT

$\overline{L}$

$\overline{W}$

COARSENESS

COMPOSITION:
- LIGNIN
- CELLULOSE
- HEMICELLULOSE

MODEL VALIDATION

TMP MILL DATA

FLOWSHEET DEVELOPED

MODELS VALIDATED

PROCESS MODELS

$$\bar{L} = \frac{A_1}{A_2} + \left(L_{in} - \frac{A_1}{A_2}\right) e^{-A_1 ZP}$$

$$\sigma_l = A_3 - A_4/\bar{L}$$

$$ZP = 10^{(NSP-A_p)/B_p}$$

(similar for $\bar{W}$)

$$S_h = 1 - \frac{1}{K} \sum_{l=1}^{n} X_i \ln \left(\frac{L_i}{2.4}\right)$$

$$K = K_o e^{K_2 \cdot NSP}$$

$$k_2 = f(NSP, \text{Consistency}, K_o)$$

$$S_h = a \ln (CSF) + b \qquad \text{(high yield)}$$

SCREENING AND CLEANING-SEPARATION EFFICIENCIES

HANDSHEET MODELS - VENKATESH

PROPERTY = f(long fibers, shives, CSF)

PROPERTY	VENKATESH	JONES*
BULK	10-20% LOW TOO SENSITIVE TO SHIVES	CLOSE NOT AS SENSITIVE
BREAKING LENGTH	TOO SENSITIVE TO SHIVES	NOT AS SENSITIVE
BURST	50% LOW	CLOSE
TEAR	REASONABLE	2 X TOO HIGH
SCATTERING	REASONABLE	2 X TOO LOW
OPACITY	CLOSE	NM
GURLEY POROSITY	INACCURATE	REASONABLE
ELONGATION AT BREAK	NM	REASONABLE
RUPTURE ENERGY	ND	ND
DRAINAGE TIME	ND	ND
WET WEB STRENGTH	ND	ND
ABSORPTION COEFFICIENT	NM	NM
Z-D TENSILE	NM	REASONABLE+

NM NO MODEL
ND NO DATA
* EXTRAPOLATION TO 100% YIELD
+ 8% SHRINKAGE

PROCESS MODELS

CSF	REASONABLE
FIBER LENGTH DISTRIBUTION	REQUIRED MINOR MODIFICATION
SHIVES	GOOD MATCH
L-FACTOR	GOOD MATCH
SEPARATIONS	REASONABLE EXCEPT AFTER MANY STAGES
CONSISTENCIES	REASONABLE EXCEPT AFTER MANY STAGES

MODIFICATIONS

ALTER LOG NORMAL DISTRIBUTION (HYRFN1)

LOCAL REVERSIBILITY IN SEPARATIONS (HYFRAC)

FINES LEAKAGE OPTION (HYFRAC)

SHEET MODULUS - DENSITY AND FREENESS

CWT 3.8μ Wet Pressing Pressure 30psi
Yield 60% Norwegian Spruce

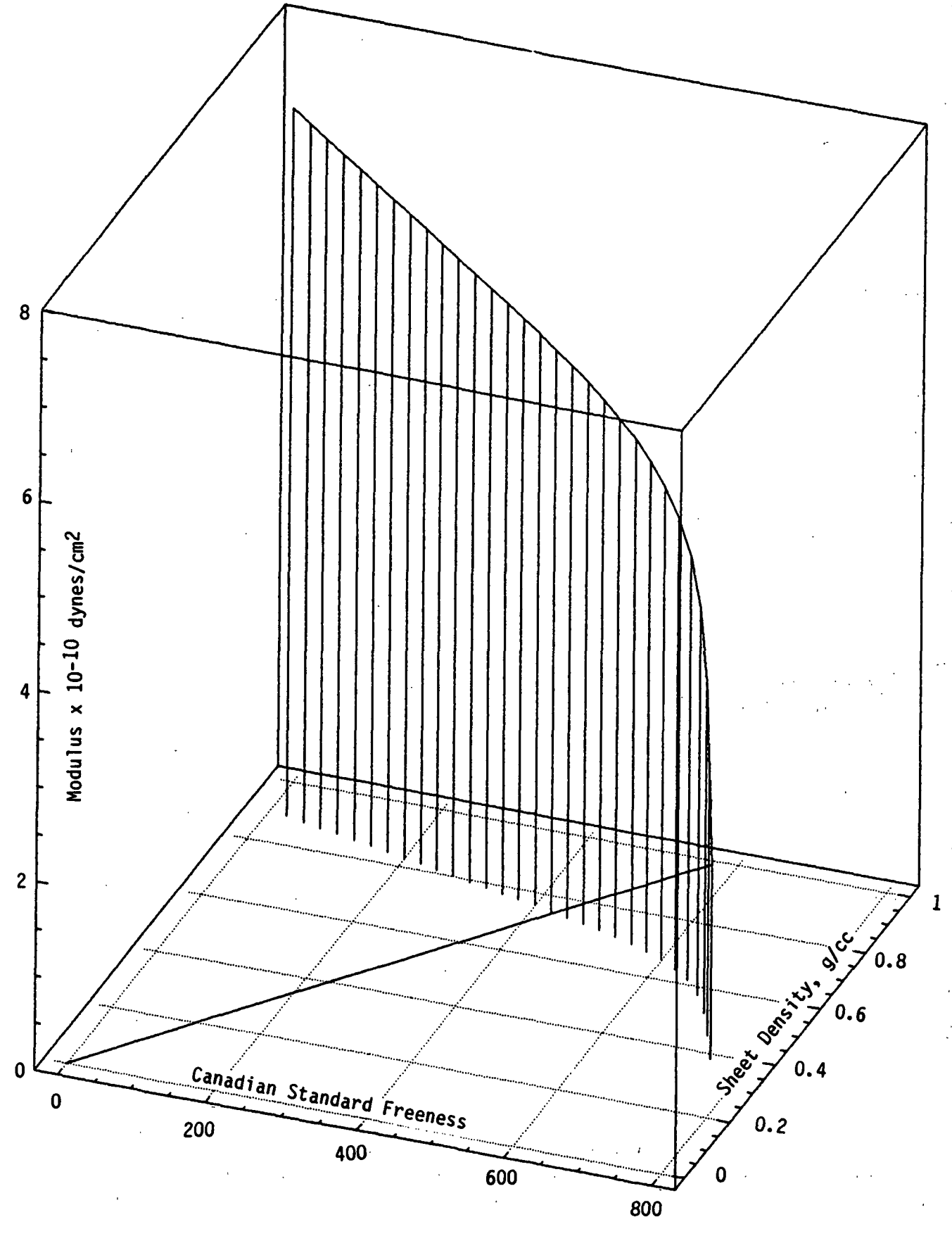

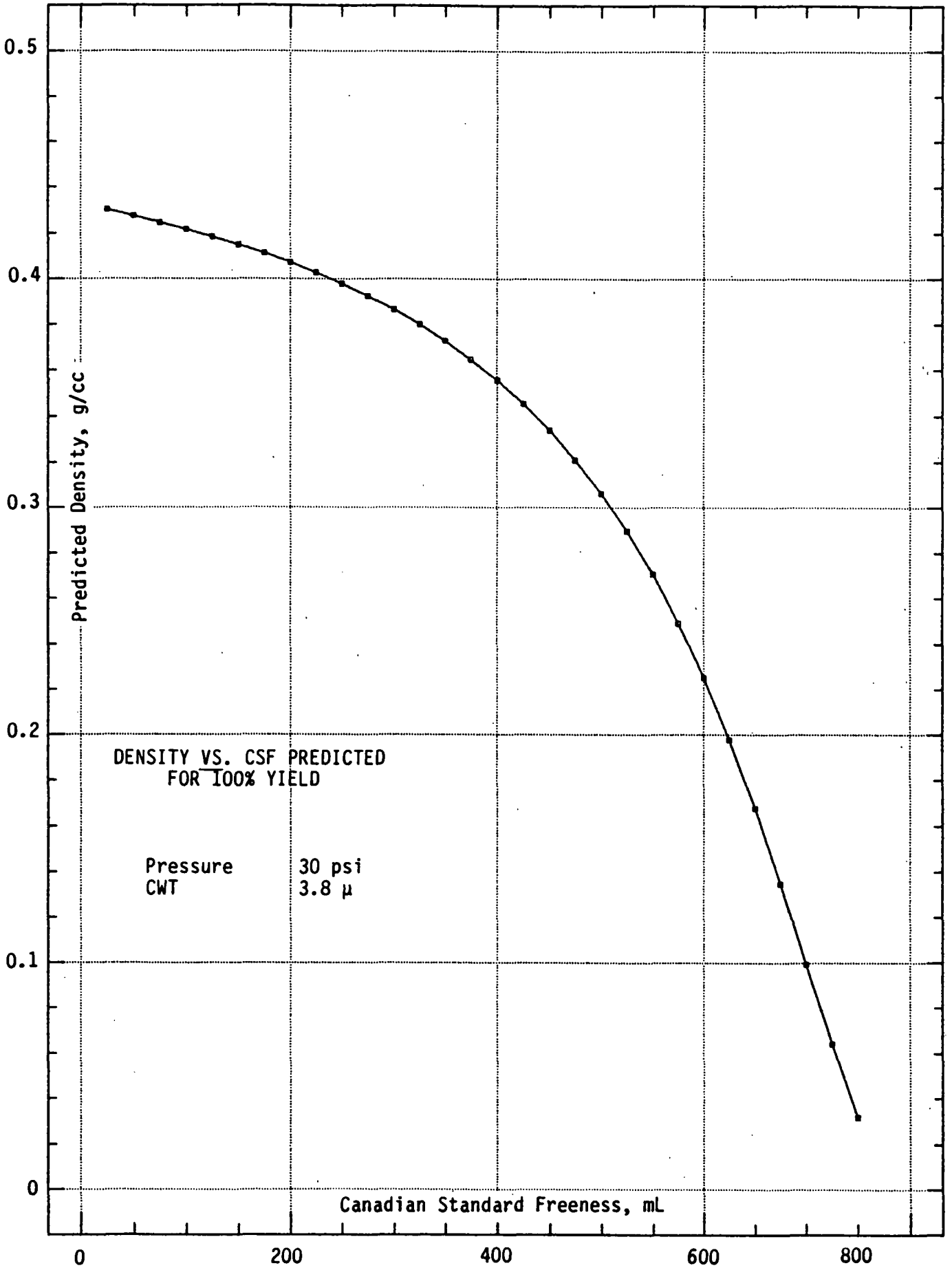
0.5
0.4
0.3
0.2
0.1
0
Predicted Density, g/cc
DENSITY VS. CSF PREDICTED
FOR 100% YIELD
Pressure 30 psi
CWT 3.8 μ
0
200
400
600
800
Canadian Standard Freeness, mL

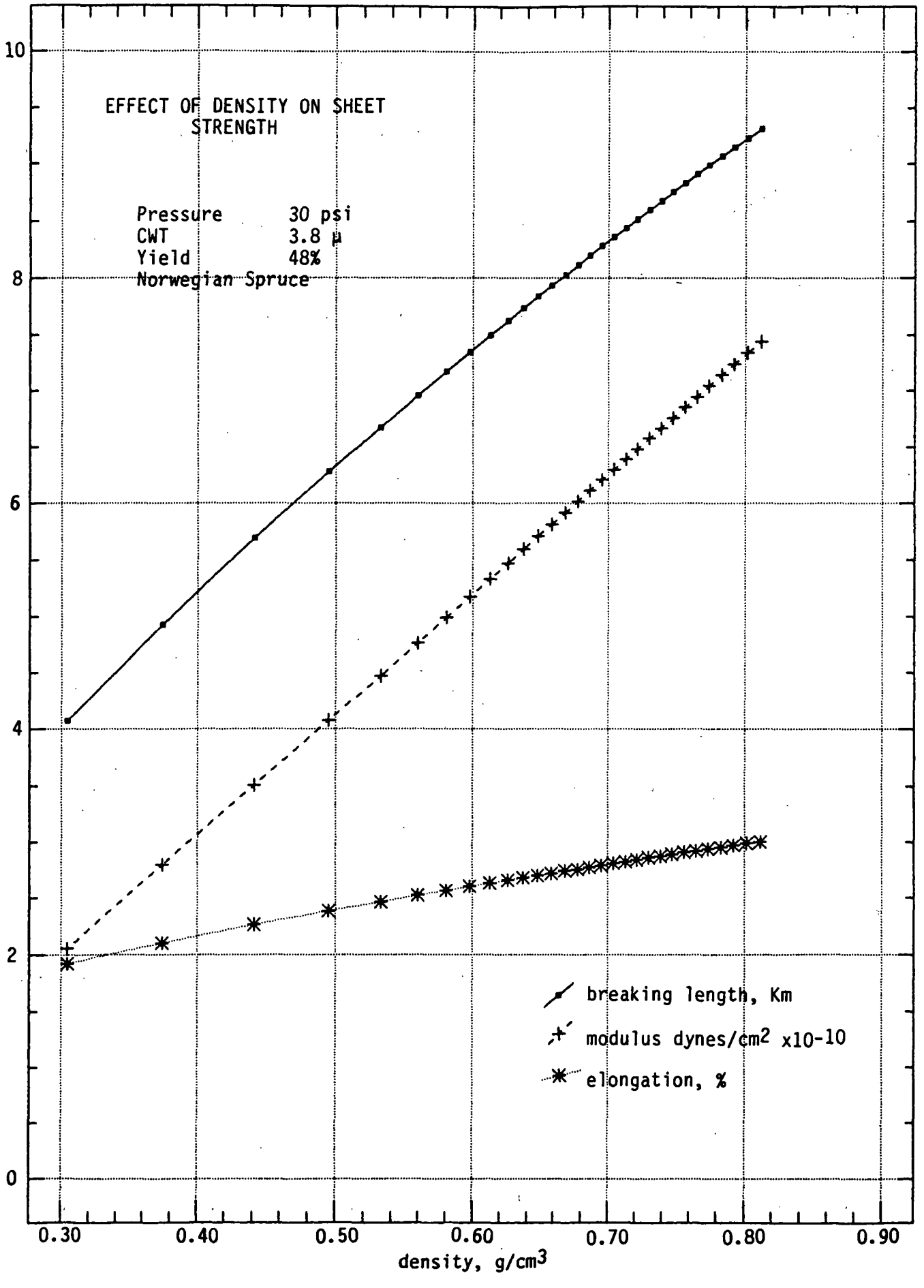
EFFECT OF DENSITY ON SHEET STRENGTH
Pressure 30 psi
CWT 3.8 μ
Yield 48%
Norwegian Spruce
10
8
6
4
2
0
0.30
0.40
0.50
0.60
0.70
0.80
0.90
density, g/cm3
breaking length, Km
modulus dynes/cm2 x10-10
elongation, %

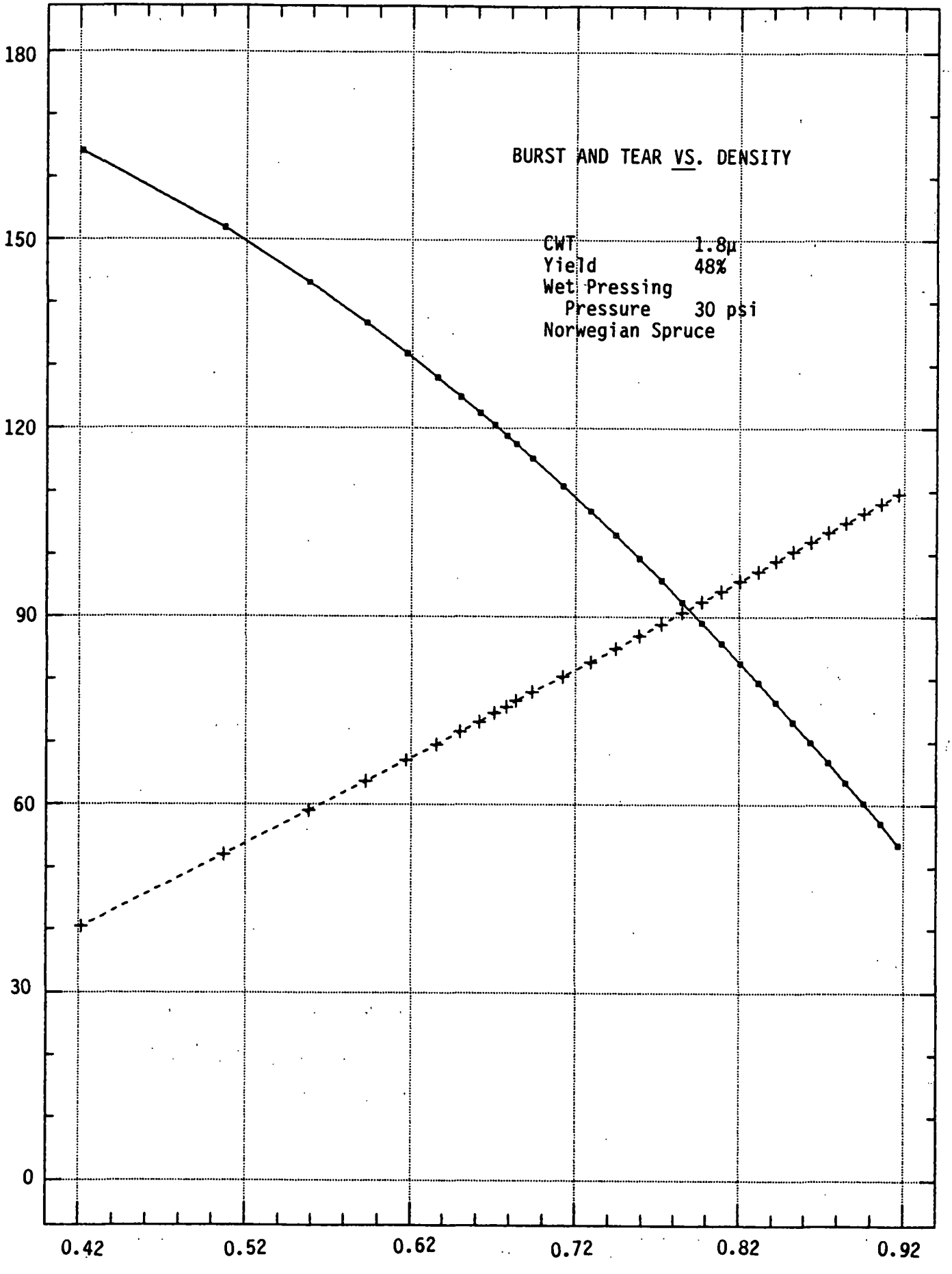
BURST AND TEAR VS. DENSITY
CWT 1.8μ
Yield 48%
Wet Pressing
Pressure 30 psi
Norwegian Spruce
180
150
120
90
60
30
0
0.42
0.52
0.62
0.72
0.82
0.92

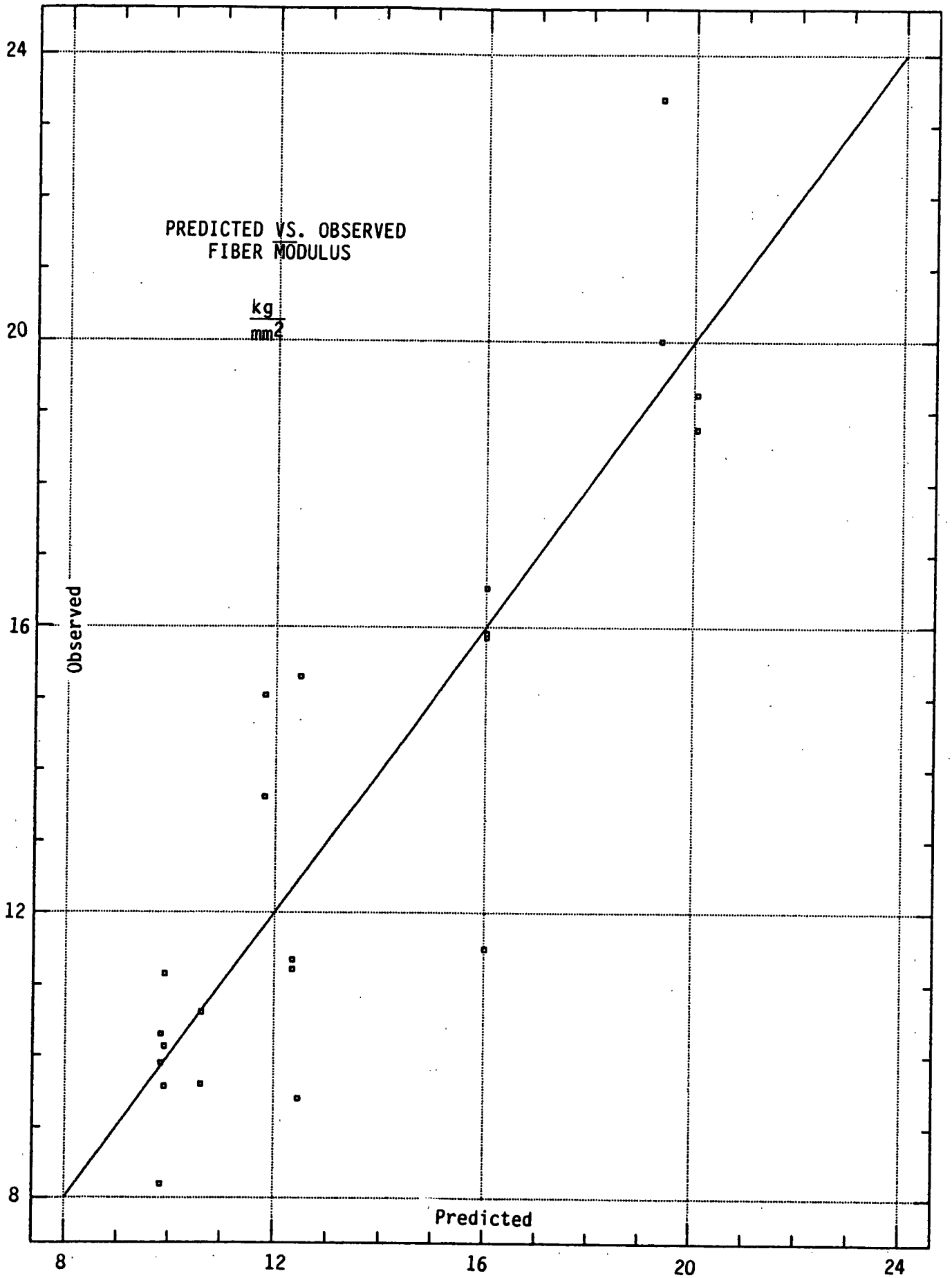
PREDICTED VS. OBSERVED
FIBER MODULUS
kg/mm2
Observed
Predicted
24
20
16
12
8
8
12
16
20
24

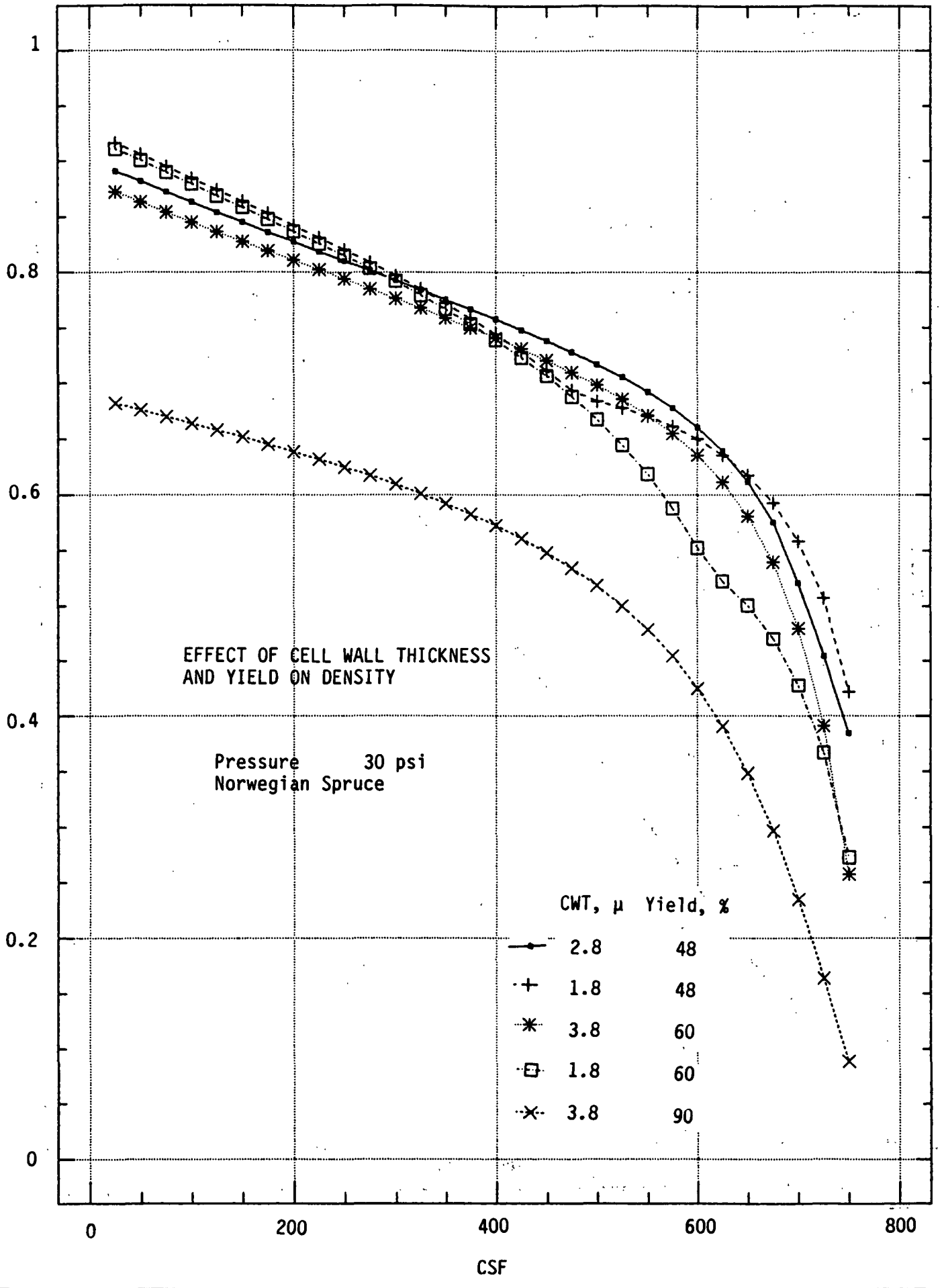
1
0.8
0.6
0.4
0.2
0
0
200
400
600
800
CSF
EFFECT OF CELL WALL THICKNESS
AND YIELD ON DENSITY
Pressure 30 psi
Norwegian Spruce
CWT, μ Yield, %
2.8 48
1.8 48
3.8 60
1.8 60
3.8 90

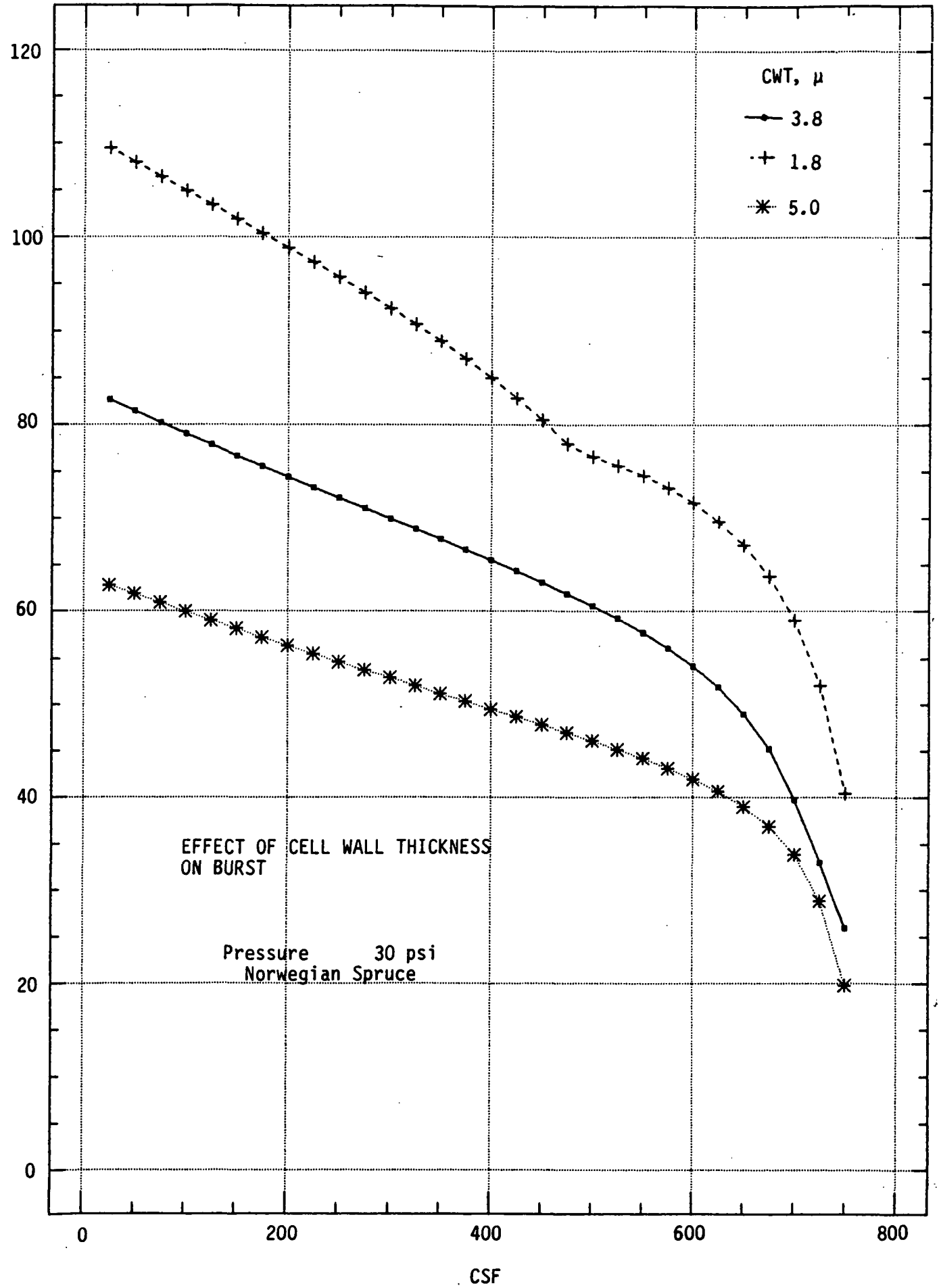
CWT, μ
3.8
1.8
5.0
120
100
80
60
40
20
0
0
200
400
600
800
CSF
EFFECT OF CELL WALL THICKNESS ON BURST
Pressure 30 psi
Norwegian Spruce

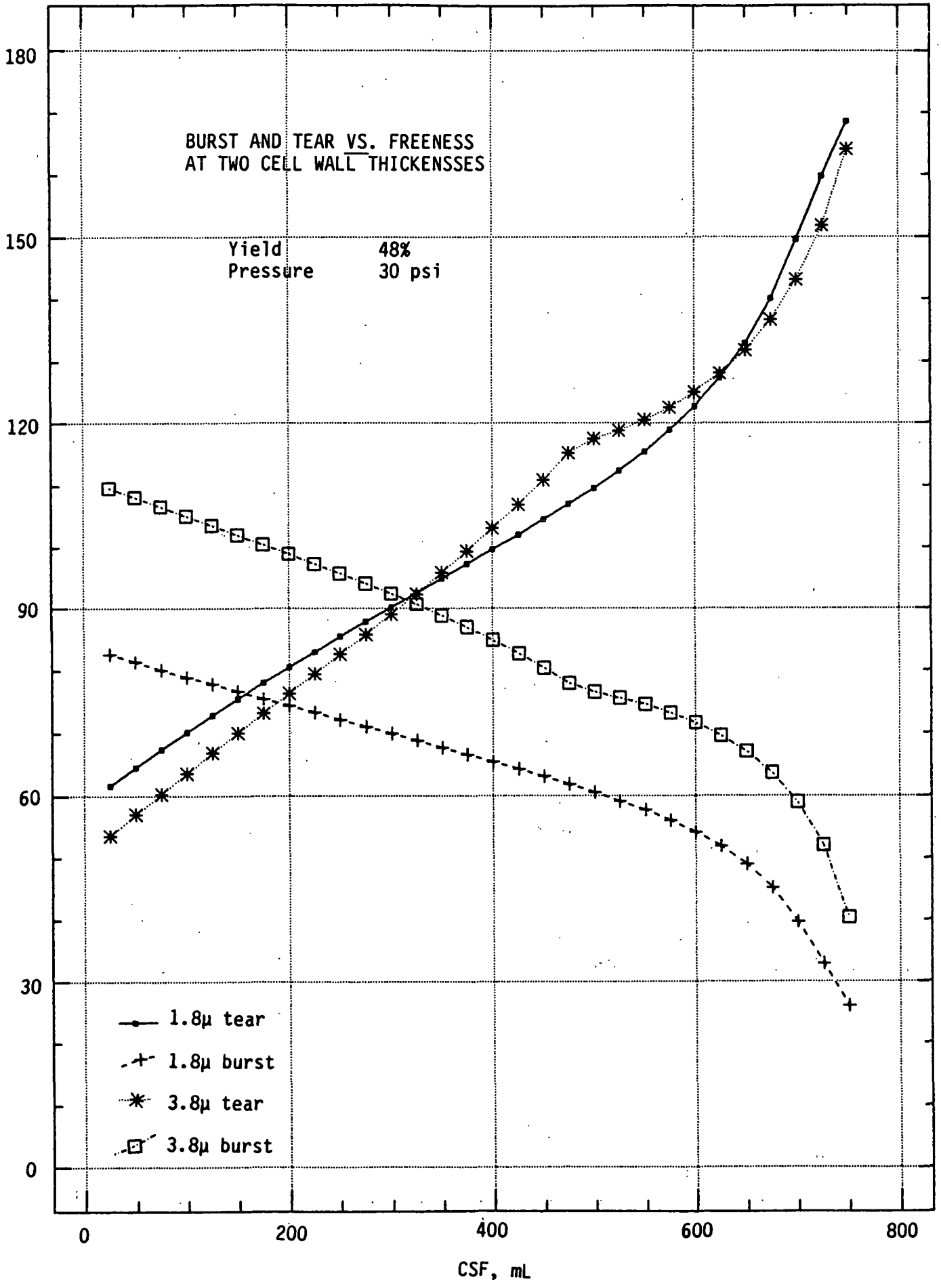
BURST AND TEAR VS. FREENESS
AT TWO CELL WALL THICKENSSES
Yield 48%
Pressure 30 psi
180
150
120
90
60
30
0
0
200
400
600
800
CSF, mL
1.8μ tear
1.8μ burst
3.8μ tear
3.8μ burst

VARIATION IN MEASURED FIBER COMPONENTS THROUGHOUT PROCESS

POSITION	
1	SECONDARY REFINER DISCHARGE
2	PRIMARY SCREEN FEED
3	PRIMARY SCREEN ACCEPTS
4	PRIMARY SCREEN REJECTS
5	SECONDARY SCREEN ACCEPTS
6	REJECT REFINER DISCHARGE
7	PRIMARY REJECT CLEANER ACCEPTS
8	THICKENER DISCHARGE

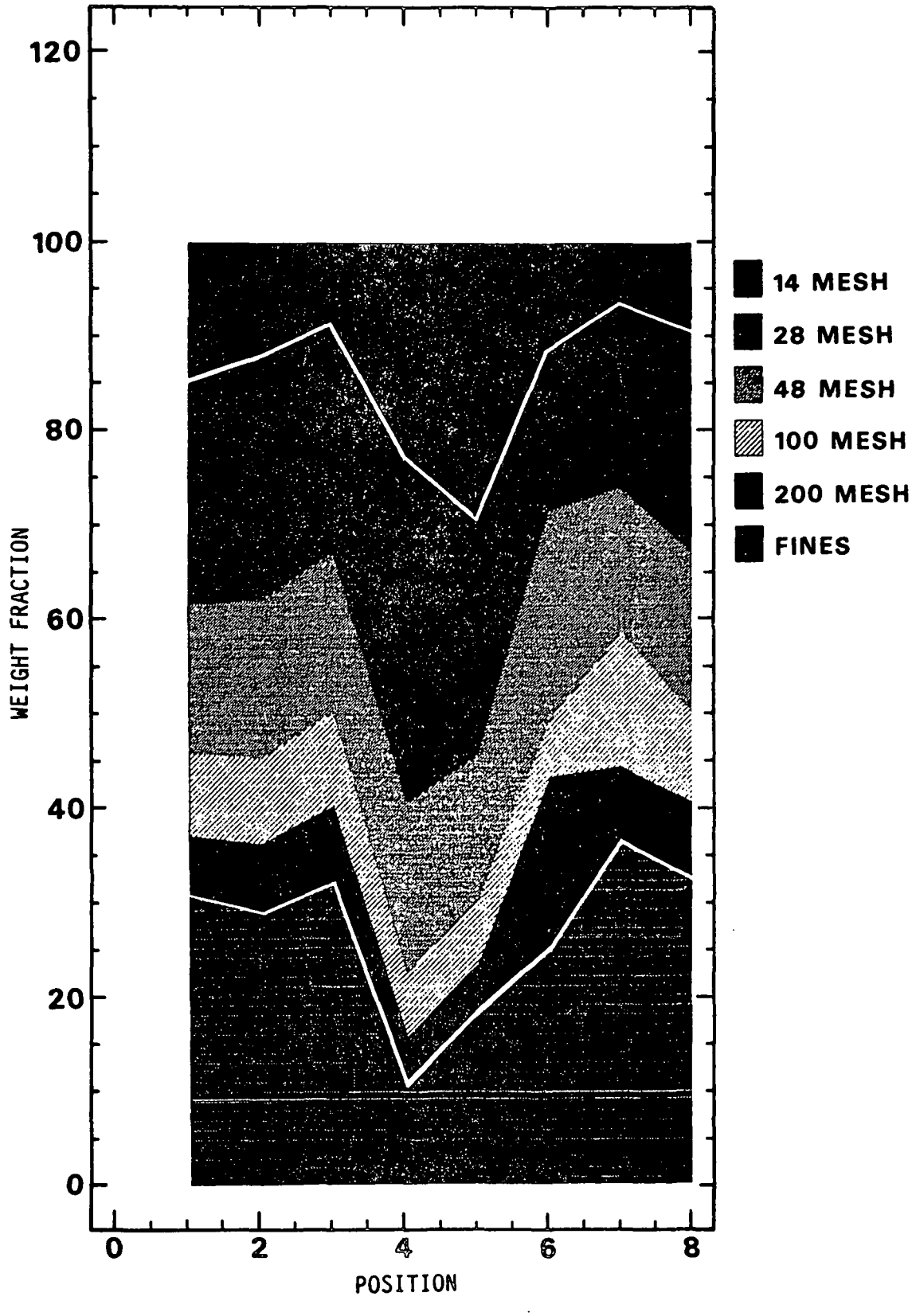
120
100
80
60
40
20
0
WEIGHT FRACTION
0
2
4
6
8
POSITION
14 MESH
28 MESH
48 MESH
100 MESH
200 MESH
FINES

Variation In Simulated Fiber Components Throughout Process

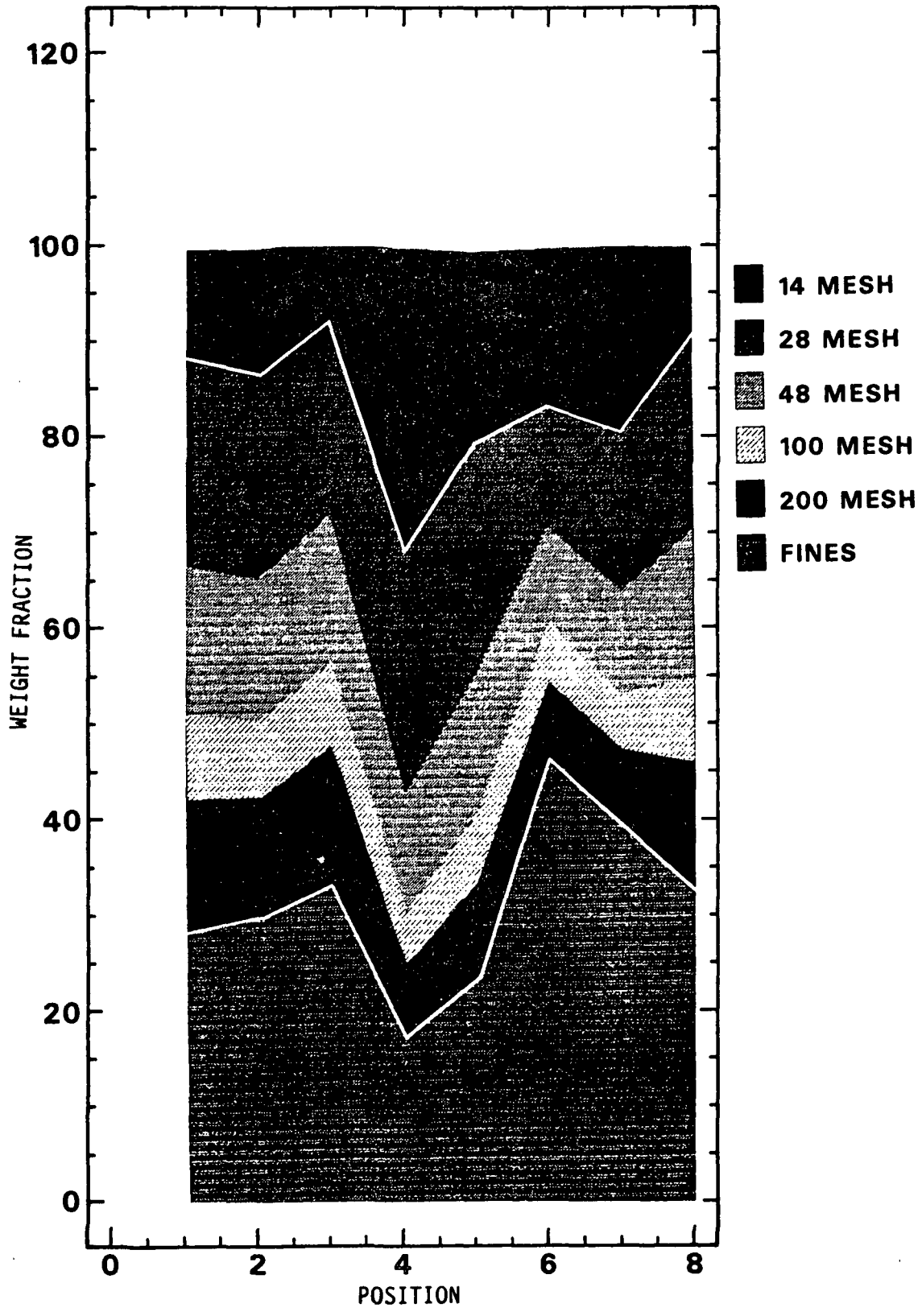

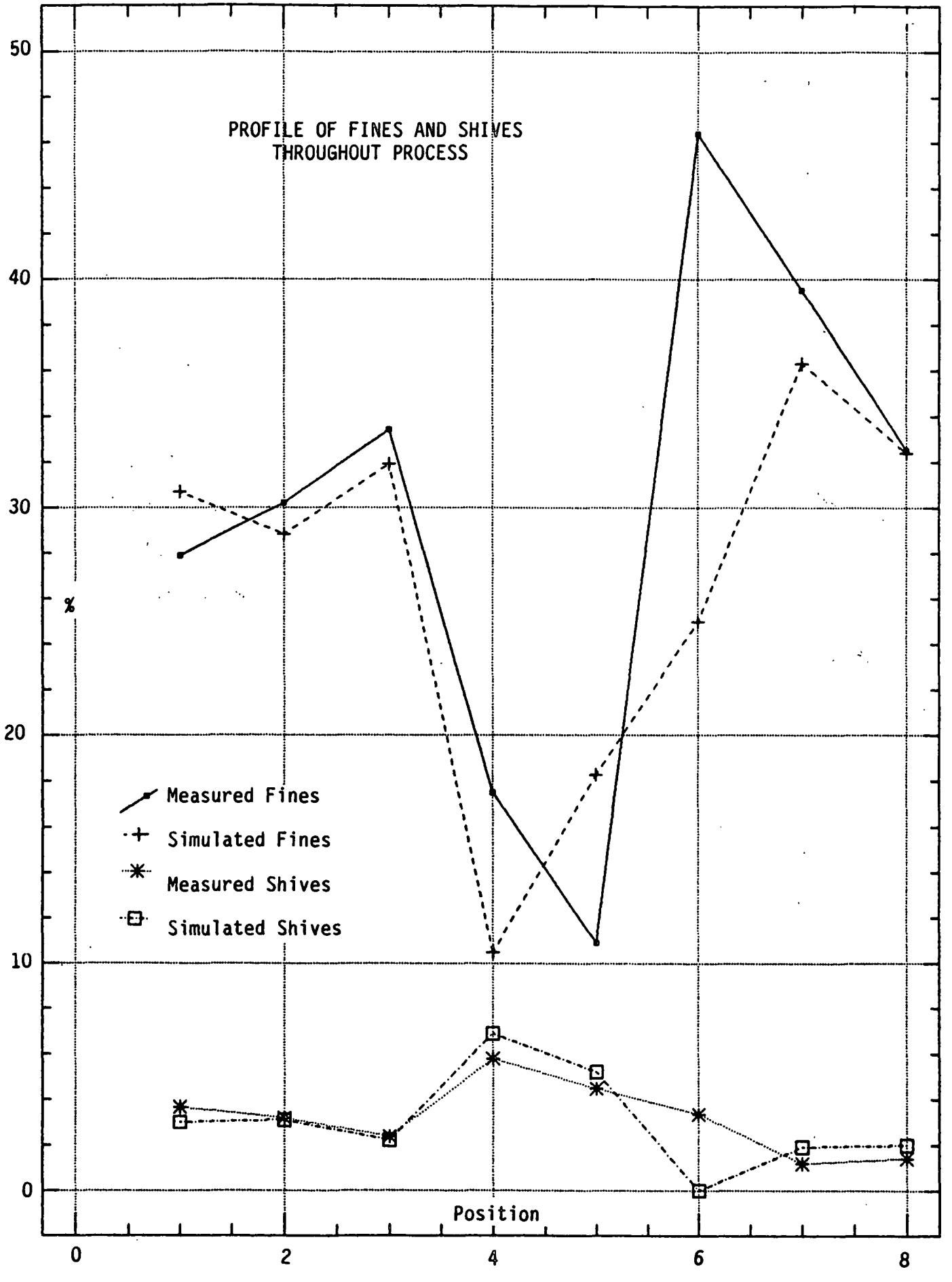
PROFILE OF FINES AND SHIVES
THROUGHOUT PROCESS
50
40
30
20
10
0
%
Measured Fines
Simulated Fines
Measured Shives
Simulated Shives
Position
0
2
4
6
8

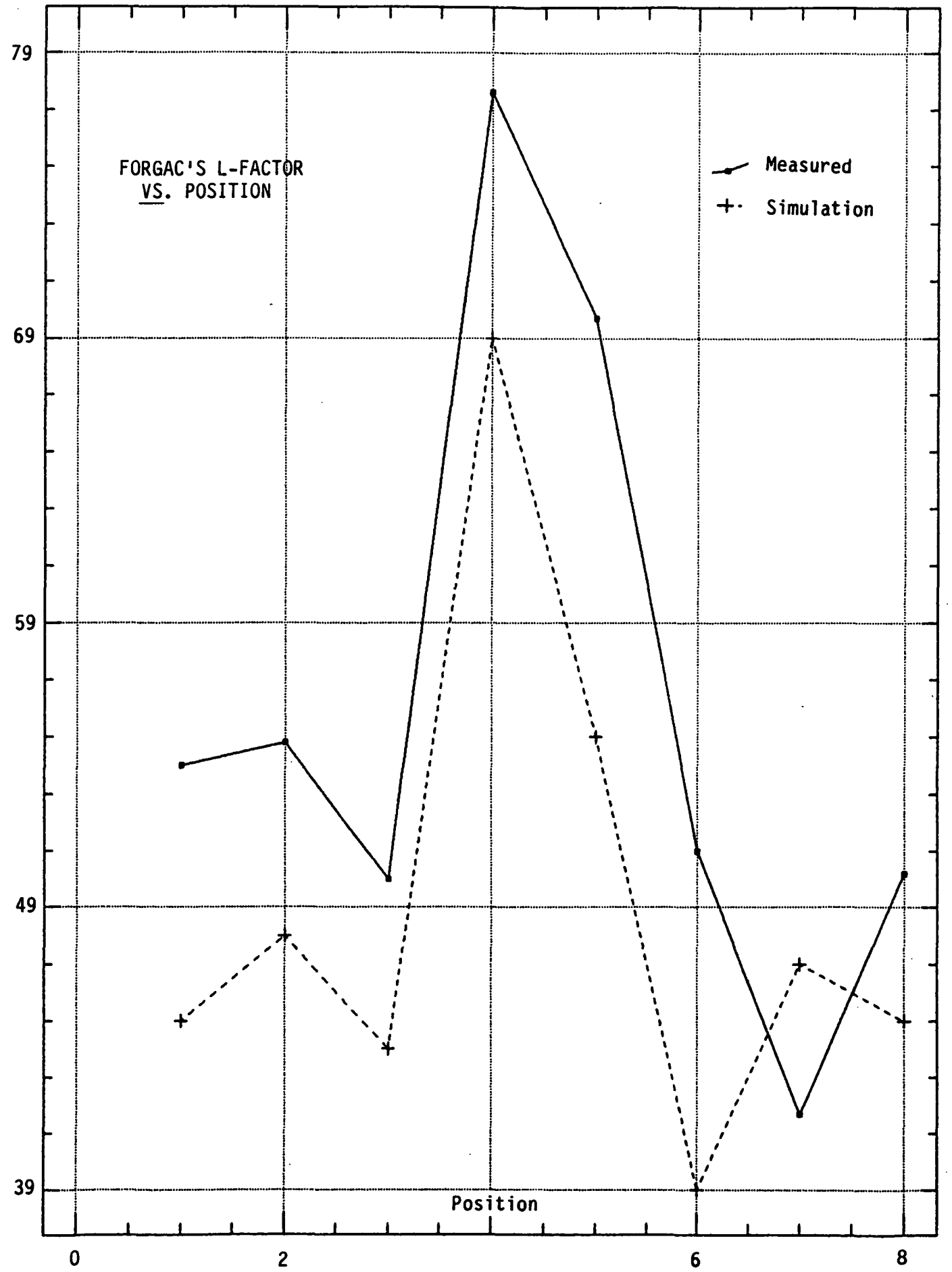
FORGAC'S L-FACTOR
VS. POSITION
Measured
Simulation
79
69
59
49
39
Position
0
2
6
8

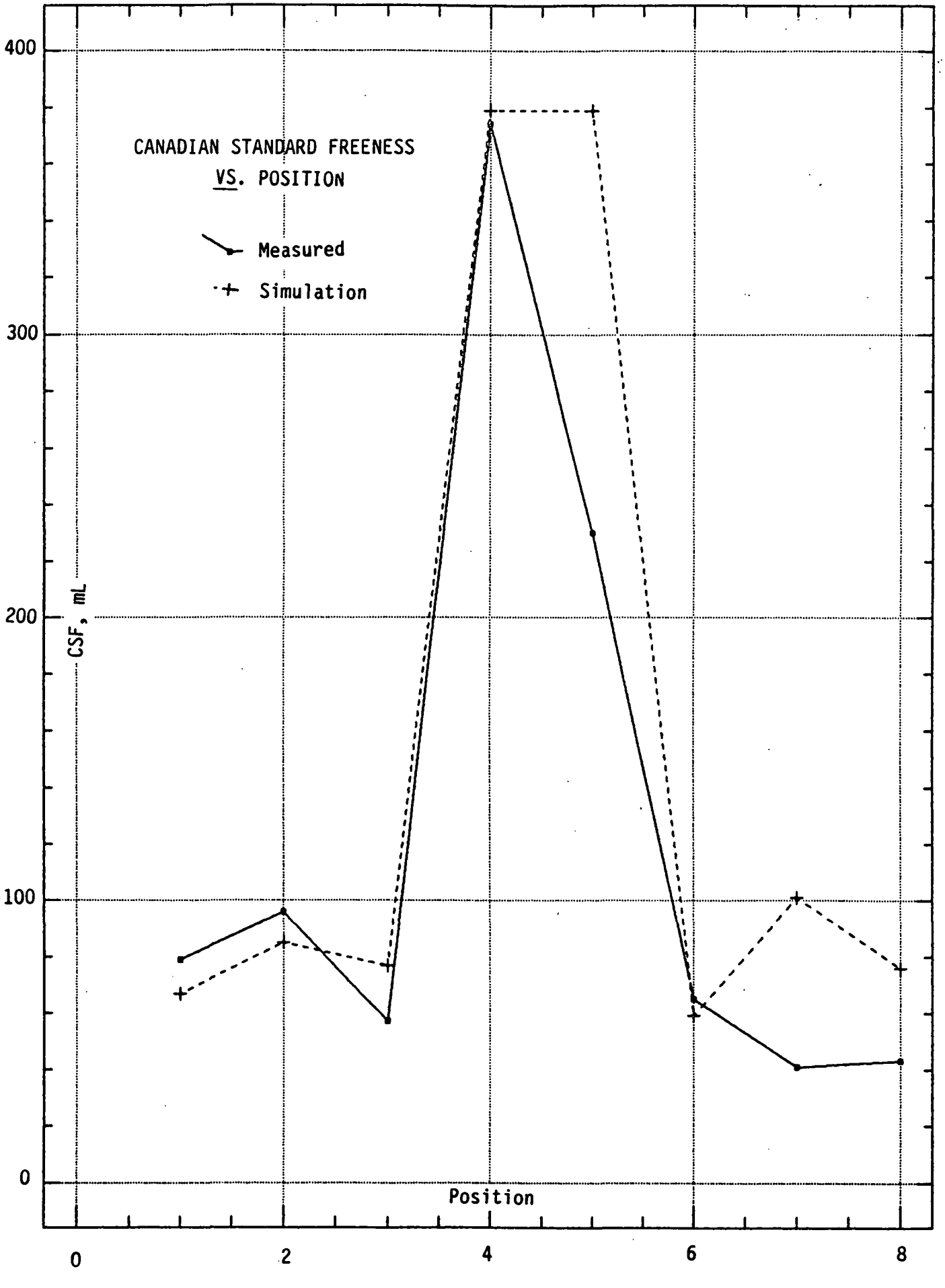
CANADIAN STANDARD FREENESS
VS. POSITION
Measured
Simulation
CSF, mL
400
300
200
100
0
Position
0
2
4
6
8

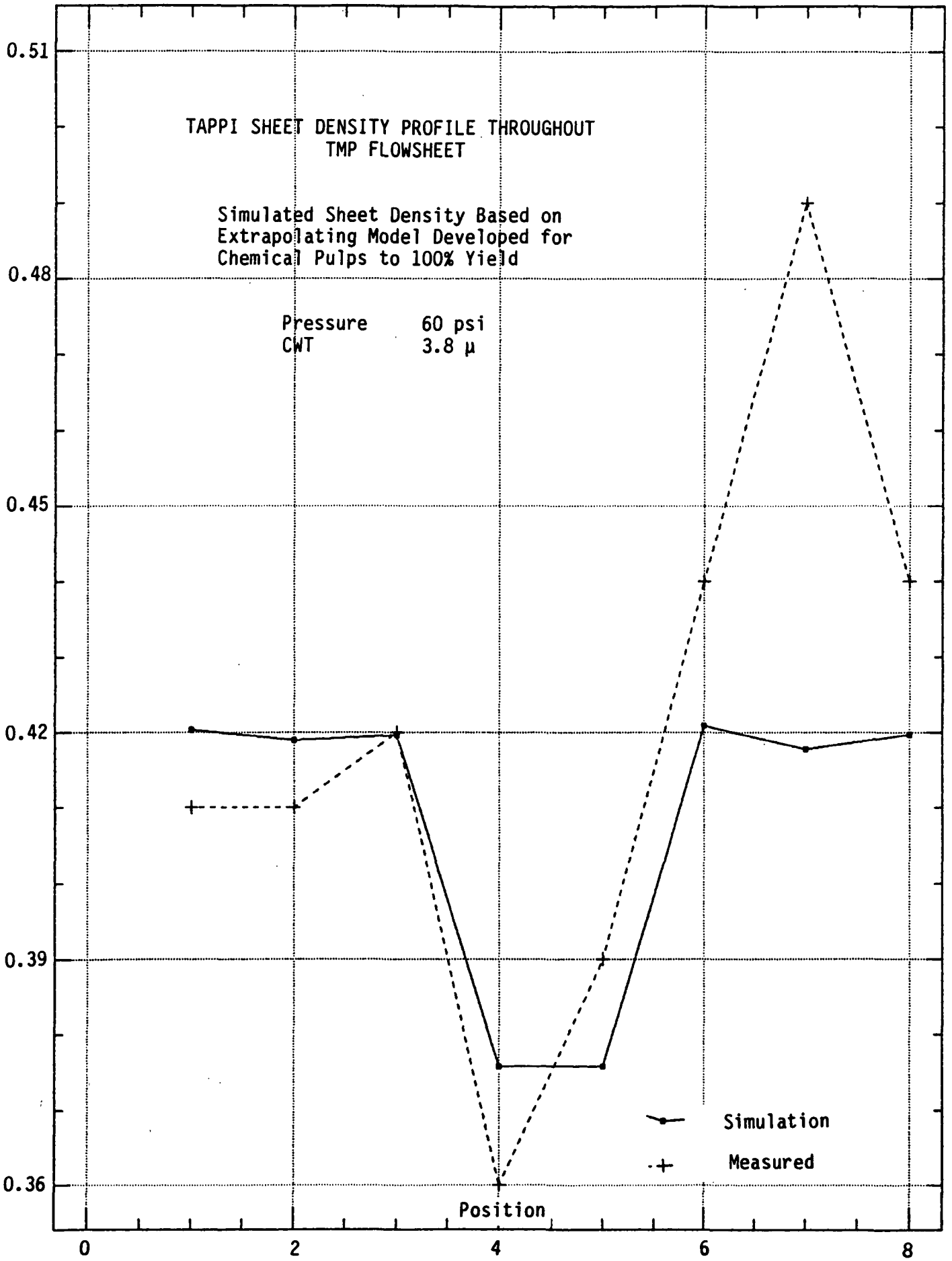
TAPPI SHEET DENSITY PROFILE THROUGHOUT
TMP FLOWSHEET
Simulated Sheet Density Based on
Extrapolating Model Developed for
Chemical Pulps to 100% Yield
Pressure 60 psi
CWT 3.8 μ
0.51
0.48
0.45
0.42
0.39
0.36
Simulation
Measured
Position
0
2
4
6
8

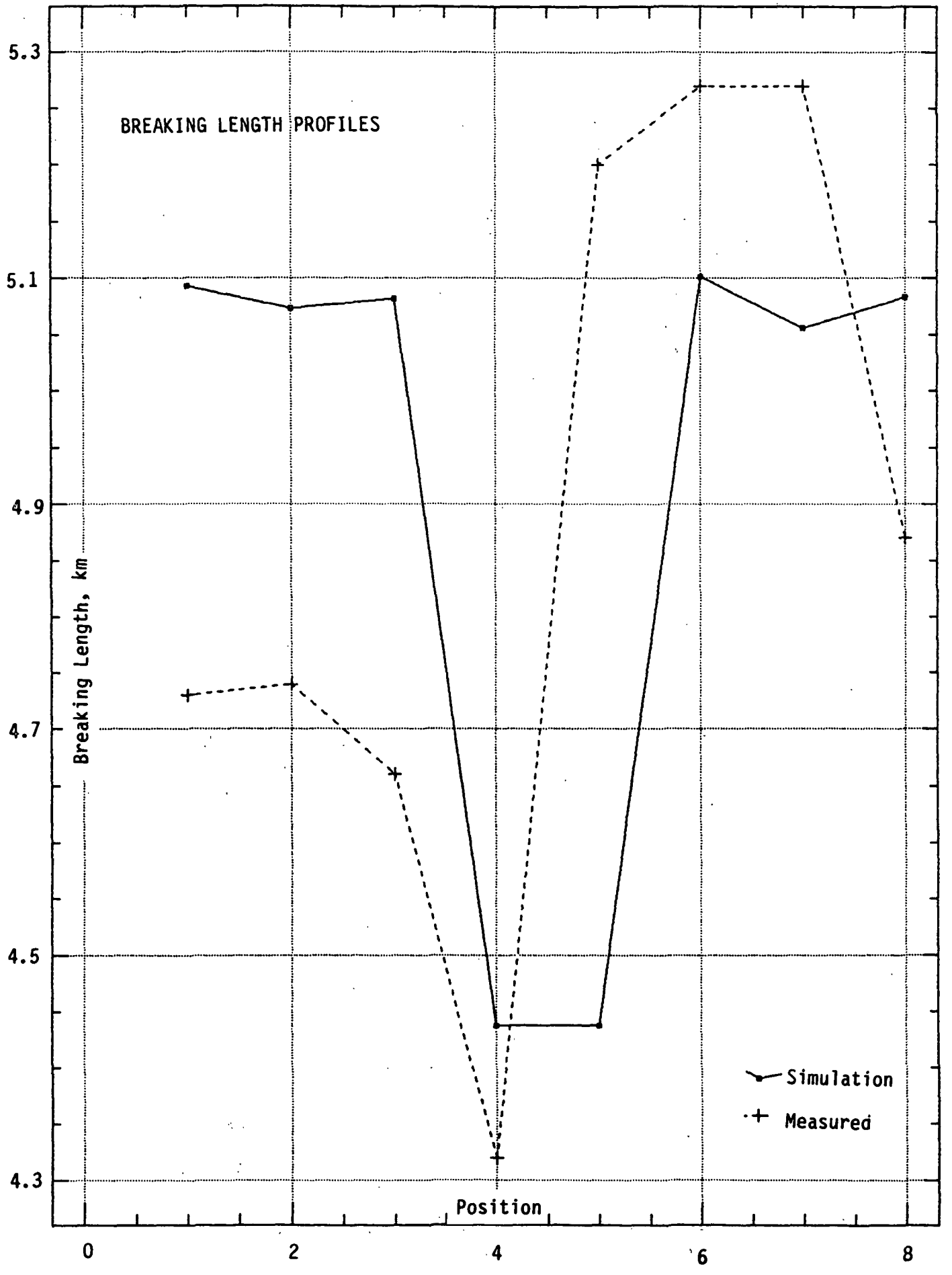
BREAKING LENGTH PROFILES
5.3
5.1
4.9
4.7
4.5
4.3
Breaking Length, km
Position
0
2
4
6
8
Simulation
Measured

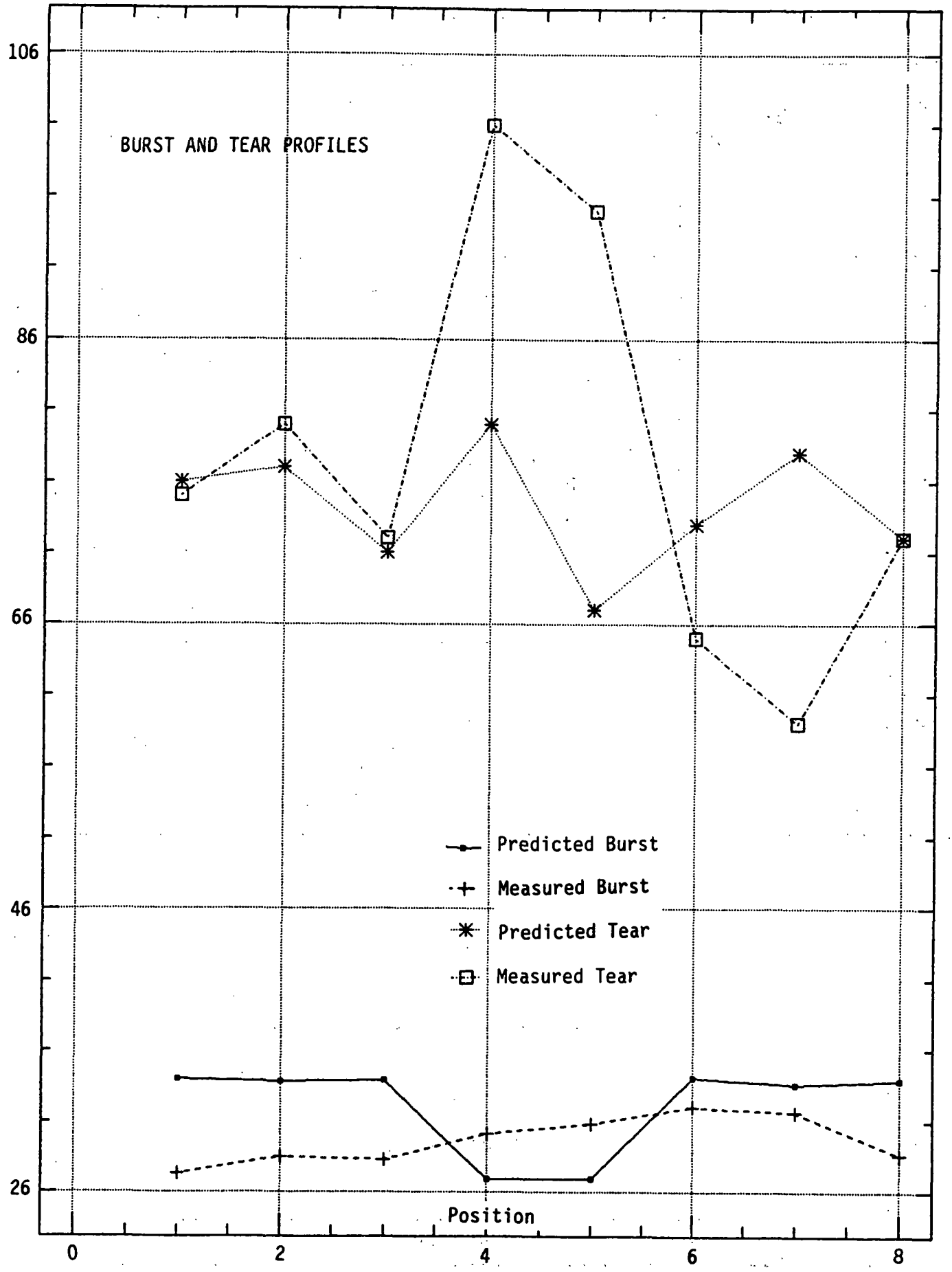
BURST AND TEAR PROFILES
106
86
66
46
26
0
2
4
6
8
Position
Predicted Burst
Measured Burst
Predicted Tear
Measured Tear

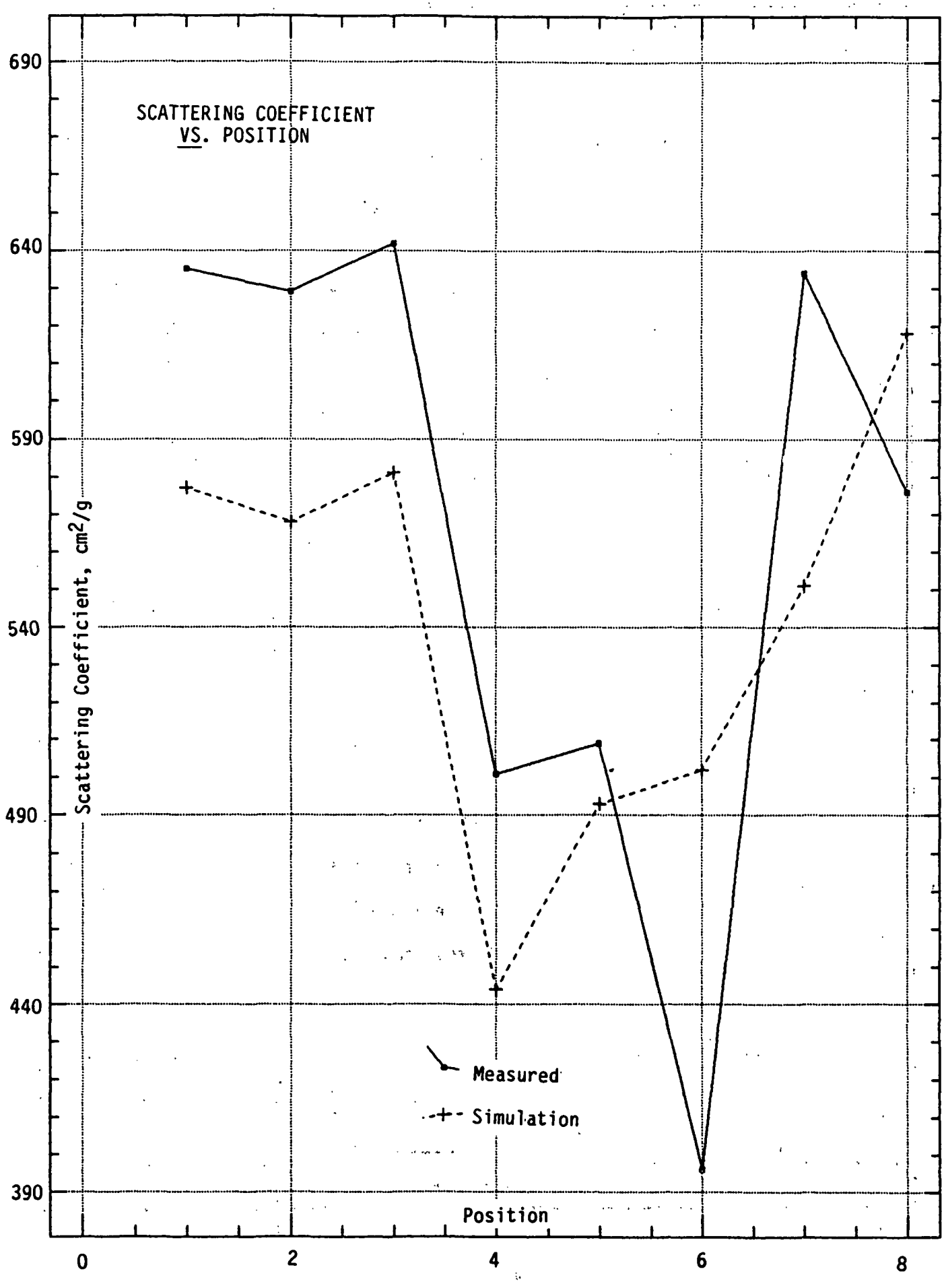
SCATTERING COEFFICIENT
VS. POSITION
690
640
590
540
490
440
390
Scattering Coefficient, cm2/g
Measured
Simulation
Position
0
2
4
6
8

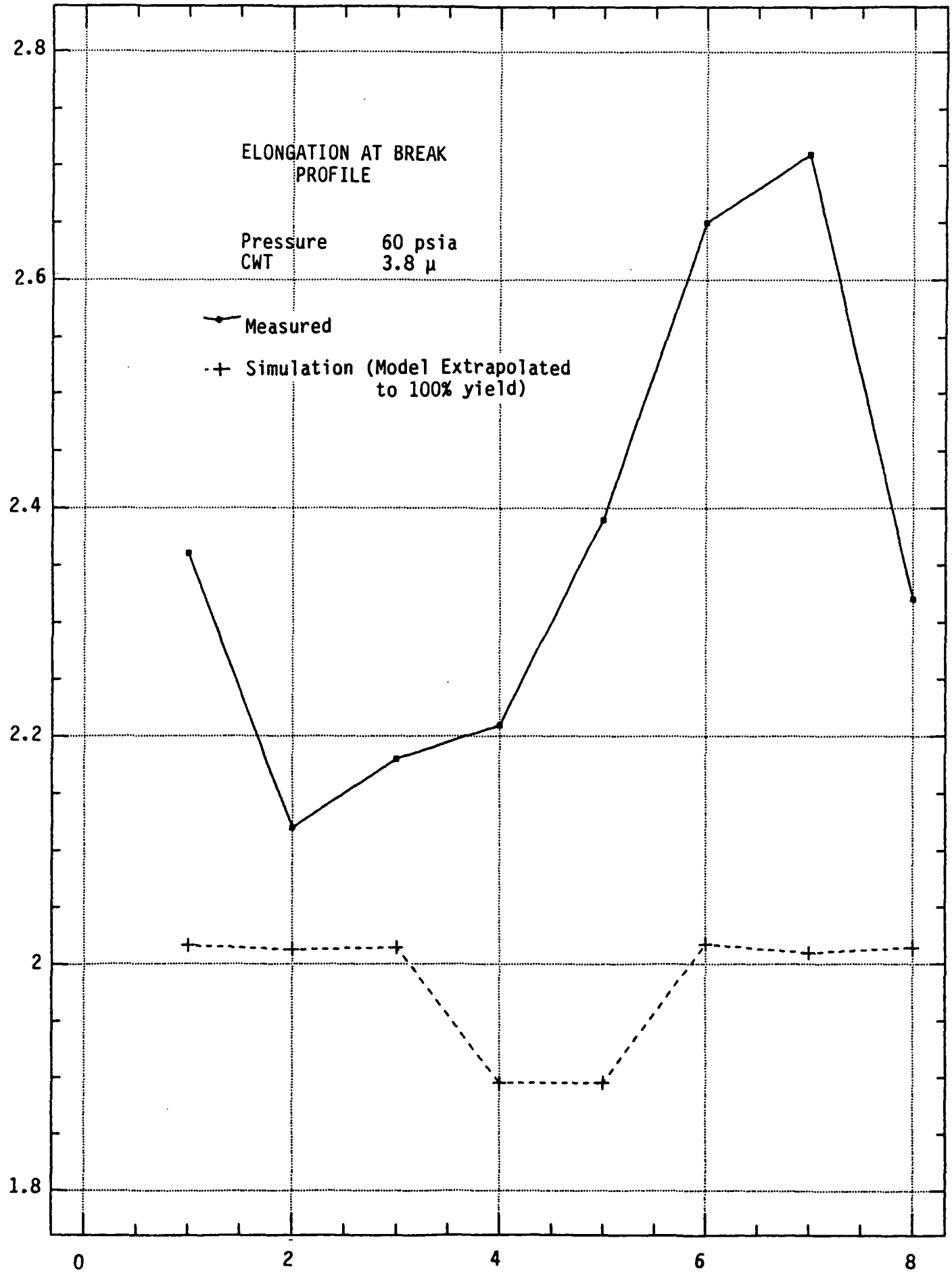
ELONGATION AT BREAK
PROFILE
Pressure 60 psia
CWT 3.8 μ
Measured
Simulation (Model Extrapolated to 100% yield)
2.8
2.6
2.4
2.2
2
1.8
0
2
4
6
8